Etudes structurales sur l'assemblage du nucléosome

Carmen Aguilar Gurrieri

THESIS/THÈSE

To obtain the title of/*Pour obtenir le grade de*

DOCTEUR DE L'UNIVERSITÉ DE GRENOBLE

Discipline/*Spécialité* : Structural biology and Nanobiology

Arrêté ministériel : 7 août 2006

Presented by/Présentée *par* **Carmen Aguilar-Gurrieri**

Thesis supervisor/*Thèse dirigée par* **Daniel Panne**

Thesis prepared at/*Thèse préparée au sein du*

European Molecular Biology Laboratory (EMBL), Grenoble Outstation

In/dans **l'École Doctorale de Chimie et Sciences du vivant**

Structural studies of nucleosome assembly

Études structurales sur l'assemblage du nucleosome

Public defense/*Thèse soutenue publiquement le* 05.07.2013

Jury members/*devant le jury composé de:*

Dr. Daniel Panne	*Thesis director/Directeur de thèse*
Dr. John McGeehan	Reviewer/*Rapporteur*
Dr. Christoph Müller	Reviewer/*Rapporteur*
Dr. Stefan Dimitrov	Examiner/*Examinateur*
Dr. Christian Häring	*Examiner/Examinateur*
Dr. Winfried Weissenhorn	President/*Président*

ABSTRACT

Assembly of chromatin is an essential process that concerns most DNA transactions in eukaryotic cells. The basic repeating unit of chromatin are nucleosomes, macromolecular complexes that consist of a histone octamer that organizes 147 bp of DNA in two superhelical turns. Although the structures of nucleosomes are known in detail, their assembly is poorly understood.

In vivo, nucleosome assembly is orchestrated by ATP-dependent remodelling enzymes, histone-modifying enzymes and a number of at least partially redundant histone chaperones. Histone chaperones are a structurally diverse class of proteins that direct the productive assembly and disassembly of nucleosomes by facilitating histone deposition and exchange. The currently accepted model is that nucleosome assembly is a sequential process that begins with the interaction of H3/H4 with DNA to form a $(H3/H4)_2$ tetramer-DNA complex. The addition of two H2A/H2B dimers completes a canonical nucleosome.

High-resolution structures of histone chaperones in complex with H3/H4 histones have resulted in detailed insights into the process of nucleosome assembly. However, our understanding of the mechanism of nucleosome assembly has been hampered by the as yet limited number of co-crystal structures of histone–chaperone complexes. In particular it remains unclear how histone chaperones mediate H2A/H2B deposition to complete nucleosome assembly.

In this work, we have investigated the role of the H2A/H2B chaperone Nap1 (Nucleosome assembly protein 1) in nucleosome assembly. We have determined the crystal structure of the complex between Nap1 and H2A/H2B and analysed the assembly by various biophysical methods. The structure shows that a Nap1 dimer binds to one copy of H2A/H2B ($Nap1_2$-H2A/H2B). A large ~550 kDa macromolecular assembly containing 6 copies of the $Nap1_2$-H2A/H2B complex is seen in the asymmetric crystallographic unit. We confirmed by both non-denaturing mass spectroscopy and negative stain electron microscopy studies that this assembly is the predominant form of the $Nap1_2$-H2A/H2B complex in solution.

We further investigated the potential interplay between p300-mediated histone acetylation and nucleosome assembly. Together, the structure and associated functional analysis

provide a detailed mechanism for the Nap1 chaperone activity, its role in H2A/H2B deposition and in nucleosome assembly.

RESUME EN FRANÇAIS

Au sein du noyau, l'ADN est organise en chromatine dont l'unité de base est le nucléosome. La structure de la chromatine est très dynamique, ce qui est nécessaire pour la plupart des opérations qui se produisent dans l'ADN telles que la réplication, la transcription, la réparation et la recombinaison. Le nucléosome est constitué de deux dimères H2A/H2B et deux dimères H3/H4 associés avec 147 paires de bases d'ADN. La protéine Nap1 est un chaperon d'histone H2A/H2B impliquée dans l'assemblage et démontage des nucléosomes. Nap1 protège les interactions non spécifiques entre l'ADN chargé négativement et les dimères H2A/H2B chargés positivement, afin de permettre la formation de la structure ordonnée des nucléosomes. Lors de l'assemblage des nucléosomes, les dimères d'histones H3/H4 sont déposés en premier lieu, suivi par le dépôt de dimères H2A/H2B. Lors du démontage du nucléosome, les dimères H2A/H2B sont retirés avant le retrait des dimères H3/H4. La determination de la structure du complexe Nap1-H2A/H2B pourra permettre une meilleure compréhension du processus d'assemblage du nucléosome.

Dans cette étude, nous voulons comprendre comment le chaperon Nap1 cible spécifiquement les dimères d'histones H2A/H2B pour l'assemblage des nucléosomes. Notre objectif est de caractériser la structure et la fonction du complexe de Nap1-H2A/H2B. Ainsi nous nous sommes tout d'abord intéresse à la stoechiometrie de ce complexe. Nous avons trouvé qu'un dimère de Nap1 s'associe à un dimère H2A/H2B ($Nap1_2$-H2A/H2B). D'autre part, l'analyse par spectrométrie de masse non-dénaturante a montré que ce complexe de base peut s'oligomériser et contenir jusqu'à 6 copies de $Nap1_2$-H2A/H2B. L'analyse de ce complexe par spectrométrie de masse non-dénaturant a montré que ce complexe peu oligomériser dans un grand complexe contenant jusqu'à 6 copies de $Nap1_2$-H2A/H2B. Nous avons également obtenu la première structure cristalline à basse résolution de ce complexe. L'analyse du même complexe par microscopie électronique à coloration négative a révélé la présence en solution du même oligomère que dans l'unité asymétrique du cristal, qui contient aussi 6 copies de $Nap1_2$-H2A/H2B. Ainsi, nous avons pu mettre en évidence de nouvelles interfaces d'interaction entre les différents composants de ce complexe qui nous permettent de mieux comprendre le processus d'assemblage des nucléosomes.

Le remodelage de la chromatine permet l'expression des gènes eucaryotes. Ce remodelage nécessite des enzymes telles que des histone acétyltransférases (HAT) et les chaperons d'histones. Les HATs acétylent les chaînes latérales des lysines. Il a été proposé que les HATs et les histones chaperons agissent en synergie pour moduler la structure de la chromatine pendant la transcription. La HAT p300 a été proposé d'interagir avec l'histone chaperon Nap1. Nous avons entrepris de caractériser cette interaction. Malheureusement, nos expériences n'ont pas pu détecter d'interaction directe entre ces protéines.

LIST OF ABBREVIATIONS

A	Å	Angstrom
	aa	amino acid
	Abs	Absorbance
	Asf1	Anti-silencing function-1
	ATP	Adenosine-5'-triphosphate
	ATRX	Alpha Thalassemia/mental Retardation syndrome X-linked
B	BMB	1,4-bis(maleimido)butane
	BMOE	Bis(maleimido)ethane
	bp	base pairs
	BRD	Bromodomain
	BRP	Bromodomain RING and PHD domain module
C	CAF1	Chromatin Assembly Factor 1
	CDAI	Congenital Dyserythropoietic Anemia type I
	CH3	Cysteine Histidine rich domain 3
	Chz1	Chaperone for H2A.Z/H2B
	CID	Collision Induced Damaged
	CKII	Casein Kinase II
D	Da	Dalton
	DAXX	Death domain-associated protein
	DEN	Deformable Elastic Network
	DMSO	Dimethyl sulfoxide
	DTT	Dithiothreitol
E	EDTA	Ethylenediaminetetraacetic acid
	EM	Electron Microscopy
	ESRF	European Synchrotron Radiation Facility
F	FT	Flow Through

G	GST	Glutathione-S-Transferase
H	HAT	Histone Acetyl-Transferase
	HBD	Histone Binding Domain
	His-tag	polyHistidine tag
I	INHAT	INhibitor of Histone Acetyl-Transferase
	IPTG	Isopropyl-β-D-thio-galactoside
	ITC	Isothermal Titration Calorimetry
K	Kap114	Karyopherin114
	kDa	kilo Dalton
L	LB	Luria Broth
	LysCoA	Lysine Co-factor A
M	mAmp	mille Amperes
	MCS1	Multiple Cloning Site 1
	mM	milliMolar
	μM	microMolar
	MME	Monomethyl ether
	MR	Molecular Replacement
	MS	Mass Spectrometry
N	NAD^+	Nicotinamide Adenine Dinucleotide
	Nap1	Nucleosome assembly protein 1
	NaCl	Sodium Chloride
	NCP	Nucleosome Core Particle
	NCS	Non-Crystallographic Symmetry
	NES	Nuclear Export Sequence
	NLS	Nuclear Localization Sequence
	nm	nanometre
	Np	Nucleoplasmin

O	OD	Optical Density
P	PAGE	Polyacrylamide gel electrophoresis
	PanNETs	Pancreatic NEuroendocrine Tumors
	PDB	Protein Data Bank
	PEG	Polyethylene glycol
	PfNapS / PfNapL	*Plasmodium falciparum* Nap1
	pI	point Isoelectric
R	Rpm	Revolutions per minute
	Rtt109	Regulation of Ty1 transposition protein 109
S	SDS	Sodium Dodecyl Sulphate
	SEC	Size-Exclusion Chromatography
	SET	SE Translocation
	SFM	Serum Free Media
	SIRT2	Human Sirtuin 2
T	TAF-1β	Template-Activating Factor-1β
	TCEP	Tris(2-carboxyethyl)phosphine
	TEV	Tobacco Etch Virus
	TMAO	Trimethylamine N-oxide
	Tris	Tris(hydroxymethyl)aminomethane
U	UV	Ultraviolet
V	V	Volts
	Vps75	Vacuolar protein sorting-associated protein 75

W	*wt*	wild-type

TABLE OF CONTENTS

1. INTRODUCTION

RÉSUMÉ EN FRANÇAIS

Dans une cellule, environ deux mètres d'ADN doivent être compactés pour tenir au sein d'un noyau de quelques microns. Malgré ce degré de compaction extrême, l'ADN doit être rapidement accessible pour réguler son métabolisme lors des événement de transcription, réplication, réparation, etc. Pour cela l'ADN s'organise dans le noyau en une structure nucleo-proteique dynamique appelée chromatine. Le nucléosome constitue un premier niveau de structuration de la chromatine. Son remodelage et le remodelage de la chromatine en général, lui confère de nouvelles propriétés structurales et fonctionnelles. Plusieurs mécanismes principaux assurent cette plasticité de la chromatine comme la modification de l'ADN par méthylation, l'incorporation de variant d'histone et la mobilisation des nucléosomes par les complexes de remodelage ainsi que la modification post-traductionnelle des histones.

Les chaperonnes d'histone jouent un rôle important dans la régulation de la structure de la chromatine. Elles s'associent avec les histones libres dans la cellule, les escortent dans le noyau et participent à leur incorporation ou à leur éviction à des endroits précis dans la chromatine. Nap1 est une chaperonne d'histones qui est impliquée dans le dépôt de l'hétérodimère H2A/H2B sur l'ADN. Des études biochimiques de Nap1 montre que cette protéine forme un dimère de base capable de s'oligomeriser. La taille de cet oligomère varie selon la force ionique du tampon et la concentration en protéine. La stoechiométrie de ces grands oligomères reste controversée et leur rôle dans l'assemblage des nucléosomes est actuellement inconnu. Afin de comprendre le rôle des chaperonnes H2A/H2B dans le processus d'assemblage du nucléosome, nous avons entrepris de caractériser la structure du complexe Nap1-H2A/H2B.

Les chaperonnes peuvent fonctionner seules ou en complexe avec des enzymes de modifications comme les HATs. Par exemple, cher *Saccharomyces cerevisiae*, l'histone chaperonne Vps75 est retrouvée en complexe avec la HAT Rtt109. Cette interaction augmente l'activité acétyle-transférase de Rtt109 et facilite le transfert des histones H3/H4 sur Vps75. De façon similaire, chez les eucaryotes supérieurs, l'homologue de Rtt109, la HAT p300/CBP, interagit avec la chaperonne d'histone Nap1. Cette association pourrait faciliter

le remodelage des nucléosomes via leur acétylation. Afin de valider cette hypothèse nous avons entrepris de caractériser l'interaction entre Nap1 et p300.

1.1. CHROMATIN STRUCTURE

Eukaryotic cells contain about two meters of DNA which must be physically organized and compacted into a nucleus with a micrometre-scale diameter (Rocha & Verreault 2008). This compaction is achieved synergistically by the arrangement of DNA with specific proteins. This combination of protein and DNA is known as chromatin. The global and local compaction / de-compaction of chromatin are essential for all the cellular processes that involves DNA, such as DNA replication, DNA transcription or chromatin sorting during cell division, thus throughout the cell cycle the extent of chromatin compaction is in dynamic equilibrium (Figure 1) (Horn 2002).

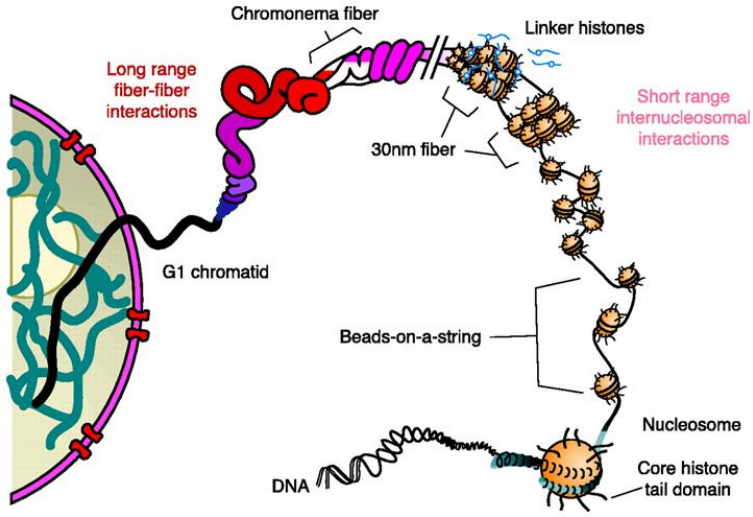

Figure 1 Schematic representation of the multiple stages of chromatin folding. *Note: figure from (Horn 2002).*

The chromatin is compacted in a hierarchical fashion through several degrees of compaction. The first stage of compaction occurs when double stranded DNA wraps around a core of histone proteins, forming a structure known as the nucleosome core particle (NCP) or nucleosome (A. L. Olins & D. E. Olins 1974). The remaining DNA between two NCPs, known as linker DNA, is protected by a linker histone, whose recruitment to NCPs results in a complex known as the chromatosome (Simpson 1978). Thousands of nucleosomes are organized as such on a continuous DNA helix, in linear strings separated by 10 to 60 base pairs (bp) of linker DNA in the genome (Hansen 2002). This “beads-on-a-string”, to which this linear nucleosomal array is referred in the literature, fibre may be considered to constitute the lowest function unit of chromatin (Horn 2002; Hansen 2002).

The second level of compaction is accomplished through histone tail-mediated nucleosome-nucleosome interaction, which promotes the formation of a 30 nm wide fibre (Horn 2002). Two models have been proposed to explain the organization of this 30 nm fibre structure: (a) the 'one-start' (solenoid) model, which consists of consecutive nucleosomes interacting with each other and following a helical trajectory via torsion of the linker DNA; and (b) the 'two-start' (zigzag) model, characterized by two rows of nucleosomes which form a two-start helix so that alternate nucleosomes become interacting partners with relatively straight linker DNA (Woodcock & Ghosh 2010; Luger et al. 2012). Even though the prevailing view is that the 30 nm fibre is organized in a 'heteromorphic' fibre *in vitro* in a more energetically favourable conformation, and both models may coexist in the genome (H. Wong et al. 2007; Grigoryev et al. 2009). However, this model remains controversial, as it has not yet been proven to reflect the true chromatin structure *in vivo* (Fussner et al. 2012).

A third level of compaction arises from the histone tail-mediated association of individual 30 nm fibres, which produces a tertiary structure known as 'chromonema' fibres (Figure 1) (Horn 2002).

The ultimate level of compaction results in the higher structural organisation of the highly recognizable X-shaped chromosomes observed at metaphase (Figure 1) (Woodcock & Ghosh 2010).

1.1.1. The nucleosome core particle: structure and assembly

The NCP is the elemental repeat unit of all known eukaryotic chromatin structures (Oudet et al. 1975; Finch et al. 1977). However, although the structure of the NCP itself is well characterized (Luger, Mäder, et al. 1997a; Davey et al. 2002), the mechanisms of its assembly and dynamics *in vivo* are not yet well understood.

The NCP consists of a histone octamer (one tetramer of histones H3/H4 and two dimers of H2A/H2B) around which 147 bp of DNA are wrapped in 1.7 turns of a tight, flat, and left-handed super-helix (Figure 2A) (Luger, Mäder, et al. 1997a). The central 80 bp of the nucleosomal DNA are organized by a heterotetramer of histones H3/H4, whereas the peripheral 40 bp of DNA on each side are bound more loosely by the H2A/H2B dimers

(Figure 2B) (Ransom et al. 2010). The penultimate 10 bp of DNA are coordinated by the amino(N)-terminal α-helix of histone H3 (Figure 2B) (Ransom et al. 2010).

The four core histone proteins (H2A, H2B, H3, and H4), which constitute the histone octamer, share a highly similar structural motif named the 'histone-fold' domain in their central regions (Figure 2C). This domain is formed of three α-helices connected by two interspersed loops, an arrangement denoted as α1-L1-α2-L2-α3 in Figure 2C, and is characteristic of this class of proteins. Due to complementary internal packing, H3 and H2A form crescent-shape heterodimers exclusively with H4 and H2B respectively through their histone fold domains. In the nucleosome core particle, the two H3/H4 heterodimers interact though a 4-helix bundle formed exclusively by the two juxtaposed H3 histone folds thus constituting the heterotetramer (Figure 2). Each H2A/H2B heterodimer interacts with the heterotetramer through a second, homologous 4-helix bundle between H2B and H4 histone folds. For more details refer to (Luger, Mäder, et al. 1997a).

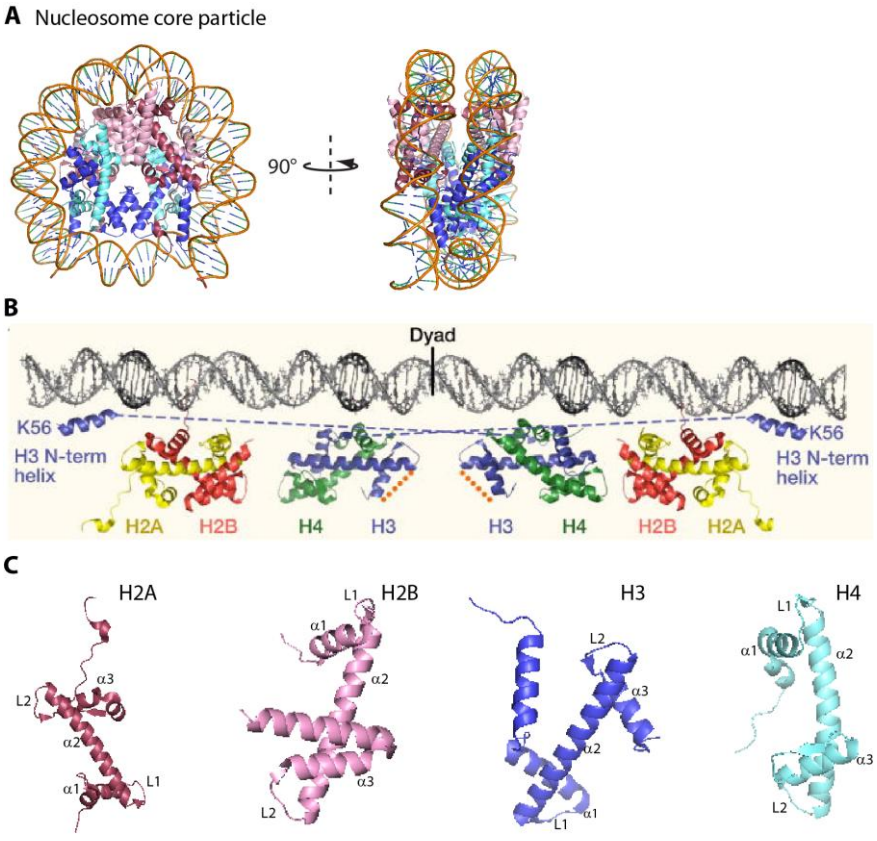

Figure 2 Nucleosome structure. (A) Nucleosome core particle structure (PDB Code: 2NQB), front and side views. (B) Unravelling of the nucleosomal DNA to indicate which region of the DNA is organized by which histone proteins. Dashed lines indicates the H3-H3 dimerization interface involved in H3/H4 tetramerization.

Note: figure from (Ransom et al. 2010). (C) Histone-fold domain of H2A, H2B, H3, and H4 (PDB Code: 2NQB). Histone H2A is colored in red, H2B in pink, H3 in blue, and H4 in cyan.

Histone tails are found at the N-terminal end of the histone-fold domain and can extend outside of the nucleosome (Luger, Mäder, et al. 1997a). These tails are extremely basic due to the high proportion of lysine and arginine that they contain and their post-translational modifications can modulate nucleosome assembly or disassembly (Luger & Richmond 1998).

The assembly of the NCP is thought to be a two-step process guided by histone chaperones in cooperation with ATP-dependent remodelling factors, and histone modification enzymes (Mello & Almouzni 2001; Ransom et al. 2010; Haushalter & Kadonaga 2003). First a tetramer of H3/H4 is deposited onto the DNA to form an intermediate known as the tetrasome (Figure 3A) (Smith & Stillman 1991). Secondly, an H2A/H2B heterodimer is initially deposited unilaterally on the tetrasome, forming the hexasome (Figure 3B); followed by a second H2A/H2B heterodimer from the other side of the central H3/H4 heterotetramer thus constituting the final NCP (Figure 3C) (Nakagawa et al. 2001). Disassembly likely occurs as a reversal of this series of events.

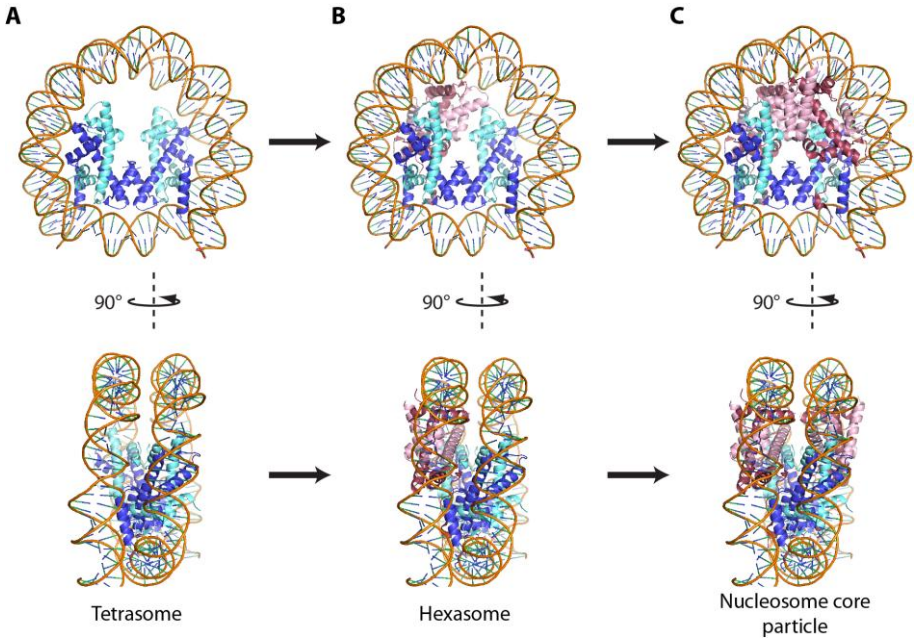

Figure 3 Nucleosome assembly process. A model for step-wise nucleosome assembly as guided by histone chaperones: (A) tetrasome, (B) hexasome, and (C) NCP. PDB Code: 2NQB. Histone H2A is colored in red, H2B in pink, H3 in blue, and H4 in cyan.

1.2. HISTONE CHAPERONES

Histones are small and highly basic proteins that have an intrinsic affinity for the negative charge of DNA (Kornberg & Thomas 1974). The association of histones and DNA *in vitro* under physiological conditions leads to the rapid formation of insoluble aggregates (Tyler 2002), thus additional factors must be required for the establishment of biologically relevant histone-DNA assemblies, such as chromatin. It has been described in the literature that the presence of additional acidic proteins, which could attenuate the charge of the histones, precludes aggregation and ensures the formation of chromatin by the regular and ordered deposition of histones on DNA (Akey & Luger 2003). Such acidic factors are known as histone chaperones. These chaperones associate with histones upon their synthesis, escort them into the nucleus, and modulate their specific association with DNA during essential processes in the cell such as DNA replication, DNA repair or transcription (Avvakumov et al. 2011; Eitoku et al. 2008; Rocha & Verreault 2008). Additionally, they are involved in histone storage which prevents their non-productive aggregation with DNA (Akey & Luger 2003). Lastly, specialized histone chaperones mediate the assembly of histone variants into the nucleosome (Campos & Reinberg 2010; Henikoff & Ahmad 2005).

The affinity and specificity for H3/H4, H2A/H2B, and linker histones varies among different classes of histone chaperones, and it is principally the variation in these attributes that determines the functional specialisation of the chaperones. For example, Anti-silencing function 1 (Asf1) interacts specifically with the core histones H3/H4 (Natsume et al. 2007; English et al. 2006), while Nucleoplasmin (Np) preferentially binds the core histones H2A/H2B (Ramos et al. 2010), thus both may be considered highly specific chaperones. Additionally, Chaperone for H2A.Z/H2B 1 (Chz1) and Death domain-associated protein (DAXX) are two histone chaperones that interact specifically with histone variants H2A.Z and H3.3, respectively (Luk et al. 2007; Elsässer et al. 2012). Conversely the histone chaperone Nucleosome assembly protein 1 (Nap1) has been reported to bind to all core histones (H2A/H2B and H3/H4) as well as the linker histone H1 (McBryant et al. 2003; Kepert et al. 2005; Park et al. 2005), meaning that Nap1 interacts with histones with considerable promiscuity.

However histone chaperones also bind other factors in addition to their histone partners to form complexes that participate in other cellular functions such as DNA replication, DNA repair, and transcription (Zlatanova et al. 2007).

In the following sections, further details about histone chaperones and their functions are described, with special emphasis on Nap family proteins, which are the predominant focus of this thesis.

1.2.1. Chaperoning histones H3/H4: Anti-silencing function 1

Asf1 is an H3/H4-specific histone chaperone, which participates in global nucleosome disassembly and replication-independent nucleosome assembly (Hansen et al. 2010). Biochemical and structural studies on the formation of Asf1-H3/H4 complexes revealed that the histone chaperone binds with a 1:1 (Asf1 monomer/ H3/H4 dimer) stoichiometry (English et al. 2005; Mousson et al. 2005). These studies also revealed that Asf1 blocks the H3-H3 dimerization interface of the H3/H4 heterodimer, impeding formation of the H3/H4 heterotetramer and allowing histones to exist as soluble, chaperone-coupled heterodimers (English et al. 2005; Mousson et al. 2005).

The crystal structure of free Asf1 showed that this chaperone consists of an elongated β sandwich with three α helices present in the loops between the β strands, which are organised into an immunoglobulin-like fold (Figure 4A) (Daganzo et al. 2003; Mousson et al. 2005). This structure revealed the presence of two major regions of Asf1 which could be available for protein-protein interactions: (a) a hydrophobic concave groove surrounded by polar and charged residues, and (b) a deep pocket with hydrophobic residues on the other site of the hydrophobic groove, between β1-β9 (Daganzo et al. 2003). The acidic C-terminal region of Asf1 is fully unfolded and thus is not represented in this structure (Figure 4A) (Mousson et al. 2005).

As demonstrated by a second structure, reporting the Asf1-H3/H4 complex, it is precisely this hydrophobic cavity where the histone H3 binds Asf1 (Figure 4B). Histone H3 interacts with Asf1 through the H3-H3 dimerization interface (helix α3 and half of the helix α2) preventing the formation of H3/H4 heterotetramers *in vitro* and *in vivo* (Figure 4C) (English

et al. 2006; Natsume et al. 2007). Accordingly, the measured affinity of Asf1 for helix α3 of H3 is 100 ± 20 μM (Mousson et al. 2005). In addition, this primary binding site of Asf1 and its correspondent surface on histone H3 have complementary charge distributions. Mutational studies of this binding interface suggest that this interaction is critical for cellular processes including transcription, DNA replication, and DNA repair (Natsume et al. 2007).

The structure of Asf1-H3/H4 ternary complex also revealed a secondary binding interface, where the C-terminus of histone H4 contacts β9 of the histone chaperone to generate a strand-swapped anti-parallel β-sheet (Figure 4B) (English et al. 2006). As that the C-terminal region of histone H4 interacts with H2A in the nucleosome structure to form a parallel β-sheet (Figure 4C), the interaction between H4 with Asf1 likely inhibits the formation of octamers by steric occlusion (Natsume et al. 2007).

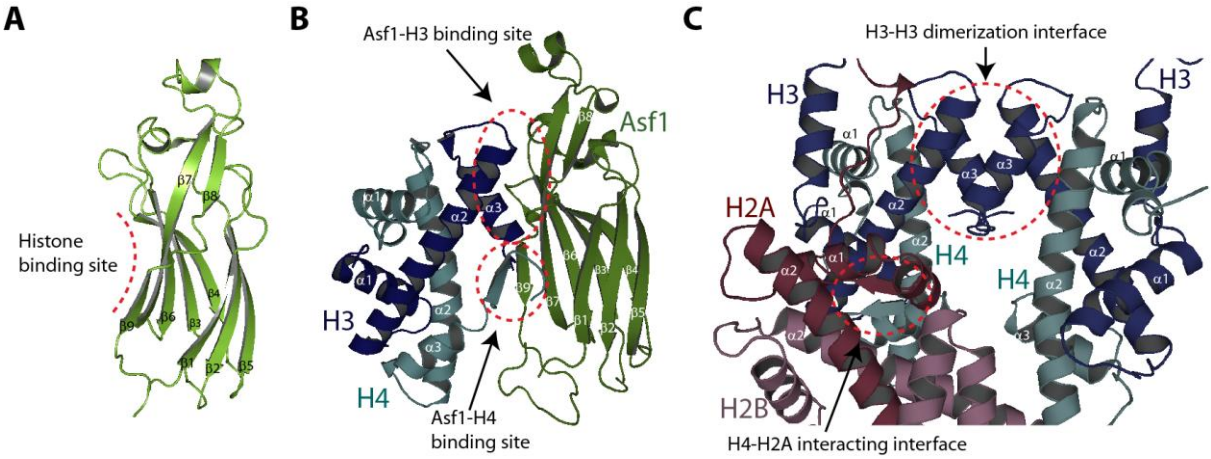

Figure 4 Structure of Asf1, Asf1-H3/H4 ternary complex, and the canonical histone hexamer. (A) Cartoon diagram of the Asf1 histone chaperone (PDB Code 1ROC). Asf1 colored in green. Dashed line highlights the binding cavity for H3/H4 dimer. (B) Cartoon diagram of the Asf1-H3/H4 complex (PDB Code 2HUE), with H3 colored in blue, and H4 in cyan. Dashed lines highlight the interaction interfaces between the histone chaperone and the histone heterodimer. (C) Cartoon diagram of the H2A-H2B/$(H3\text{-}H4)_2$ hexamer in the nucleosome structure (PDB Code 1ID3, with H2A colored in red and H2B in pink. Dashed lines highlight relevant dimerization interfaces.

The crystal structure of Asf1-H3/H4 ternary complex discussed here is likely to represent an intermediate of the Asf1-mediated nucleosome assembly/disassembly reaction (Natsume et al. 2007). In the chromatin assembly process, the presence of DNA apparently triggers H3/H4 dimer release from Asf1 and deposition of the H3/H4 tetramer on DNA. Both, DNA

interaction and tetramerization of H3/H4 are suggested to drive the binding equilibrium from the Asf1-H3/H4 complex towards H3/H4 tetramers (English et al. 2006).

Conversely, the "strand-capture" model has been proposed to explain the chromatin disassembly process (English et al. 2006). Initially, a H2A/H2B chaperone would remove the two H2A/H2B dimers from the tetrasome structure. Then, Asf1 may bind to the C-terminus of histone H4, and this would trigger the disruption of the H3/H4 heterotetramer and the final disassembly of the nucleosome. *In vivo* and *in vitro* mutational studies showed defects in chromatin disassembly and transcription silencing, which supports this model (English et al. 2006).

1.2.2. Chaperoning histones H2A/H2B: Nucleoplasmin

Np was the first histone chaperone discovered (Laskey et al. 1978; Earnshaw et al. 1980). It interacts predominantly with H2A/H2B dimers, but can also interact with H3/H4 tetramers albeit to a lesser extent (Dutta et al. 2001). Functionally, therefore, and for the purpose of this thesis, it can be considered an H2A/H2B chaperone. Np has thus far been found to be represented exclusively in higher eukaryotes, which suggests an evolutionarily specialised role for this histone chaperone (Akey & Luger 2003). Most studies on Np have been conducted in *Xenopus* oocytes, where is one of the most abundant non-histone proteins found in the nucleus (Woodland & Adamson 1977; Mills et al. 1980).

The Np monomer is comprised of a conserved, N-terminal domain (also known as Np-core), which contains a small acidic tract (A1), and a flexible C-terminal tail, with two larger acidic tracts (Figure 5A). The crystal structure of Np, at 2.3 Å resolution (PDB Code 1K5J), reveals a pentameric ring conformation, in which each monomer consists of eight β-sheets forming a β-barrel with a jellyroll topology (Figure 5A). Oligomerization, up to and including pentamers, is facilitated by a β-hairpin present between β-4 and β-5 (Figure 5A) (Dutta et al. 2001). This β-hairpin also features in other histone chaperons, such as Nap1, and has been proposed to play a role in oligomerization (Park et al. 2008). Research on Np suggests that these higher order complexes may function as a histone storage entity (Akey & Luger 2003);

furthermore the conservation of the β-hairpin in Nap1 implies that histone:chaperone oligomerization may be a common mechanism amongst related chaperones.

However, the exact extent of this oligomerization remains controversial. In the Np crystal form described above, two Np pentamers are packed face-to-face to generate a decamer (Figure 5B). Analytical ultracentrifugation studies also indicated the presence of a pentamer-decamer equilibrium governed by the properties of the pentamer-decamer interface (Dutta et al. 2001). Conversely, SAXS experiments confirmed the presence of pentamers but were in contention with the proposed existence of a decamer in solution (Taneva et al. 2009).

Characterization of the Np-H2A/H2B complex showed that the pentameric ring conformation of Np can accommodate five H2A/H2B dimers, yielding a stoichiometry of 1:5 (pentamer/dimer) (Taneva et al. 2009). Accordingly, an electron microscopy model of this complex reveals two circular discs, wherein the Np pentamer and the H2A/H2B dimers are positioned atop each other (Figure 5C). Superimposition of the available Np pentamer and H2A/H2B crystal structures presents five candidate linker regions where the C-terminal regions of the Np molecules may reside, and interact with the histones (Figure 5C) (Ramos et al. 2010). The role of such higher oligomeric 'storage' complexes *in vivo*, however, requires further clarification.

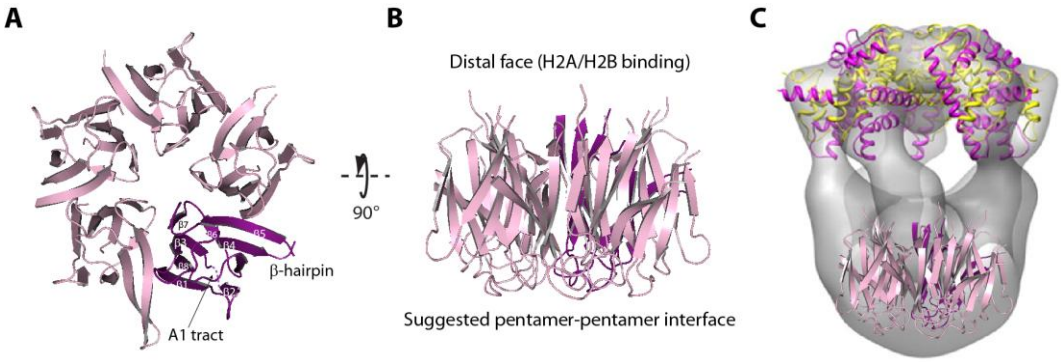

Figure 5 Structure of Np-H2A/H2B complex. A) Cartoon diagram of the Np histone chaperone (PDB Code 1K5J). Np colored in pink, one subunit colored in purple. (B) Cartoon diagram of the Np histone chaperone rotated 90°. (C) Representation of the EM map of the Np-H2A/H2B complex with a superimposition of the crystal structures of both components. Histones colored in yellow and pink. Note: *adapted from (Ramos et al. 2010).*

Understanding of how Np oligomerizes and binds to histones provides a general model for how H2A/H2B chaperones might function. Current evidence suggests that: (a) chaperones may effectively dimerize to form a surface which allows histones to bind as pairs of H2A/H2B dimers (meaning tetramers), (b) histone binding may require stereospecific interactions with the chaperone in addition to charge neutralization, and (c) conformational plasticity may be required to allow efficient histone binding (Akey & Luger 2003).

1.2.3. Nucleosome assembly proteins

Nap1 was the first nucleosome assembly protein identified in HeLa cells as a histone chaperone that facilitates nucleosome assembly by binding to two histones pairs: H2A/H2B and H3/H4 (Ishimi et al. 1987). Orthologues of Nap1 were subsequently identified in other organisms, such as *Saccharomyces cerevisiae* (Ishimi & Kikuchi 1991), *Drosophila* (Ito et al. 1996), *Xenopus* (Steer et al. 2003), *Arabidopsis* (Zhu et al. 2006), and *Plasmodium* (Gill et al. 2009; Gill et al. 2010). Members of the Nap family can be classified into (a) Nap1 proteins (or Nap1-L1 in higher eukaryotes), (b) Nap1-like proteins (Nap1-L2 through Nap1-L6) in metazoans, including the yeast homolog Vacuolar sorting-associated protein 75 (Vps75), and (c) SE Translocation (SET) proteins (Park & Luger 2006a; Hansen et al. 2010).

1.2.3.1. Nap1 proteins

Genome-wide expression analysis in *Saccharomyces cerevisiae* showed that approximately 10% of genes are regulated by Nap1 (Ohkuni et al. 2003). Nap1 interacts with all four core histones (H2A/H2B and H3/H4) *in vitro* (McQuibban et al. 1998); however *in vivo* interaction is exclusive to H2A/H2B dimers (Ito et al. 1996; Mosammaparast et al. 2001). Therefore Nap1 is mainly considered a H2A/H2B-specific chaperone and performs a plethora of functions related to this role. Nap1 is involved in the nuclear import of H2A/H2B dimers (and not H3/H4 dimers) by engaging with the karyopherin Kap114 (Mosammaparast et al. 2002; Mosammaparast & Pemberton 2004). It has also been associated with gene activation, through putative interactions with transcriptional activators and co-activators, such as p300 (Ito et al. 2000; Asahara et al. 2002).

1.2.3.2. Nap1-like proteins

Nap1-L2 has been described to play an important role in neuronal precursor cells, where it might present the histones H3/H4 to HAT enzymes for acetylation (Attia et al. 2007). Nap1-L3 is a brain-specific member of the Nap family, and may contribute to the regulation of brain-specific gene expression by modulating the structural states of chromatin in co-operation with other factors (Shen et al. 2001). Collectively, these studies, and other, studies indicate tissue-specific expression and function of some members of the Nap1-like class, which would be congruent to the presence of a large family of proteins in higher eukaryotes.

Naturally, diversity of function is not solely achieved by the evolution of isoforms. It has been shown that post-translational modifications of Nap family members affect their localization throughout the cell cycle. For example, phosphorylation of Nap1-L4 (also named Nap2) by Casein Kinase II (CKII) retains Nap1-L4/histone complexes in the cytoplasm, whereas its dephosphorylation permits its transport into the nucleus complete with histone cargo (Rodriguez et al. 2000).

1.2.3.3. Vps75

Vps75 was the most recently identified member of the Nap family. Surprisingly, in contrast to other Nap proteins, Vps75 preferentially binds histone H3/H4 in their tetrameric form (Selth & Svejstrup 2007). It has been proposed that Vps75 influences chromatin dynamics by interaction with the histone acetyltransferase (HAT) Regulation of Ty1 transposition protein 109 (Rtt109) (Tang et al. 2008; Berndsen et al. 2008; Kolonko et al. 2010). Formation of the Vps75-Rtt109 complex increased acetyltransferase activity and histone deposition activity of both components and enhanced specificity for histone H3-lysine9 acetylation (H3K9ac) (Berndsen et al. 2008), which revealed a HAT-chaperone complex that combines histone modification with nucleosome assembly.

1.2.3.4. SET/INHAT/TAF-1β

SET (also named INHAT or TAF-1β) is a histone chaperone that binds preferentially to histones H3/H4 and dsDNA (Muto et al. 2007). It has been proposed that binding of DNA by SET is a requisite step in its histone chaperone activity, leading to the formation of a pre-nucleosome complex to which histones are then recruited (Muto et al. 2007). In this scenario, SET could then guide the dsDNA onto specific sites of the core histones and thereby determine the initiation site for DNA-winding (Muto et al. 2007). In addition, SET has been shown to play an important role in transcription (Gamble et al. 2005; Seo et al. 2001). Here, SET strongly inhibits HAT/co-activator-mediated acetylation of core histones and nucleosomes by binding to histones and occluding them from serving as acetylase substrates (Seo et al. 2001). Such a property of SET has been refer to as “histone masking” (Seo et al. 2001).

1.2.3.5. Chaperoning histone variants: Chz1 and DAXX

The preceding chapters of this thesis have focused on histone chaperones which exhibit some specificity in their association with the major classes of histones, known as canonical histones. Subsequent to the discovery of histones, variants were identified exclusively for H2A and H3 which participate in more nuanced roles in the cell (Henikoff & Ahmad 2005). In this section, two examples of a second class of histone chaperones, which recognise H2A and H3 variants, are described: (a) Chz1 which is the chaperone of H2A.Z/H2B and (b) DAXX, which specifically binds H3.3/H4 heterodimers.

As histone variants are thought to be incorporated into pre-existing nucleosomes by displacement of their canonical equivalents (Henikoff et al. 2004), replacement of H2A/H2B dimers by H2A.Z/H2B dimers is an energetically unfavourable process due to the necessity to disrupt histone-histone and histone-DNA contacts in the nucleosome, and it is thus additionally catalysed by the ATP-dependent chromatin remodelling complex SWR1 (Swi2/Snf2-related ATPase) (Mizuguchi et al. 2004; Wu et al. 2005). In this process, the histone chaperone Chz1 delivers an H2A.Z/H2B dimer to the Swr2 subunit of the SWR1 complex, and possibly also captures the ejected H2A/H2B dimer (Wu et al. 2005; Luk et al. 2007). Biochemical characterization of the Chz1-H2A.Z/H2B complex showed that its

stoichiometry is 1:1 (chaperone/histone dimer) (Luk et al. 2007). Chz1 binds to the H2A.Z/H2B dimer through contacts with both histones via a conserved central region (named CHZ motif), although the contribution of the histones to this interface is somewhat asymmetric in favour of H2A.Z (Figure 6A) (Luk et al. 2007; Zhou et al. 2008). This is entirely concordant with the notion that Chz1 specifically recognizes variant H2A-containing H2A/H2B dimers. Intriguingly, the helix αN on Chz1 also prevents the interaction of the histone dimer with DNA (Zhou et al. 2008), implying a mechanism by which inappropriate histone-DNA interactions may be avoided.

Incorporation of H3.3/H4 heterodimers at transcription factor binding sites (TFBS), telomeres, and pericentric chromatin is similarly catalysed by an ATP-dependent remodelling factor, ATRX (Goldberg et al. 2010; L. H. Wong et al. 2010; Drane et al. 2010), which belongs to the Swi/Snf complex component SNF2 (SNF2) family of helicases/ATPases. Current evidence suggests that ATRX recruits DAXX, an H3.3-specific histone chaperone, to telomeres where both factors cooperate to deposit H3.3/H4 dimers into nucleosomes (Lewis et al. 2010). In the DAXX-H3.3/H4 complex, the DAXX histone-binding domain (DAXX HBD) adopts an all α-helical fold (α1-α6) that wraps around the H3.3/H4 dimer with a stoichiometry of 1:1 (monomer/dimer) and making multiple contacts with both histones (Figure 6B) (Elsässer & D'Arcy 2012; C.-P. Liu et al. 2012). Comparison of the H3.3/H4 heterodimer as it is found in the context of DAXX HBD or the nucleosome reveals that the H3.3/H4 heterodimer undergoes several conformational changes, indicating that DAXX prevents DNA-histone contacts and H3.3/H4 tetramer formation (Elsässer et al. 2012; C.-P. Liu et al. 2012).

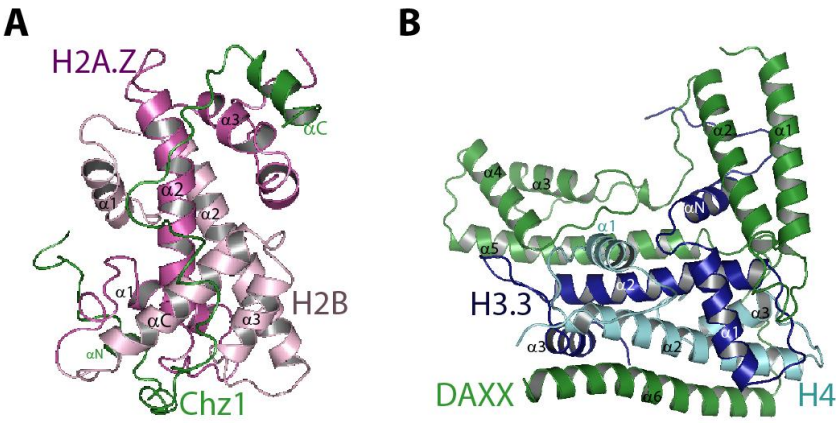

Figure 6 Structure of Chz1-H2A.Z/H2B and DAXX-H3/H4 complexes. (A) Cartoon diagram of the Chz1-H2A.Z/H2B complex (PDB Code 2JSS), with Chz1 colored in green, H2A.Z in magenta, and H2B in pink. (B) Cartoon diagram of the DAXX-H3.3/H4 complex (PDB Code 4H9N), with DAXX colored in green, H3.3 in blue, and H4 in cyan.

1.3. Nap1 – p300 COOPERATION IN TRANSCRIPTION

Nucleosomes are highly stable protein-DNA complexes that physically block access of the transcriptional apparatus to DNA templates, thus their assembly and disassembly are fundamental to the regulation of transcription (Avvakumov et al. 2011). During transcription initiation, histone chaperones cooperate with ATP-dependent chromatin remodelers and histones modifying enzymes, such as HATs, to alter and/or remove key nucleosomes at promoter regions (B. Li et al. 2007; Avvakumov et al. 2011). Subsequently, histone chaperones also play a role in transcription elongation, where they coordinate with other factors to promote the progression of the RNApol II along coding regions (B. Li et al. 2007; Avvakumov et al. 2011). Finally, histone chaperones mediate histone recycling and nucleosome reassembly after transcription, restoring DNA to a heterochromatic state (Avvakumov et al. 2011).

CBP/p300 is known to acetylate lysine residues in all four core histones and contains multiple conserved domains which serve as platforms for protein-protein interactions. This enzyme is organized into three regions: N-terminal, central and C-terminal regions (Yuan & Giordano 2002). At the N-terminus residues a nuclear receptor-interacting domain RID, a cysteine/histidine-rich region composed of a zinc finger motif called TAZ1, and the CREB-binding domain (KIX) (Figure 7). The C-terminal region is composed of a glutamine/proline-

rich (QP) domain that associates with other coactivators and HAT proteins (Figure 7) (Yuan & Giordano 2002).

Until recently CBP/p300 was thought to comprise three domains: a Bromodomain, a PHD finger (which constitute the effector module), and a HAT domain (catalytic domain) (Yuan & Giordano 2002). However, unpublished results from our laboratory revealed that there is also a RING domain inserted at N-terminal of the PHD finger (Delvecchio 2011). In close proximity to this central region, there is a cysteine-histidine-rich (CH3) domain, which includes two zinc-binding motifs designated ZZ (Legge et al. 2004) and TAZ2 (De Guzman et al. 2000) (Figure 7). The CH3 domain is thought to be involved in molecular scaffolding of factors such as p53 (De Guzman et al. 2000) or Nap1 (Shikama et al. 2000), thus it is this region which is of particular interest to this thesis.

The direct interaction between Nap1 and p300 has been studied in the field. Mammalian two-hybrid assays showed that human p300 interacts with Nap2 (also called Nap1-L4) via the CH3 domain (Figure 7) (Shikama et al. 2000). In addition, pull-down assays using cell extracts showed that the KIX domain of the mouse ortholog of CBP/p300 appeared to be capable of binding mNap1, suggesting that this complex is stabilized by multiple surface contacts (Figure 7) (Asahara et al. 2002). However, the direct interaction between Nap1 and p300 *in vitro* remains to be definitively established. Confirmation of such interaction would establish a direct link between acetyltransferases and histone chaperones.

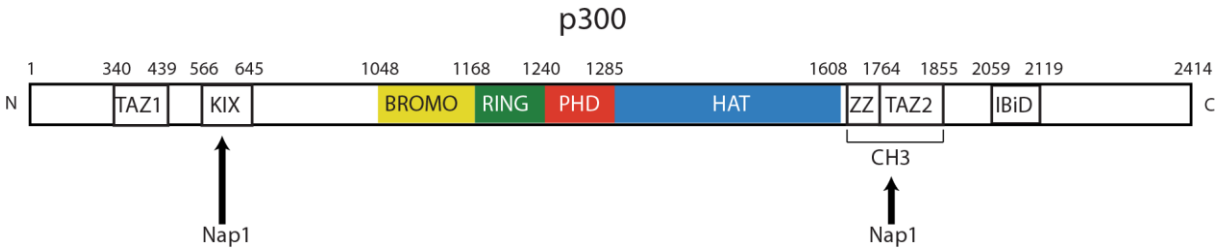

Figure 7 Schematic representation of CBP/p300 domain organization and Nap1 interaction.

In higher eukaryotes nucleosome disassembly during transcription depends on the acetyltransferase activity of CBP/p300, where the acetylation of the four core histones serves to destabilize nucleosomes, (Sharma & Nyborg 2008) and on the capacity of Nap1 to act as a histone acceptor, facilitating their removal from DNA (Ito et al. 2000). Two likely

causes for this effect have been postulated: initial acetylation might reduce the affinity of H2A/H2B for nucleosomes, with subsequent removal of the H2A/H2B dimers from chromatin by Nap1; or the acetylation of H2A/H2B might increase the affinity of H2A/H2B dimer for Nap1 (Ito et al. 2000). It has not been possible to distinguish between these possibilities, and so it remains unclear which one of the two has a major impact in this process. It is also entirely possible that the reality represents a synthesis of both theories, as they are not mutually exclusive.

Accordingly, a model has been proposed to explain the sequential events in acetylation-dependent nucleosome eviction at the promoter regions (Luebben et al. 2010), where disassembly of the histone octamer from the promoter DNA is independent of ATP-dependent remodellers (Sharma & Nyborg 2008). In this model, p300 is recruited to the promoter via interactions with transcription activators, whereupon it acetylates the histone tails of the promoter-associated nucleosomes. Following H3K14 acetylation, Nap1 is recruited by p300 and mediates disassembly of the nucleosome octamer from the promoter DNA, producing a nucleosome-free region that is permissive to the assembly of the general transcription apparatus (Figure 8) (Luebben et al. 2010).

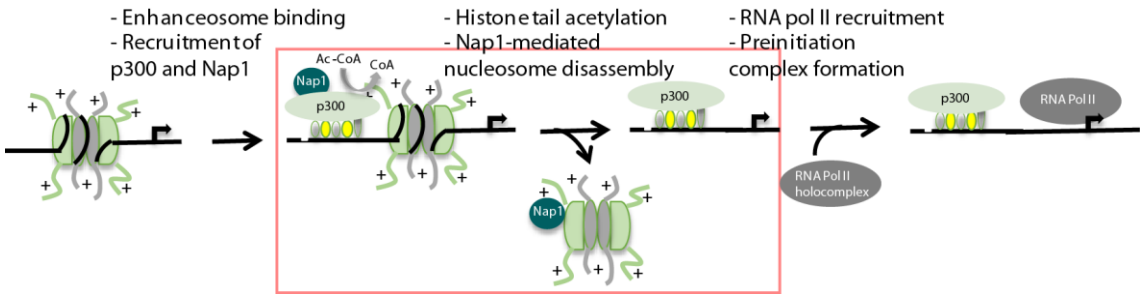

Figure 8 Model showing the sequential events in acetylation-dependent nucleosome disassembly. The process studied in this thesis is highlighted with a red box. *Note: adapted from (Luebben et al. 2010).*

1.4. NUCLEOSOME ASSEMBLY PROTEIN 1

In this work, we focus our attention on the histone chaperone Nap1. In *Saccharomyces cerevisiae* Nap1 (yNap1) is a markedly acidic 48-kDa protein with a calculated pI of 4.23, attributable to a high aspartic and glutamic acid content, which contributes 24% of the total primary sequence. This Nap1 orthologue has been shown to bind to all core histones *in vitro*, as well as the linker histone H1, and to function as a chromatin remodelling factor *in vivo* (Fujii-Nakata et al. 1992; Kepert et al. 2005). In addition, Nap1 plays a role in histone transport, transcription and cell-cycle regulation, and apoptosis (Park & Luger 2006a; Zlatanova et al. 2007).

The relative promiscuity of the interactions between Nap1 and all four core histones (H2A/H2B and H3/H4) has been shown to persist uniquely *in vitro* (McQuibban et al. 1998; McBryant et al. 2003); by contrast, it apparently interacts with H2A/H2B dimers *in vivo* (Ito et al. 1996; Mosammaparast et al. 2001). The precise stoichiometry of Nap1 with histone H2A/H2B or H1 remains controversial, as two binding stoichiometries have been proposed. The first postulates that yNap1 may bind to one histone H2A/H2B heterodimer or one linker histone H1 (1:1) (McBryant et al. 2003; Tóth et al. 2005; Zlatanova et al. 2007; Kepert et al. 2005), and the second that yNap1 may bind two histone H2A/H2B heterodimers or two linker histones H1 (1:2) (Andrews et al. 2008; McQuibban et al. 1998). Analyses of Nap1 complexes from *Xenopus* were in agreement with a stoichiometry of a single Nap1 dimer bound to one histone H2A/H2B heterodimer (Newman et al. 2012) or one linker histone B4 monomer (Shintomi et al. 2005). The general consensus of these papers advances a 1:1 stoichiometry, however recent studies of human Nap1 (hNap1) complexes reported that both stoichiometries can be detected depending on sample preparation (Noda et al. 2011). The question of the Nap1-H2A/H2B stoichiometry therefore remains essentially unresolved and needs further investigation.

The interaction of Nap1 with histones facilitates the assembly and disassembly of the nucleosome *in vitro* (McQuibban et al. 1998; Levchenko & Jackson 2004). The affinity of Nap1 for H3/H4 appears to be lower than that of H3/H4 for DNA, which biases the exchange H3/H4 towards DNA and the formation of the tetrasome (Mazurkiewicz et al. 2006; Andrews et al. 2010). In contrast, the affinity of Nap1 for histones H2A/H2B has been

estimated around 8 nM (Andrews et al. 2008; Hieb et al. 2012), which is higher to that of H2A/H2B for free DNA (Mazurkiewicz et al. 2006; Andrews et al. 2010). That has been suggested to prevent release of H2A/H2B onto free DNA and the subsequent formation of improper histone-DNA complexes (Andrews et al. 2010). However once the tetrasome is formed by initial deposition of H3/H4 complexes, this may then provide a higher affinity binding platform for H2A/H2B dimers such that the hexasome and nucleosome particles form in a stepwise manner wherein the tetrasome ultimately competes against Nap1 for H2A/H2B (Mazurkiewicz et al. 2006; Andrews et al. 2010). Finally, Nap1 facilitates the deposition of the linker histone H1 on its preferred binding structure, the NCP, leading to the formation of the final chromatosome (Mazurkiewicz et al. 2006).

In addition to the core histones and the linker histone H1, Nap1 has been found to bind the variant histone H2A.Z/H2B heterodimer. In this context, Nap1 exhibits overlapping functions with the specialized H2A.Z/H2B histone chaperone Chz1 (Luk et al. 2007). However, it has been proposed that they play distinct roles in the cell: Nap1 might be necessary for maintaining the soluble pool of H2A.Z in the cytoplasm and could serve as a cofactor for H2A.Z/H2B import by the importing Kap114, while Chz1 appears to be strictly nuclear and therefore probably functions exclusively in the nucleus (Straube et al. 2010).

1.4.1. Nap1 structure

To date, four members of the Nap superfamily have been crystallized and their structures resolved: yNap1 (Park & Luger 2006b), which was the first member to be crystallized, *Plasmodium falciparum* Nap1 (PfNapS and PfNapL) (Gill et al. 2009; Gill et al. 2010), *Saccharomyces cerevisiae* Vps75 (Berndsen et al. 2008; Tang et al. 2008), and *Homo sapiens* SET (hSET) (Muto et al. 2007). These proteins constitute a complete structural representation of each Nap family lineage. Overall the structures share a distinctive gross morphology, however some discrepancies are observed.

Biophysical studies suggested that Nap1 exists in solution as a dimer (McBryant & Peersen 2004), which was confirmed by the yNap1 structure that revealed the formation of an obligate dimer with a dome-shaped complex. The N- and C-termini are disordered in these structures and do not appear to contribute to the overall architecture of the dimer.

Moreover, it was described that the central region (the Nap domain or core) is sufficient for histone binding and nucleosome assembly (Fujii-Nakata et al. 1992), suggesting that these N- and C-terminal tails extruding from the core are not important for the function of Nap proteins. However, the C-terminal segment of Nap proteins is highly acidic, which might indicate a supportive role of this region in neutralizing the positive charge of the histones. Furthermore it was also shown that this acidic segment is important for H2A/H2B disassembly from the nucleosome (Park et al. 2005).

As stated previously, the domain architecture and the overall fold of the Nap family members have been shown to be very similar. These histone chaperones adopt an anti-parallel, symmetrical dimeric form that has a "headphone"-like shape with two distinct domains per monomer (Figure 9). Domain I contains a long α-helix (α2) "head" segment of the headphone that interacts in an antiparallel fashion with the "head" of the opposing subunit via exclusively hydrophobic interactions. This dimerization interface is further stabilized by the α2-α3 loop, the helix α3 and the α3-α4 loop which wrap around the base of the helix α2 of the dimerization partner in yNap1 (Figure 9). Domain II contains the α/β globular "earmuff" segments of the headphone. These globular domains are on opposite ends and sides of the domain I dimerization element and contain a four-stranded antiparallel β-sheet (β1-β4), with five helices (α4-α8), arranged below the β-sheet surrounding a hydrophobic cavity (Figure 9). Comparison of the arrangement of domain II in antiparallel β-sheets of Nap family members with other histone chaperons such as Asf1 and Np reveals that such a distribution is not unique Nap1 and all histone chaperones characterized thusly share this feature (Park & Luger 2006b). It is tempting therefore to speculate that this configuration might be relevant to their functions in chromatin assembly or histone binding.

Despite the similarities between the Nap members noted above, there are two main points of divergence that are worth mentioning. First, an accessory domain that is only present in yNap1 and not in other members of the superfamily, such as hSET, Vps75, and PfNapS. Amino acid sequences alignment analysis additionally predicted that xNap1, dNap1, and hNap1 contain this subdomain (Park & Luger 2006b), indicating this feature is well conserved within the Nap1 subfamilly. The yNap1 accessory domain consists of helix α3 and two loops that link domain I and II. In close proximity to this subdomain, yNap1 contains a

nuclear export sequence (NES) located at the N-terminal end of helix α2, whose activity has been confirmed *in vivo* (Mosammaparast et al. 2002; Miyaji-Yamaguchi et al. 2003). In the yNap1 structure, the accessory domain obscures the upper part of the NES and is thought to be rather flexible based on the poor electron density in the yNap1 structure (Park & Luger 2006b) (Figure 9). However, it remains unclear what its function in nuclear shuttling.

The second and final deviation is found in domain II where yNap1, in contrast to other family members, possesses a β-hairpin structure (β5-β6) (Figure 9), which extends from the earmuff and contains a nuclear localization sequence (NLS). This region corresponds to helix α5 in Vps75 and to a disordered region in hSET, neither of which contains an NLS. This divergence may indicate a functional specialization of that region in Nap1 proteins. It has been suggested that the β-hairpin in yNap1 triggers protein oligomerization (Park et al. 2008), while Vps75 and hSET have not been reported to do so.

Analysis of the electrostatic potential of the yNap1 structure indicates that the convex surface of the dimer exhibits a relatively non-distinct charge distribution. In contrast, the concave underside of the dimer is highly acidic (Figure 9). This cavity is considered too small to accommodate an entire histone dimer, however it has been proposed to bind and neutralize the basic N-terminal histone tails, which may enable Nap1 to distinguish H3/H4 from H2A/H2B dimers (Park & Luger 2006b; McBryant et al. 2003).

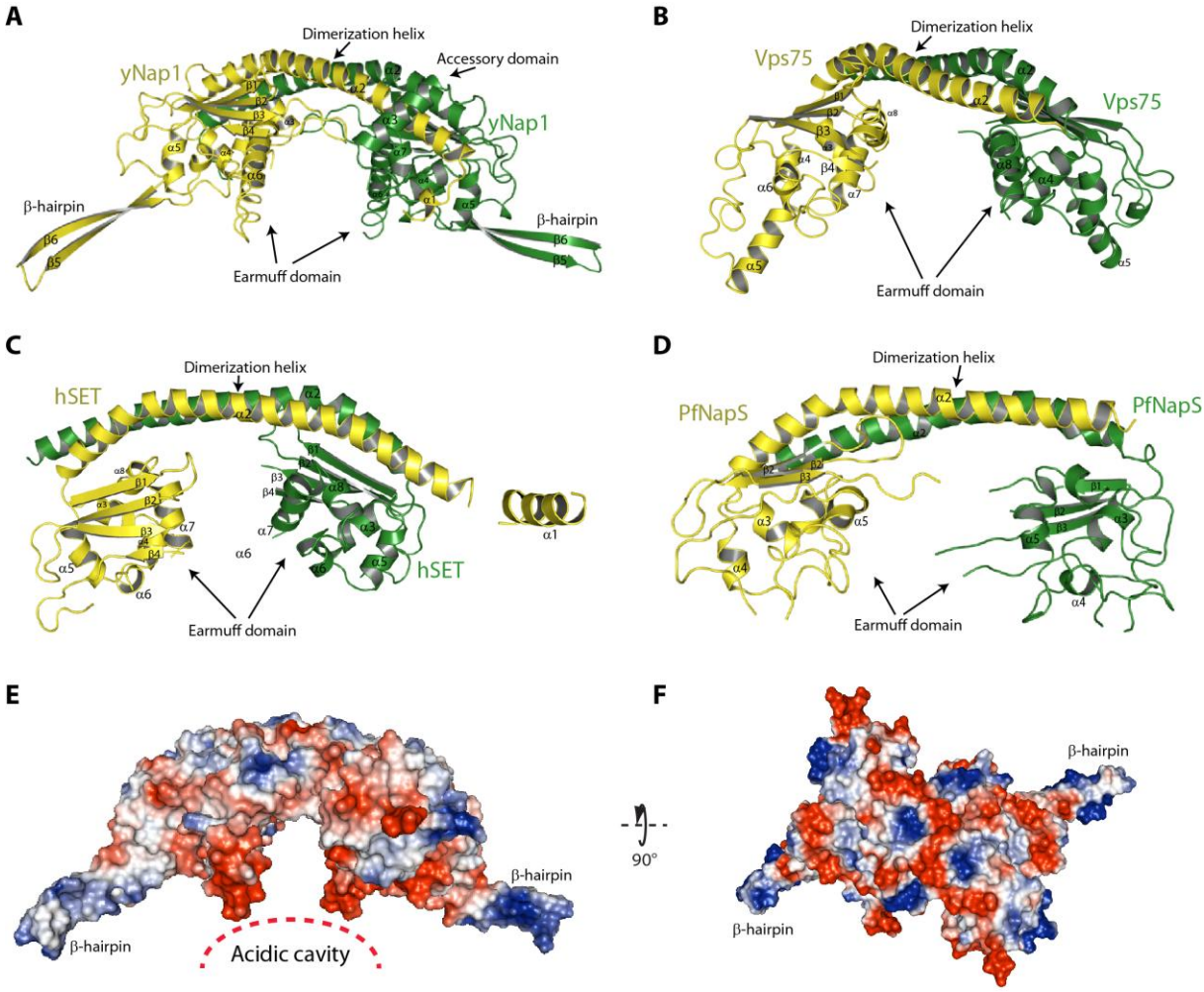

Figure 9 Structure of Nap family members: yNap1 (A), Vps75 (B), hSET (C), and PfNapS (D). Each monomer is colored in either yellow or green. Dimerization helix, earmuff domain accessory domain and β-hairpin are indicated. (PDB Codes: 2Z2R, 3DM7, 2E5O, and 3KYP, respectively).

1.4.2. Nap1 oligomerization

Considerable efforts have been made to characterize the nature and extent of higher order Nap1-histone complexes in solution. As described previously, Nap1 is able to bind H2A/H2B dimers, H3/H4 tetramers (*in vitro*), and linker histone H1 with a distinct stoichiometry. In this section, the oligomeric state of Nap1 alone and in complex with histones H2A/H2B will be described in detail.

Solution studies on yNap1 strongly support the formation of an elongated and stable dimer as its elemental oligomerization state, which further may self-associate to generate higher species (McBryant et al. 2003; McBryant & Peersen 2004). At high ionic strength (500 mM NaCl), Nap1 is mostly a dimer, however at lower ionic strength (150 mM NaCl), which would

be considered physiological, Nap1 tends to oligomerize into higher order species (McBryant & Peersen 2004; Tóth et al. 2005; Park et al. 2008). Analytical ultracentrifugation experiments at physiological ionic strength support a dimer-octamer-hexadecamer equilibrium, which is also detected when H2A/H2B dimers are bound to Nap1 (Figure 10A) (Tóth et al. 2005).

Additionally, structural studies of the yNap1 central region (residues 75 to 365) revealed that the β-hairpin structure (β5-β6) (Figure 9) extrudes from the core and interacts with the β-hairpin of a neighbouring yNap1 dimer through an extensive hydrogen-bonding network over its entire length. It is thought that this crystal-packing interface also explains dimer oligomerization *in vitro* as mutational analysis indicates that disruption of this interface indeed abolishes oligomerization, even in conditions of low ionic strength (Park et al. 2008).

This oligomerization phenomenon is not unique to yNap1 and it has also been observed in *Xenopus* and human Nap1 (xNap1 and hNap1). Cryo-electron microscopy studies of xNap1-H2A/H2B and xNap1-H3/H4 revealed a large ring-like structure that could form the basis for a scaffold that allows the controlled assembly and exchange of histones in chromatin (Figure 10B) (Newman et al. 2012). Concordantly, biophysical characterization of hNap1 alone showed that hNap1 dimers oligomerize up to a tetradecamer and its assembly might occur through a circular arrangement (Noda et al. 2011). In both proteins, it has been posited that the oligomerization of Nap1 is due to the β-hairpin similarly to that of the yeast homolog.

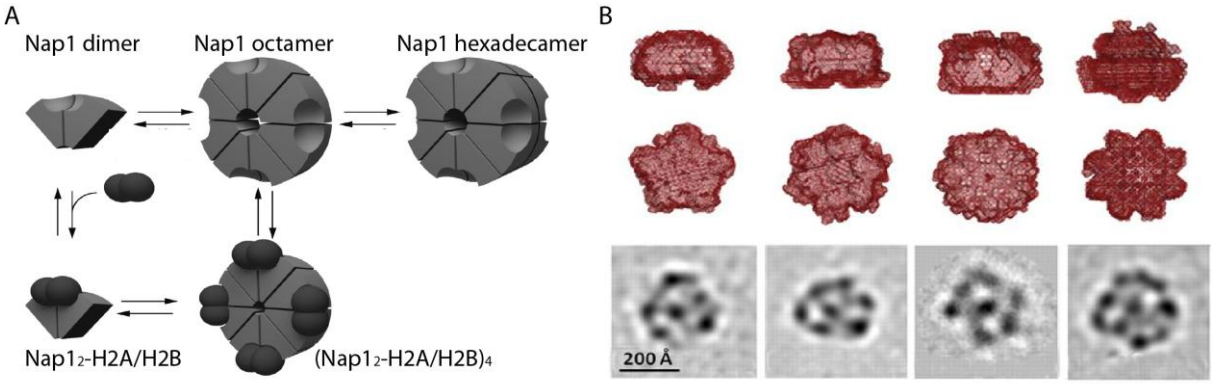

Figure 10 Association states of Nap1. (A) Model of association states of Nap1 (triangles) alone and in complex with H2A/H2B heterodimers (spheres) in solution. *Adapted from* **(Tóth et al. 2005)**. (B) Two orientations of SAXS (upper panels) and cryo-EM images (lower panels) of xNap1-H2A/H2B complexes. *Results from* **(Newman et al. 2012)**.

However, the physiologically relevant association states adopted by Nap1 remain to be elucidated, as well as their implications in nucleosome assembly. Therefore, detailed structural information pertaining to a Nap1-H2A/H2B complex is expected to be extremely valuable in advancing the field.

1.4.3. Nap1 localization and histone shuttling

The subcellular localization of Nap1 throughout the cell cycle has been extensively studied in yeast and higher eukaryotes. These studies indicate that *Drosophila* Nap1 (dNap1), yNap1, and hNap2 are typically cytoplasmic, normally maintaining a minimal nuclear fraction, but that significant translocation into the nucleus occurs during S phase (Ito et al. 1996; Miyaji-Yamaguchi et al. 2003; Tóth et al. 2005; Rodriguez et al. 2000). Phosphorylation of Nap1 proteins by Casein Kinase II (CKII) has been suggested to regulate the exchange of Nap1 between the nucleus and cytoplasm (M. Li et al. 1999; Rodriguez et al. 2000; Tóth et al. 2005; Calvert et al. 2008). In this model, phosphorylation of Nap1 anchors the protein in the cytoplasm, in complex with histones during the G0 and G1 (Figure 11), whereas its dephosphorylation triggers its transport into the nucleus during S phase (Figure 11), alongside its histone cargo. The cycle resolves at the end of S phase when Nap1 is again phosphorylated and exported to the cytoplasm (Tóth et al. 2005; Rodriguez et al. 2000).

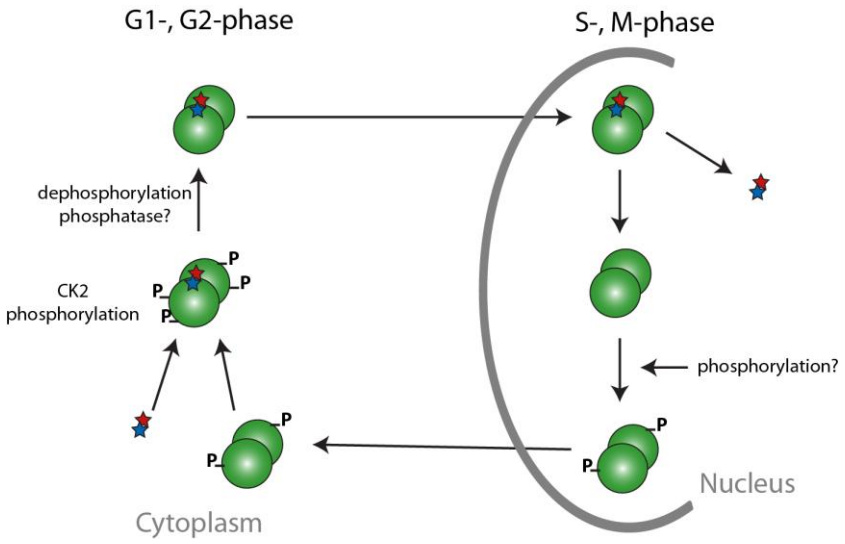

Figure 11 Cell cycle distribution of Nap1-H2A/H2B complex. *Note: adapted from (Rodriguez et al. 2000).*

According to the previous model, the Nap1 phosphorylation and dephosphorylation cycle may function as a switch to determine whether Nap1 acts as a histone donor or acceptor in chromatin assembly during S phase (Calvert et al. 2008). However, it remains unclear.

Nuclear import of yNap1-H2A/H2B complexes is thought to be facilitated by the importin Kap114 (Mosammaparast et al. 2001). This hypothesis is supported by the fact that Nap1, H2A, H2B and Kap114 form a complex *in vivo* and *in vitro* (Mosammaparast et al. 2002). The biological process though which these proteins interact and participate in H2A/H2B nuclear import is thought to occur as follows: Nap1 binds to H2A/H2B dimers as they are synthesized in the cytoplasm and this complex is translocated into the nucleus upon interaction with Kap114, where they are released to fulfil their various functions (Mosammaparast et al. 2001; Mosammaparast et al. 2002). Unloading of Nap1-H2A/H2B complexes from Kap114 in the nucleus has been attributed to RanGTP. In absence of RanGTP, Kap114 inhibits Nap1-mediated incorporation of H2A/H2B into chromatin by remaining bound to the Nap1-histone complex (Mosammaparast et al. 2005).

Experimental evidence indicating a correlation between phosphorylation of Nap1 and nuclear import of the Kap114-Nap1-H2A/H2B complex however is thus far not apparent, despite the stark effect Nap1 phosphorylation has upon its localisation (Calvert et al. 2008). Biochemical studies have demonstrated that the phosphorylation state of Nap1 does not regulate its interaction with Kap114 (Calvert et al. 2008). Ultimately, further investigation is needed to elucidate the exact relationship between post-translational modifications, histone shuttling and chromatin assembly. Furthermore the biological importance of Nap1 oligomerization within all these processes also remains to be established.

1.5. SCIENTIFIC AIMS

Even though the structure of the nucleosome is known in detail (Luger, Mäder, et al. 1997a), its mechanism of assembly is poorly understood. Structural studies on the chaperone-histone complex, Asf1-H3/H4, yielded important insights into the first step of this process (English et al. 2006). However, it remains unclear how histone chaperones mediate H2A/H2B deposition to complete nucleosome assembly. Similarly to the Asf1-H3/H4 complex, understanding of the architecture of the Nap1-H2A/H2B ternary complex will bring forth our knowledge of the nucleosome assembly and disassembly mechanism. So that, the main focus of this work was to obtain structural information regarding the yNap1-H2A/H2B complex. To this end, the ternary complex was studied by X-ray crystallography and negative stain EM. As of the writing of this thesis, there are no available histone chaperone – H2A/H2B complex structures, this work is therefore of seminal importance to the field as it provides structural and molecular basis for their assembly.

Nap1 alone and in complex with H2A/H2B heterodimers assembles into large complexes (Fujii-Nakata et al. 1992; McBryant & Peersen 2004; Tóth et al. 2005; Park et al. 2008; Noda et al. 2011; Newman et al. 2012). Yet the roles of these higher-order histone-chaperone complexes are unclear. In addition, the stoichiometry of Nap1-H2A/H2B complex remains controversial (McBryant et al. 2003; Tóth et al. 2005; Zlatanova et al. 2007; Kepert et al. 2005; Newman et al. 2012; Andrews et al. 2008; McQuibban et al. 1998; Noda et al. 2011), as well as the elemental repeating unit of the oligomers. Knowledge of the basic stoichiometry and the oligomerization of Nap1-H2A/H2B complex is vital for understanding the roles of these higher-order histone-chaperone complexes in the cell. Here, biophysical and structural characterization (by non-denaturing MS, X-ray crystallography and negative stain EM) of this complex was performed in order to resolve the controversy regarding the specific stoichiometry interactions of the Nap1 and H2A/H2B. This study also attempts to comprehend Nap1-H2A/H2B oligomerization and bring some light to its role.

In addition, understanding H1 deposition by Nap1 is required to elucidate the mechanism of chromatin compaction into higher orders of complexity. Thus characterization of the Nap1-H1 complex is another of the aims of this study, as Nap1 has been shown to participate in H1 deposition.

Finally, as Nap1 has been reported to interact with non-histone partners, such as the histone acetyltransferase p300 (Shikama et al. 2000; Asahara et al. 2002) and play a role in regulation of transcription (Sharma & Nyborg 2008; Luebben et al. 2010). We aim to biochemically characterize the direct interaction between Nap1 and p300. In addition, we wondered if the CH3 domain of p300, which was considered to mediate the interaction with Nap1 (Shikama et al. 2000; Asahara et al. 2002), could participate in the auto-regulation of the p300 HAT activity and performed biochemical assays in order to address this question.

2. MATERIALS AND METHODS

RÉSUMÉ EN FRANÇAIS

Dans ce chapitre, sont décrits les techniques suivantes: clonage, expression et purification des protéines relatives à ce projet de thèse. En particulier, l'expression des protéines hétérologues a été réalisée dans *E. coli* BL21 (DE3) ou dans des cellules d'insectes Hi5. Toutes les protéines ont été purifiées de façon homogène ainsi leur pureté a été vérifiée par électrophorèse sur gel de polyacrylamide en condition dénaturante et par spectrométrie de masses (MS).

Les méthodes biochimiques, biophysiques et structurales qui ont été utilisées pour la caractérisation des ces macromolécules, sont décrites dans ce chapitre. Il s'agit notamment de l'analyse des protéines d'intérêt après leur digestion partielle par des protéases et l'identification des peptides obtenus par séquençage du N-terminal. Il s'agit aussi des tests d'interaction entre l'histone chaperonne Nap1 et les dimers d'histones H2A/H2B, l'histone d'union H1, et l'enzyme p300/CBP (pull-downs, non-denaturing MS). Enfin, la caractérisation structurale du complexe formé par Nap1 et les histones H2A/H2B (cristallographie par diffraction des rayons X et microscopie électronique) a été réalisée.

2.1. MOLECULAR BIOLOGY

A list of constructs characterized during this study is presented in Table 1. yNap1 and mouse Nap1 (mNap1) constructs were cloned into the pACYC-Duet1 and pET-21a vectors (Novagen), respectively. These vectors both contain an N-terminal 6x His-tag (polyhistidine, HHHHHH) followed by a TEV recognition site (ENLYFQG) upstream of the multiple cloning site 1 (MCS1), which allows cleavage of the His-tag. hNap1 constructs, cloned as a GST fusion proteins into the pGEX-4T1 vector (Amersham Pharmacia Biotech), were a gift from Dr. Saadi Khochbin (Institute Albert Bonniot, Grenoble). GST-yNap1 construct was cloned into the pETM33 vector (EMBL). GST-yNap1 were obtained using the QuikChange® Lightning Site-directed mutagenesis kit (Agilent Technologies).

Histone H1 constructs were also a gift from the Dimitrov lab (Institute Albert Bonniot, Grenoble). These constructs were cloned into the pET-3d vector (Novagen) and as such are untagged. Histones H2A and H2B construct were cloned into the pET-Duet1 (Novagen) and pET-21a vectors.

p300short, p300'core' and its mutants and variants (detailed later in this section), as well as p300_HAT constructs, were already available in the Panne Group (EMBL, Grenoble). The first two constructs (and subsequent mutants) were cloned into the pFASTBAC1 (Invitrogen) and contained an N-terminal FLAG tag (DYKDDDK) and GST tag, respectively, each followed by a TEV recognition site. p300_HAT was cloned into the pET-21a and contains a TEV cleavable N-terminal 6x His-tag. p300_BRP and p300_BPΔR were cloned into pETM33, which contains a TEV cleavable N-terminal GST sequence. p300_CH3 was cloned into pGEX-4T1, which introduces an N-terminal GST-tag.

p300'core'_ZZ, p300'core'_ZZ_TAZ2 constructs and all their mutants and variants were cloned into a pFASTBAC1 vector. This vector contains a GST tag and a TEV recognition site upstream of the MCS. These constructs were generated by introducing the nucleotides corresponding to the ZZ and the ZZ_TAZ2 domains into the already available p300'core' constructs, following the In-Fusion® HD Cloning kit (Clontech) procedure.

The His-SIRT2 construct into pFASTBAC1 vector was a gift from Dr. Carey Laboratory (University of California, LA).

Table 1 Summary of all constructs used in this study.

Construct	Organism	Residues	Vector	Tag	Mutations and variants
yNap1	*Saccharomyces cerevisiae*	1-417	pACYC-Duet1	His	*wt*, core (residues 74-365), coreΔ284-308, Δ1-73, Δ366-417
yNap1	*Saccharomyces cerevisiae*	1-417	pETM33	GST	*wt, D201R, D205R, E310R, E332R, D333R, E336R,*
mNap1	*Mus musculus*	1 – 391	pET-21a	His	*wt*, Δ36, Δ50, Δ63, core (residues 63-347)
hNap1	*Homo sapiens*	-	pGEX-4T1	GST	L1 (*wt*, like-1, residues 1-391) L2 (*wt*, like-2, residues 1-460) L4 (*wt*, like-4, residues 1-375)
p300_short	*Homo sapiens*	324 – 2094	pFASTBAC1	Flag	
p300_CH3	*Homo sapiens*	1609 – 1855	pGEX-4T1	GST	
p300_HAT	*Homo sapiens*	1286 – 1608	pET-21a	His	
p300_BRP	*Homo sapiens*	1048 – 1285	pETM33	GST	*wt*, BPΔR
p300'core'	*Homo sapiens*	1048 – 1666	pFASTBAC1	GST	*wt*, ΔloopY1467F (Δ1520-1580)
p300'core'_ZZ	*Homo sapiens*	1048 – 1764	pFASTBAC1	GST	*wt*, ΔloopY1467F (Δ1520-1580)
p300'core'_ZZ_TAZ2	*Homo sapiens*	1048 – 1855	pFASTBAC1	GST	*wt*, ΔloopY1467F (Δ1520-1580)
H1Δ100	*Mus musculus*	1 – 127	pET3-d	No tag	*wt*, GH1 (residues 40-112)
dH2A_FL	*Drosophila melanogaster*	1-130	pET-Duet1	No tag	*wt*
xH2AΔ14	*Xenopus leavis*	14 – 130	pET-3d	No tag	*wt*
xH2A14-109	*Xenopus leavis*	14 – 109	pET-21a	No tag	*wt*
dH2B_FL	*Drosophila melanogaster*	1-126	pET-Duet1	No tag	*wt*
xH2BΔ28	*Xenopus leavis*	28 – 126	pET-3d	No tag	*wt*
xH2BΔ36	*Xenopus leavis*	36 – 126	pET-21a	No tag	*wt*
SIRT2	*Homo sapiens*	Full-length	pFASTBAC1	His	*wt*

2.2. PROTEIN EXPRESSION

2.2.1. Bacterial expression

All constructs expressed in bacteria were transformed into *E. coli* BL21 (DE3).

The histone H2A and H2B constructs were expressed using LB media. Cells were grown under agitation at 37ºC until they reached an OD_{600} = 0.6, then protein expression was induced by addition of IPTG (400 mM final concentration) at 37ºC for 3 to 5 hours. Cell cultures were centrifuged for 20 minutes at 6000 rpm (JA-14 rotor from Beckman) and cell pellets were resuspended in lysis buffer (see composition in Table 2).

Histone H1 constructs as well as His- and GST- tagged proteins, excluding p300 variants, were expressed using auto-inducing media ZYP-5052 (Studier 2005). Cells were grown under agitation at 37ºC until they reached an OD_{600} of 0.6 – 0.8, the temperature was then decreased to 20ºC and expression was continued overnight. Cell cultures were centrifuged for 15 minutes at 7000 rpm (JLA-8.1 rotor from Beckman) and cell pellets were resuspended in lysis buffer (Table 2).

p300 constructs were expressed in LB medium enriched with 100 μM $ZnCl_2$. Cells were grown under agitation at 37ºC until they reached an OD_{600} of 0.6 – 0.8, then temperature was decreased to 18ºC overnight. For p300 constructs, protein expression was induced with IPTG (1 mM final concentration) at 18ºC overnight. Cell cultures were centrifuged for 15 minutes at 7000 rpm (JLA-8.1 rotor from Beckman) and cell pellets were resuspended in lysis buffer (Table 2).

Seleno-methionine substituted His-tagged yNap1 constructs were expressed using minimal media M9 enriched with trace elements and vitamins. Cells were grown at 37ºC until they reached an OD_{600} of 0.6 – 0.8, then amino acids were added as solids (including seleno-methionine) and protein expression was induced by IPTG (1 mM). The temperature was decreased to 20ºC overnight and moderate agitation was maintained. Cell cultures were centrifuged for 15 minutes at 7000 rpm (JLA-8.1 rotor from Beckman) and 4ºC. Cell pellets were resuspended in lysis buffer (Table 2).

2.2.2. Baculovirus cultivation

Recombinant baculoviruses were propagated in Sf21 cells with Sf900-II SFM medium (Invitrogen). For protein production, Hi5 cells in Express Five SFM medium (Invitrogen) were infected with recombinant baculoviruses at a multiplicity of infection of 2.0, maintained in shake flasks at 27ºC and harvested by centrifugation after 72 hours of infection. Cell pellets were resuspended and frozen in lysis buffer (Table 2).

Table 2 List of lysis buffers used in this study. All buffers were freshly supplemented with one tablet of Complete Protease Inhibitors EDTA-Free from Roche Applied Science, and for proteins expressed in insect cells 10 U of Benzonase (New England Biolabs).

Protein	Lysis buffer
Histone H2A **Histone H2B**	50 mM Tris/HCl pH 7.5, 100 mM NaCl, 1 mM Na-EDTA, 5 mM β-mercaptoethanol
Histone H1	50 mM HEPES pH 8.0, 150 mM NaCl, 1 mM DTT
Nap1	50mM Tris/HCl pH 8.0, 150 mM NaCl, 1 mM DTT (a small spoon of methionine was added for SeMet substituted protein)
p300_BRP **p300_BPΔR** **p300'core'** **p300'core'_ZZ**	50mM Tris/HCl pH 8.0, 300 mM NaCl, 5 μM $ZnCl_2$, 1 mM DTT
p300_CH3 **p300'core'_ZZ_TAZ2**	50mM Tris/HCl pH 7.0, 500 mM NaCl, 5 μM $ZnCl_2$, 1 mM DTT

2.3. PROTEIN PURIFICAITON

2.3.1. Purification of recombinant histones

2.3.1.1. Purification of Histones H2A and H2B

Histone H2A and H2B were obtained from inclusion bodies produced in *E. coli* BL21 (DE3).

Bacteria lysis was performed by sonication on ice 6 to 12 times for 30 seconds at amplitude of 50 mAmp with 45 seconds off rest between. The lysate was cleared by centrifugation at 19000 rpm (JA-20 rotor from Beckman) for 20 minutes and the resultant supernatant discarded. Pellet washes were then conducted; twice with triton wash buffer (lysis buffer

containing 1% v/v Triton X-100) and twice with lysis buffer; the washes were carried out by centrifugation (20 minutes at 19000 rpm, JA-20 rotor from Beckman) rinsing of the pellets, which contain the inclusion bodies, with buffers as described. Once the last centrifugation was completed, the pellets were resuspended in unfolding buffer (20 mM Tris/HCl pH 7.5, 7 M Guanidinium-HCl, 10 mM DTT) and incubated for 1 hour at room temperature, with gentle stirring. The dissolved inclusion bodies were then centrifuged as above and the supernatant was retained. The solution was then dialyzed overnight at room temperature against 2 l of SAU-200 buffer (20 mM Sodium acetate pH 5.2, 200 mM NaCl, 7 M Urea, 1 mM Na-EDTA, 5 mM β-mercaptoethanol).

After dialysis, the solution was centrifuged for 10 minutes at 10000 rpm (A-4-44 rotor from Eppendorf) and 4ºC and the supernatant was loaded on a 5-ml HiTrap SP HP column (GE Healthcare) pre-equilibrated with SAU-200 buffer. The column was washed with SAU-200 buffer and eluted using a gradient from SAU-200 to SAU-600 buffer (SAU-200 containing 600 mM NaCl). The eluted sample was then dialyzed against water overnight at 4ºC stirring with a magnet. The final products, isolated H2A and H2B, were aliquoted as single unfolded histones, flash frozen in liquid N_2, lyophilized and stored at -80ºC until required for H2A/H2B dimer reconstitution. SDS-PAGE gels were run to verify purity of the preparation.

2.3.1.2. Purification of histone H1

Bacteria lysis was performed by sonication on ice 6 to 12 times for 30 seconds at amplitude of 50 mAmp with 45 seconds off rest between. The lysate was cleared by centrifugation at 14000 rpm (JA-14 rotor from Beckman) for 45 minutes; the supernatant was retained for further purification whilst the pellet was discarded. The supernatant was loaded on a 5-ml HiTrap SP HP column pre-equilibrated with buffer A (50 mM HEPES pH 8.0, 150 mM NaCl, 1 mM DTT). The column was washed with buffer A and the protein eluted using a gradient from buffer A to buffer B (buffer A containing 1.5 M NaCl). SDS-PAGE gels were run to verify purity of the preparation.

2.3.2. Purification of His-tagged proteins

Bacterial pellets were thawed and then lysed using a Microfluidizer (Microfluidics). Clarification of the lysate was carried out by centrifugation at 14000 rpm (JA-14 rotor from Beckman) for 45 minutes and the supernatant was applied to a 5-ml HisTrap FF crude column (GE Healthcare) pre-charged with Ni^{2+} and pre-equilibrated in binding buffer (20mM Tris/HCl pH 8.0, 150 mM NaCl, 20 mM imidazole). The column was washed with binding buffer and the protein was eluted in a single step using elution buffer (binding buffer containing 500 mM imidazole). The eluate was concentrated to a final volume between 10 ml and 15 ml; the His-tag was then cleaved with TEV protease (1:100 w/w) in dialysis overnight at 4ºC using 2 l of dialysis buffer (binding buffer containing 10 mM imidazole, 1 mM DTT) while stirring. The His-tag and the His-TEV were then removed from the preparation with a second His-affinity purification step. Cleaved protein was collected in the flowthrough.

The purification of SeMet substituted proteins was carried out in essentially the same was as described above, except, all SeMet buffers were supplemented with a spoonful of methionine and 1 mM DTT.

2.3.3. Purification of GST-tagged proteins

Cells were lysed using a Microfluidizer when proteins were expressed in bacteria and by sonication when proteins were expressed in insect cells. The lysate was cleared by centrifugation at 19000 rpm (JA-20 rotor from Beckman) for 45 minutes and the supernatant was loaded on to a Glutathione Sepharose 4 Fast Flow resin (GE Healthcare), pre-equilibrated with binding buffer (Table 3). The resin was washed with binding buffer and incubated on the beads with TEV protease (1:100 w/w) overnight at 4ºC. The protein sample was then washed off the column using binding buffer and loaded onto an IMAC Sepharose 6 Fast Flow resin (GE Healthcare) pre-charged with Ni^{2+} ion and pre-equilibrated in binding buffer. The His-TEV protease was thus removed from the protein sample during the His affinity purification step.

When cleavage of the tag was not necessary, the GST-tagged protein was eluted using elution buffer (Table 3). The final protein was concentrated to 10 mg/ml and SDS-PAGE gels were run to verify purity of the sample. Aliquots were flash frozen in liquid N_2 and stored at -80ºC.

Table 3 Summary of buffers used in GST-tagged proteins purification.

Protein	Binding buffer	Elution buffer
Nap1	20 mM Tris/HCl pH 8.0, 150 mM NaCl, 1 mM DTT	Binding buffer with 10 mM reduced glutathione
p300_BRP **p300_BPΔR**	20 mM Tris/HCl pH 8.0, 300 mM NaCl, 5 μM $ZnCl_2$, 1 mM DTT	-
p300_CH3	20 mM Tris/HCl pH 7.0, 500 mM NaCl, 5 μM $ZnCl_2$, 1 mM DTT	Binding buffer with 10 mM reduced glutathione

2.3.4. Size-exclusion chromatography

After cleavage of the tag, proteins were further purified by size-exclusion chromatography using a HiLoad 16/60 Superdex 75 (or 200) prep grade column (GE Healthcare) pre-equilibrated in SEC buffer (Table 4). The final protein was concentrated to minimum 10 mg/ml and SDS-PAGE gels were run to verify purity of the sample. Aliquots were flash frozen in liquid N_2 and stored at -80ºC.

Table 4 Summary of buffers used in SEC.

Protein	SEC buffer
Histone H1 **Nap1**	20 mM HEPES pH 8.0, 150 mM NaCl, 1 mM DTT
p300_BRP **p300_BPΔR** **p300'core'** **p300'core'_ZZ**	20 mM HEPES pH 7.5, 300 mM NaCl, 5 μM $ZnCl_2$, 0.5 mM TCEP
p300_CH3 **p300'core'_ZZ_TAZ2**	20 mM HEPES pH 7.0, 500 mM NaCl, 5 μM $ZnCl_2$, 0.5 mM TCEP

2.4. COMPLEX RECONSTITUTION

2.4.1. Reconstitution of H2A/H2B dimers

Histone heterodimer refolding was performed as necessary. Equimolar amounts of each histone H2A and H2B were dissolved in unfolding buffer and incubated at room temperature for 30 minutes before mixing them and incubating the mixture for a further hour. After incubation, the histone mixture was dialyzed, whilst stirring, for 2 hours in refolding buffer (10 mM Tris/HCl pH7.5, 2 M NaCl, 1 mM Na-EDTA, 5 mM β-mercaptoethanol) and overnight in refolding buffer containing 500 mM NaCl at 4ºC. The sample was then loaded on a HiLoad 16/60 Superdex 75 prep grade pre-equilibrated with refolding buffer containing 500 mM NaCl. After analysis of the fractions by SDS-PAGE gel, the protein peak was pooled and concentrated to 10 mg/ml. Aliquots of the histone dimers were then stored in a 50% glycerol at -20ºC until required.

2.4.2. Reconstitution of Nap1-Histone complexes

Reconstituted H2A/H2B dimers were added at a twofold molar excess to Nap1, thus giving a 2 histone dimer: 1 Nap1 dimer ratio. The mixture was incubated for 30 minutes on ice. After incubation, the sample was centrifuged for 15 minutes at 10000 rpm (F45-24-11 rotor from Eppendorf) and run on a pre-equilibrated Superose 6 10/300 GL column (GE Healthcare) in SEC Buffer (20 mM HEPES pH 8.0, 0 to 250 mM NaCl, 1 mM DTT). Following analysis of the fractions by SDS-PAGE gel, the protein peak was pooled and concentrated to 10 mg/ml. Aliquots of the final complex were flash frozen in liquid N_2 and kept at -20ºC.

After purification of mNap1 and histone H1 as individual components as described in chapter 2.3, the protein complex was reconstituted *in vitro* by mixture of mNap1 (mNap1FL, mNap1Δ36, mNap1Δ50 and mNap1Δ63) and H1Δ100 in a 1:2 ratio and incubated on ice for 30 minutes. After incubation, the samples were centrifuged for 15 minutes at 10000 rpm (F45-24-11 rotor from Eppendorf) and injected on a Superdex 200 10/300 GL column pre-equilibrated in SEC buffer (20 mM HEPES pH 8.0, 150 mM NaCl, 1 mM DTT).

2.5. ANALYSIS BY NATIVE PAGE GELS

6% polyacrylamide native-PAGE gels were used to visualize Nap1-H2A/H2B and mNap1-H1 oligomers. Samples were prepared in 20 mM HEPES pH 8.0, 1 mM DTT, 10% glycerol and several salt concentrations and were incubated from 30 minutes to 1 hour on ice and directly loaded onto a pre-run native-PAGE gel. Visualization of the proteins was performed using Coomassie® Brilliant Blue G 250 pure (SERVA Electrophoresis GmbH).

2.6. LIMITED PROTEOLYSIS

Proti-Ace™ and Proti-Ace™ 2 kits (Hampton Research) were used for time-course limited proteolysis experiments. These two kits contain a total of twelve proteases (α-chymotrypsin, trypsin, elastase, papain, subtilisin, endoproteinase Glu-C, proteinase K, clostripain, pepsin, thermolysin, bromelain and activase). Nap1 alone and in complex with the histones were diluted to 1 mg/ml in buffer containing 20 mM HEPES pH 8.0 and 1 mM DTT and digestion was initiated by the addition of diluted protease to the protein mix (molar ratio 1:500 of protease:proteins). Samples were taken at several time points. At each time point, proteolysis was inactivated by addition of SDS-loading buffer and boiling of the sample for 10 minutes. Samples were loaded and run on a SDS-PAGE gel and protein fragments visualized by Coomassie® Brilliant Blue G 250 pure. N-terminal sequencing and mass spectrometry were used for identification of protein fragments.

2.7. PULL-DOWNS

2.7.1. GST Pull-downs

GST pull-downs were carried out with recombinant GST-tagged human Nap1 (GST-hNap1) and p300_CH3 (GST-p300_CH3) constructs, which were expressed and purified as described.

GST-hNap1 and its putative binding partners were mixed in binding buffer (100 mM Tris/HCl pH 8.0, 150 mM NaCl and 1 mM DTT) at a 1:2 molar ratio. Glutathione Sepharose 4 Fast Flow resin was pre-equilibrated in binding buffer and resuspended in a 50% v/v suspension. The

resin was then added to the protein mix (25 μl final resin for 12 μM final GST-hNap1). The samples were incubated with the resin for 3 hours on a rotating wheel at 4ºC. After incubation, the resin was pelleted and the supernatant containing unbound protein was removed. The resin was washed three times with binding buffer, to further exclude unbound material. Elution was performed by addition of 3xSDS loading buffer to the resin and the samples were boiled for 10 minutes. Protein samples were run a 15% SDS-PAGE gel and visualized by Coomassie® Brilliant Blue G 250 pure.

GST-yNap1FL (wt and mutants) and untagged H2A/H2B dimers were mixed in binding buffer (20 mM Tris/HCl pH 8.0, 250 mM NaCl and 1 mM DTT) at an equimolar ratio (1 Nap1 dimer: 1 histone dimer). Glutathione Sepharose 4 Fast Flow resin was pre-equilibrated in binding buffer and resuspended in a 50% v/v suspension. The resin was then added to the protein mix (30 μl final resin for 10 μM final GST-yNap1FL). The samples were incubated with the resin for 2 hours on a rotating wheel at 4ºC. After incubation, the resin was pelleted and the FT was removed. Then the resin was washed three times with wash buffer (binding buffer containing 0.1% Tween-20). Finally, the samples were eluted and analysed as described above.

For GST-p300_CH3 pull-downs, Glutathione Sepharose 4 Fast Flow resin was pre-equilibrated in binding buffer (20 mM Tris/HCl pH 7.0, 500 mM NaCl, 5 μM $ZnCl_2$ and 0.5 mM TCEP) and resuspended in a 50% v/v suspension. The resin was then added to the GST-p300_CH3 at 25 μM for 25 μl of resin and incubated for 2 hours on a rotating wheel at 4ºC. After incubation, the resin was pelleted and the supernatant, containing unbound proteins, was removed. The resin was washed three times with binding buffer, again to further exclude unbound material, and resuspended in a 50% v/v solution. The bound GST-tagged protein was added to the putative partners (final concentration of 18 – 25 μM) and incubated for 2 hours on a rotating wheel at 4ºC. After incubation, the resin was again pelleted, the supernatant was removed and the resin was washed three times with wash buffer (binding buffer containing 0.1% Tween-20). Elution and analysis of the samples was performed the same way as for the GST-hNap1 pull-downs.

2.7.2. His pull-downs

His pull-downs were performed with full-length recombinant His-tagged mouse Nap1 (His-mNap1FL), produced in *E. coli* BL21 (DE3) and proteins were purified as described in section 2.2.2.

His-mNap1FL and its putative binding partners were mixed in binding buffer (100 mM Tris/HCl pH 8.0, 150 mM NaCl and 1 mM DTT) at a 1:4 ratio. IMAC Sepharose 6 Fast Flow resin was pre-charged with Ni^{2+} ion and pre-equilibrated in binding buffer as a 50% v/v suspension. The resin was then added to the protein mix (75 μl final resin for 12 μM final His-mNap1FL). The samples were incubated with the resin for 3 hours on a rotating wheel at 4ºC. After incubation, the resin was pelleted and the supernatant was removed. The resin was then washed three times with binding buffer. Elution and analysis was performed as described in chapter 2.4.1.

2.8. NON-DENATURING MASS SPECTROMETRY

All proteins were expressed and purified as described in chapters 2.2 and 2.3 respectively. Subsequent reconstitution of complexes using purified proteins is described in chapter 2.4.

Prior to non-denaturing MS analysis, 30 μl of sample was buffer exchanged into 100 mM Ammonium acetate pH 7.5, 1 mM DTT using micro Bio-Spin®6 columns (Bio-Rad) or 10 kDa amicon vivaspin concentrators (Millipore). For all measurements, 2 μl of sample was loaded into a capillary needle and spectra were recorded. Typical instrument conditions used for non-denaturing MS conditions were as follows: capillary voltages 1.8 kV and cone voltage up to 100 V; for collision induced damage experiments, the collision voltage was increased up to 180 – 200 V, extractor voltage 5 V, analyser pressure 8.15×10^{-4} mbar, and ToF 8.42×10^{-6} mbar. All mass spectra were calibrated externally using 100 mg/ml caesium iodide in water and data were acquired and processed with MassLynx V4.1 software (Waters) with minimal smoothing and no background subtraction.

This work was performed in collaboration with the Robinson Laboratory at the University of Oxford (United Kingdom).

2.8.1. Phosphorylation of Nap1 by CK2

Yeast and mouse Nap1 samples alone and in complex with H2A/H2B dimers and H1Δ100 respectively were *in vitro* phosphorylated by Casein Kinase 2 (New England Biolabs). 100 pmol of substrate protein and 100 units of enzyme were mixed in presence of ATP. Phosphorylation reaction was permitted for 1 hour at 30ºC. The samples were then flash frozen in liquid nitrogen and stored at -80ºC. Analysis of the samples was performed by regular mass spectrometry and non-denaturing mass spectrometry as described above.

2.9. CRYSTALLIZATION TRIALS AND X-RAY DATA COLLECTION

Initial crystallization trials of a number of proteins and protein complexes, listed below, were performed using a screen of 576 crystallization conditions in 96-well sitting-drop plates (100 nl drops). The trials were established at a starting protein concentration of 10 mg/ml and incubation temperatures of 20°C and 4°C. Ideal crystallisation conditions for complexes of interest were thus identified and are described below.

Those trials were set up at a starting protein concentration of 10 mg/ml and at 20 and 4ºC.

List of proteins and protein complexes used for X-ray crystallography:

- yNap1 all constructs in complex with all H2A/H2B dimers variants, as well as seleno-methionine labelled
- mNap1 in complex with H1
- p300'core'_ZZ and p300'core'_ZZ_TAZ2

2.9.1. Crystallization of Nap1 in complex with H2A/H2B dimers and data collection

All yeast Nap1 and histone H2A/H2B dimers variants generated were reconstituted as complexes in all possible Nap1-H2A/H2B combinations and set up for crystallization at protein concentrations ranging from 2.5 to 30 mg/ml at 4°C and 20°C.

Small crystals of the yNap1FL-dH2A/dH2B complex were obtained at 4ºC under a single condition: 0.1 M Tris pH 8.0, 20% w/v PEG2000 MME and 0.2 M TMAO. These crystals were manually reproduced at different pH and precipitate concentrations around the initial condition. Crystal size was increased by micro-seeding into conditions containing lower PEG concentrations. Resultant crystals were cryo-protected in 25% glycerol and tested at the ID14-4 beamline (ESRF, Grenoble) however they showed poor diffraction. 20 crystals were extensively washed and analysed by silver stained SDS-PAGE gel.

yNap1core-xH2AΔ14/xH2BΔ28 were also crystallized at both temperatures 4ºC and 20ºC under conditions containing 10-15% w/v PEG3350 and 200 mM Na/K/Li salts. These crystals were further refined by manual dehydration (using the EasyXtal 15-Well tool from Qiagen) and increasing the PEG concentrations in the reservoir up to 35% w/v PEG3350); *in situ* proteolysis (1:500 and 1:5000 of α-chymotrypsin and trypsin proteases), as well as the Additive Screen from Hampton Research. Presence of all components of the ternary complex in the crystal was analysed by silver stain SDS-PAGE, after washing the crystals extensively with cryo-solution.

Several cryo-solutions were tested: glycerol, ethylene glycol, PEG3350 as well as a cryo-free method. Crystals were tested on ESRF ID14-4 and ID23-2 beamlines; several low-resolution data sets were collected. Diffraction data for these crystals was collected using the EDNA strategy program as a guide. A dehydration device and on-beam annealing were also used on ID14-4 beamline (ESRF, Grenoble).

yNap1core-xH2A14-109/xH2BΔ36 was crystallised at both temperatures, 4°C and 20°C, and two datasets were collected at 6.7 Å resolution. However this was not an improvement as compared to the previous data obtained. Seleno-methionine labelled yNap1core-xH2AΔ14/xH2BΔ28 complex was crystallised under a unique condition containing 12.5% w/v PEG3350, 0.2 M Potassium nitrate. Diffraction data were collected from 8 derivative crystals on ID14.4 beamline (ESRF, Grenoble). These crystals diffracted only to low-resolution (around 15 Å) and no complete dataset was collected.

A number of positive hits in crystallisation trials with the yNap1coreΔ284-308-xH2AΔ14/xH2BΔ28 complex lead to the formation of needle-like clusters of crystals at 20°C under conditions containing 15 – 20% w/v PEG3350 and 0.2 M Potassium thiocyanate.

Additionally the yNap1core∆284-308-xH2A14-109/xH2B∆36 complex also crystallised under these chemical conditions, albeit at 4°C. Several crystals were tested on ID14.4 (ESRF, Grenoble) and diffracted to low-resolution.

2.9.1.1. yNap1core-xH2A∆14/xH2B∆28 complex crystal structure determination and structural analysis

The intensities obtained from the best diffracting crystals were integrated and scaled using the program XDS (Kabsch 2010). These crystals belonged to the space group $P2_1$ and diffracted to 6.7 Å. The structure was determined by molecular replacement with the program Phaser (McCoy et al. 2007) using the structure of yNap1 (PDB code 2AYU) and the structure of histone H2A/H2B heterodimer from the nucleosome structure (PDB code 1AOI) as the search models. A single round of rigid body refinement was applied using the program Phenix Refine (Afonine et al. 2012). The final model was refined using DEN Refinement (Schröder et al. 2010; O'Donovan et al. 2012; Schröder et al. 2007)).

2.9.1.2. What is Deformable Elastic Network Refinement?

Today, in structural biology, increasingly complex and thus increasingly challenging systems, including large proteins and protein assemblies, are under study. One limitation for structural studies is that crystals of large assemblies often diffract weakly to low resolution making structure determination and subsequent refinement challenging. Nevertheless, interpretation of low-resolution diffraction data is often desirable as it provides information about the interaction of individual components or insights about large-scale conformational changes between different states of a system. Methods that allow refinement at low resolution are improving; one of these methods is the Deformable Elastic Network (DEN) Refinement (Schröder et al. 2007).

The DEN Refinement employs previously determined high-resolution structures as a reference model. This method adapts only those degrees of freedom for which the density map at low-resolution actually provides information and keeps all other degrees of freedom as close to the initial structure as possible (Schröder et al. 2007). By using a reference model,

the DEN constraints reduce over-fitting at resolutions lower than 3.5 Å where this can be a significant problem. The reference model can simply provide a model for initial refinement, or it serve as a homology or predictive model that provides external information (Brunger et al. 2012).

During the process of torsion angle refinement, the DEN distance restraints are gradually adjusted in order to fit the diffraction data (Brunger et al. 2012). Two parameters are particularly important in this process: γ and W_{DEN}, whose values are optimized in a global grid search against R_{free} (Schröder et al. 2010). For the success of the DEN refinement, it is essential to perform a global search for an optimal parameter pairing (γ, W_{DEN}) (Brunger et al. 2012).

The parameter γ, also referred to as the "deformation factor", controls the extent of deformation and provides the magnitude of the adjustment of initial distance restraints. It balances the influences of the diffraction data and the reference model (Schröder et al. 2010). It can range from 0 to 1. When $\gamma = 0$, no deformable elastic network is being applied and refinement keeps the structure close to the reference model (Schröder et al. 2010). Large γ values (for example $\gamma = 1$) allow larger structural deviations from the reference model (O'Donovan et al. 2012). In summary, larger γ values indicate that little information from the initial structure is incorporated during refinement. Its optimal value can be estimated using cross-validation (Schröder et al. 2007).

The parameter W_{DEN} controls the weight of the DEN distance restraints (Brunger et al. 2012). It can range from 0 to 300. When $W_{DEN} = 0$, the DEN constraints have no effect on the refinement process. While when $W_{DEN} = 300$ and $\gamma = 0$ the DEN term is high enough to effectively constrain the refined structure to the reference-model. Its value depends on the overall similarity between the refined structure and its reference model (O'Donovan et al. 2012).

- General DEN Refinement Guidelines

Web service is now available at the SBGrid Science Portal (http://sbgrid.org); it requires that all users register. It provides a standard framework that can support specialized structure-determination computation. The extensive opportunistic resources of the Open Science Grid (OSG) provide the computational power of the portal.

The user needs to prepare two files prior to submission. (a) The DEN refinement input file (`*.inp`). The `refine_den.inp` file from the DEN tutorial of the CNS website (http://www.cns-online.org) should be used as template. It must be modified to reference the diffraction data set, the initial model and the reference structure, which are included in the archive file. (b) The archive file (`*.tar` or `*.zip`) containing the diffraction data set, the initial model and reference coordinates. It can also include special parameter files or non-crystallographic symmetry files. Once these files are ready, submission of the job can be carried out through the SBGrid Science Portal. The uploaded files are checked for correctness and consistency. Typically, a DEN refinement job takes around 10 to 12 hours of calculations. The output of the DEN refinement will consist of a set of heat maps showing the best R_{free} under different parameter conditions, a table displaying all salient results and output data files. From these results, the user is able to choose the most promising (lowest Rfree) parameters and use this for subsequent remodelling and refinement cycles.

For detailed explanation of the DEN refinement procedures refer to (O'Donovan et al. 2012).

2.9.2. Crystallization of p300 constructs

After purification of the p300'core'_ZZ and p300'core'_ZZ_TAZ2 from Hi5 cells, the samples were deacetylated overnight at room temperature, following equilibration into a specific reaction buffer, detailed below, and supplementation with SIRT2 at a 1:10 SIRT2:p300 ratio. The reaction buffer used contained 20 mM HEPES pH7.5, 300 mM NaCl, 5 μM $ZnCl_2$, 0.5 mM TCEP, 5 mM $MgCl_2$, and 1 mM NAD^+. Following completion of the incubation time, p300 and SIRT2 were separated by size exclusion chromatography using a Superdex 200 10/300 GL column equilibrated in buffer containing 20 mM HEPES pH 7.5, 300 mM NaCl, 5 mM $ZnCl_2$, and 0.5 mM TCEP. The deacetylated p300 was then concentrated to 10 mg/ml and incubated on ice for 30 minutes with a 3-fold molar excess of LysCoA, an inhibitor previously reported to stabilize the HAT domain (X. Liu et al. 2008). The deacetylated p300-LysCoA complex was finally centrifuged at 13000 rpm (F45-24-11 rotor from Eppendorf) for 15 minutes and set up for crystallization.

2.10. NEGATIVE STAIN ELECTRON MICROSCOPY

Four µL of the yNap1/H2A/H2B sample (~0.1 mg/ml) were loaded between the mica-carbon interface as described in (Franzetti et al. 2002). The sample was stained using 2% uranyl acetate pH 4.5 and air-dried. Images were taken under low-dose conditions in a CM12 Philips electron microscope working at 120 kV and with a nominal magnification of 40,000 using an Orius SC1000 CCD camera.

3. STRUCTURAL CHARACTERIZATION OF NAP1 – HISTONE COMPLEXES

RESUME EN FRANÇAIS

Le yNap1-H2A/H2B complexe et le mNap1-H1 complexe ont été reconstitués *in vitro* avec succès en utilisant différents mutants de toutes les protéines. Ce succès nous a permis d'obtenir matériel suffisaient pour analyser stoechiométrie et la composition des oligomères formés par ce complexe, qui demeurent controversées. En utilisant la spectrométrie de masse non-denaturalitzant, nous avons élucidé la stoechiométrie du complexe comme 1:1, un homodimère de Nap1 par un hétérodimére d'histone H2A/H2B ou un monomère de H1. A partir de cette unité de base, le complexe peut former un oligomère contenant jusqu'à six exemplaires de cet unité: $(yNap1_2\text{-}H2A/H2B)_6$, et jusqu'à deux exemplaires de $(mNap1_2\text{-}H1)_2$.

Il a été possible de produire des cristaux du yNap1-H2A/H2B complexe pour la caractérisation structurale par rayon X. Un model à basse résolution (6.7 Å) a été obtenu par le traitement des données recueillies pour un de ces cristaux sur la ligne ID14-4 (ESRF, Grenoble). Il y a six copies du complexe dans l'unité asymétrique, qui peut ressembler l'oligomère présente en solution et détecter par spectrométrie de masse non-denaturalitzant et microscopie électronique. Cette structure montre aussi un stoechiométrie de 1:1, où les deux monomères de yNap1 interagirent principalement avec l'histone H2A.

Il n'a pas été possible d'obtenir de l'information structurale sur le complexe mNap1-H1. Mais des études d'interaction par pull-down ont démontrais que le domaine globulaire de l'histone H1 n'est pas suffisant et que le C-terminus de mNap1 est essential pour la union a H1.

3.1. STRUCTURAL STUDIES ON YEAST NAP1 – HISTONE COMPLEXES

It is known that Nap1 binds H2A/H2B dimers to form a stable complex (McQuibban et al. 1998). However, much controversy surrounds the binding stoichiometry for the Nap1-H2A/H2B complex. One of the most widely accepted hypothesis is that one Nap1 homodimer binds to one H2A/H2B heterodimer (McBryant et al. 2003; Newman et al. 2012). In contrast, others have suggested that one Nap1 homodimer binds to two H2A/H2B heterodimers (Andrews et al. 2008), resulting in a 1:2 stoichiometry. In this study, we attempt to provide more evidence to distinguish between these two hypotheses.

Nap1 has the propensity to oligomerize in solution and considerable efforts have been made to characterize the oligomerization of Nap1 alone and in complex with histones (Fujii-Nakata et al. 1992; McBryant & Peersen 2004; Tóth et al. 2005; Park et al. 2008; Noda et al. 2011; Newman et al. 2012). Here we aim to understand the Nap1 oligomerization process and the biological relevance of higher-order Nap1 complexes.

3.1.1. Reconstitution of Nap1-H2A/H2B complexes

A number of mutants of the yNap1 protein have been used in this study. First wild-type yNap1*wt* was cloned, recombinantly expressed in *E. coli* BL21 (DE3) and purified to homogeneity. Second, we designed the yNap1core construct, which corresponds to the minimal region required for histone binding and nucleosome assembly (Fujii-Nakata et al. 1992) and has been crystallized (Park et al. 2008). Further, we designed a construct containing a deletion of residues 284-308 comprising a β-hairpin that has been implicated in Nap1 oligomerization (Park et al. 2008). Finally, we decided to investigate the role of the yNap1 N- and C-termini flexible tails in H2A/H2B binding and oligomerization using two constructs containing a deletion of the N- and C-termini respectively. It has been shown that the ability of yNap1 to disassemble H2A/H2B dimers from the nucleosome depends on its acidic C-terminal patch (Park et al. 2005). A schematic representation of all these mutants is shown in Figure 12A.

The yNap1-H2A/H2B complex was assembled *in vitro* by mixing $yNap1_2$ with H2A/H2B heterodimers in a 1:2 ratio (dimer/dimer). The ternary complex was then isolated by size-

exclusion chromatography (Figure 12B). Fractions corresponding to the elution peak were analysed by SDS-PAGE gel and showed the formation of the ternary complex (Figure 12C).

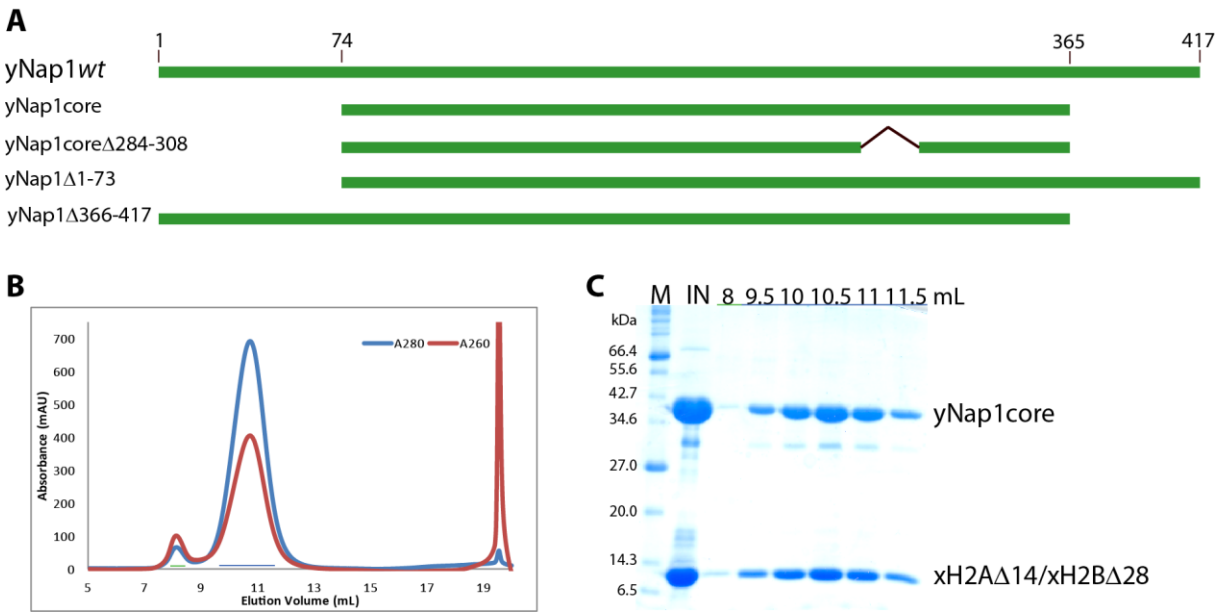

Figure 12 In vitro reconstitution of yNap1-H2A/H2B complex. (A) Schematic representation of the yNap1 constructs used in this study. (B) Chromatogram showing the elution profile of yNap1core-xH2AΔ14/xH2BΔ28 complex using a Superdex 200 gel filtration column. Absorbance at 280 nm and 260 nm were measured to detect protein and nucleic acid elution, respectively. (C) SDS-PAGE gel showing the protein content of the fractions from the elution peak. The name of the proteins as well as the molecular weight (kDa) of the protein marker is given. *Note that H2A and H2B migrate at equivalent positions on this gel.* For clarity, only one example of *in vitro* reconstituted complex is shown here.

3.1.2. Characterization of the oligomeric states of yNap1–H2A/H2B complexes

We investigated the stoichiometry of the Nap1-H2A/H2B complex as well as its oligomerization using biochemical approaches. Native-PAGE gel analysis showed that yNap1*wt* alone is not a single species; two bands were identified most likely corresponding to an yNap1*wt* dimer (major species) and a tetramer (minor species) (Figure 13). Titration of the yNap1*wt* with increasing concentration of dH2A/dH2B dimer revealed the formation of four distinct species with unknown stoichiometry (Figure 13).

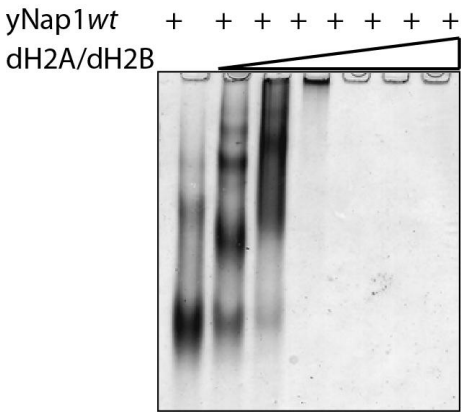

Figure 13 Oligomerizaiton of the yNap1*wt*-dH2A/dH2B complex. Titration of yNap1*wt* with increasing concentration of dH2A/H2B dimers, analysis by Native-PAGE gels and visualization by Coomassie blue staining.

Next, we performed non-denaturing mass spectrometry (MS) experiments in collaboration with Dr. Carol Robinson Laboratory (University of Oxford, United Kingdom). These experiments allowed us to elucidate the binding stoichiometry and the oligomeric state of yNap1 alone or in complex with H2A/H2B.

Prior to the complex characterization, the role of different regions of yNap1 for complex formation and oligomerization was analysed by using the mutants shown in Figure 12A. All mutants were individually buffer exchanged into 100 mM ammonium acetate buffer immediately prior to analysis. At this ionic strength, all yNap1 variants showed two major series of resolved peaks with different charge states corresponding to yNap1 dimers and tetramers (Figure 14). We conclude from this data that yNap1 predominantly is a dimer in solution. yNap1 constructs containing the C-terminal deletion revealed the presence of a trimer upon application of collision induced damaged (CID) suggesting that the acidic C-terminal region of Nap1 stabilizes the tetramer (Figure 14C-E).

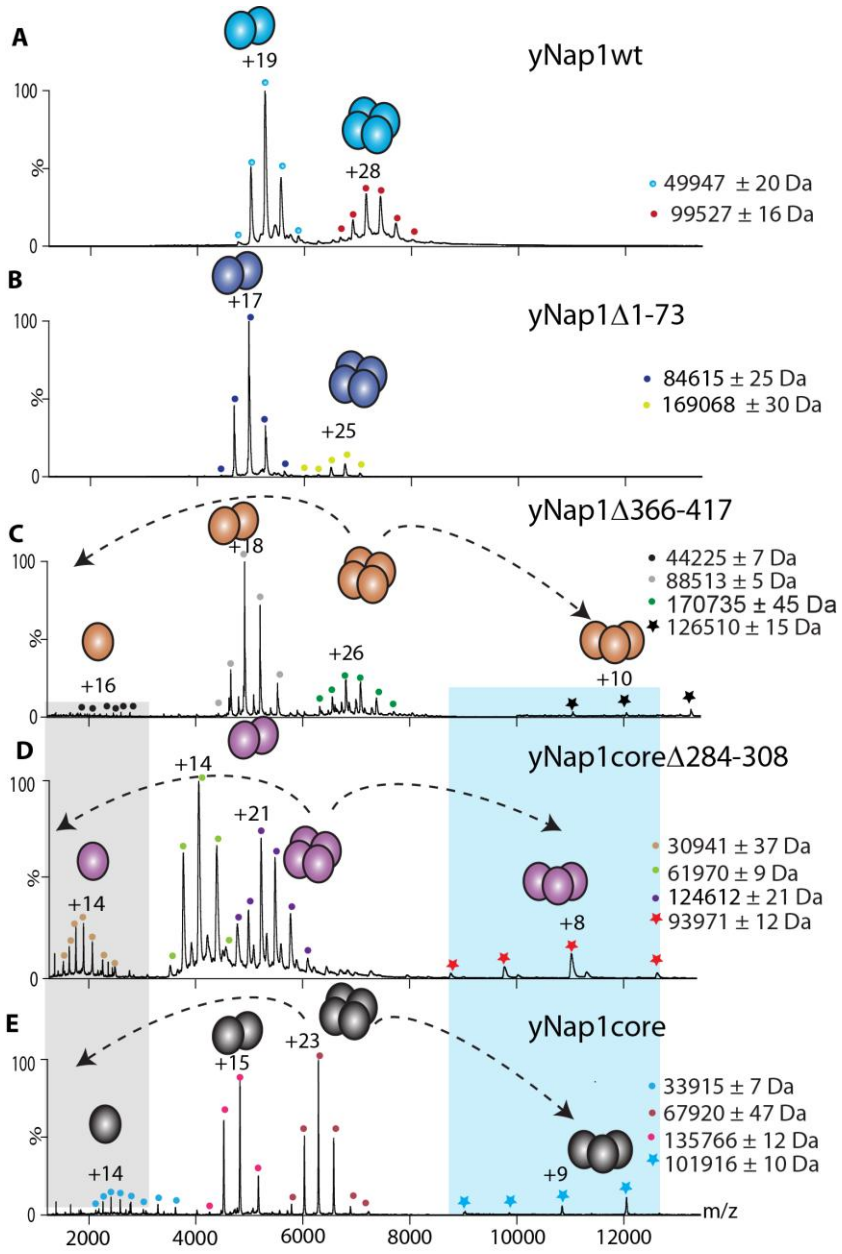

Figure 14 Oligomeric states of yNap1 alone. Non-denaturing mass spectrometry profiles of yNap1*wt* (A), yNap1Δ1-73 (B), yNap1coreΔ284-308 (C), yNap1Δ366-417 (D) and yNap1core (E). Experimental molecular masses are given in Da. Cartoons representing the proteins are displayed.

Next, the yNap1 mutants described above were analysed in complex with histone H2A/H2B heterodimers by the same technique. Complex reconstitution was performed as described in section 3.1 and buffer exchanged to 100 mM ammonium acetate immediately prior to analysis by non-denaturing MS. Analysis of the yNap1*wt*-dH2A/dH2B complex showed that one $(yNap1wt)_2$ homodimer binds to one histone H2A/H2B heterodimer (Figure 15A). Together with the yNap1core-xH2AΔ14/xH2BΔ28 X-ray crystal structure described in section

3.1.3, these results show that the stoichiometry of the complex as a ratio of 1:1 (yNap1wt_2-dH2A/dH2B). This complex further assembles into an oligomer containing up to two copies of this unit (yNap1wt_2-dH2A/dH2B)$_2$. CID analysis of the dimer and tetramer peak show that these complexes dissociate into several subspecies (Figure 15B-C), again confirming the stoichiometry obtained in the first experiment and the presence of a repeating unit from which the oligomerization is assembled.

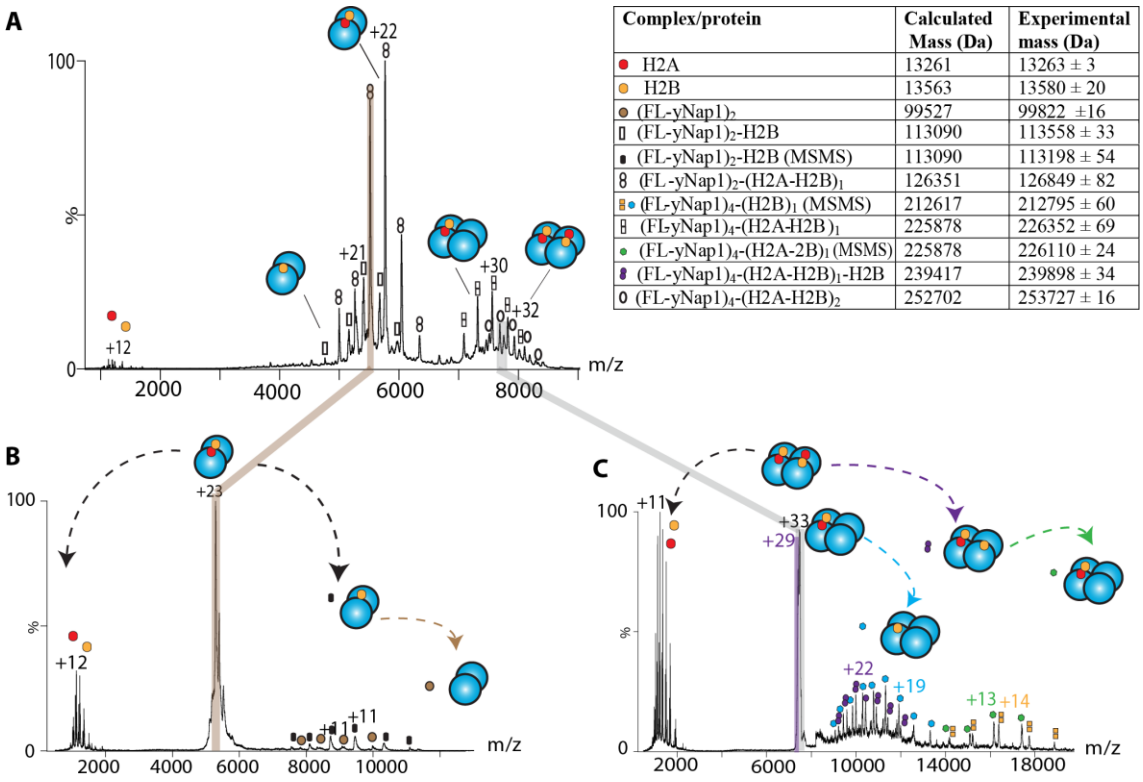

Complex/protein	Calculated Mass (Da)	Experimental mass (Da)
H2A	13261	13263 ± 3
H2B	13563	13580 ± 20
(FL-yNap1)$_2$	99527	99822 ±16
(FL-yNap1)$_2$-H2B	113090	113558 ± 33
(FL-yNap1)$_2$-H2B (MSMS)	113090	113198 ± 54
(FL-yNap1)$_2$-(H2A-H2B)$_1$	126351	126849 ± 82
(FL-yNap1)$_4$-(H2B)$_1$ (MSMS)	212617	212795 ± 60
(FL-yNap1)$_4$-(H2A-H2B)$_1$	225878	226352 ± 69
(FL-yNap1)$_4$-(H2A-2B)$_1$ (MSMS)	225878	226110 ± 24
(FL-yNap1)$_4$-(H2A-H2B)$_1$-H2B	239417	239898 ± 34
(FL-yNap1)$_4$-(H2A-H2B)$_2$	252702	253727 ± 16

Figure 15 Oligomeric states of (yNap1*wt*)$_2$-dH2A/H2B complex. (A) Non-denaturing MS spectrum of the complex including cartoons of the proteins. (B) MS/MS isolation of the +23 charge state of (yNap1*wt*)$_2$-dH2A/dH2B complex including cartoons of the proteins and CID sub-complexes. (C) MS/MS isolation of the +29 and +33 tetramer of ((yNap1*wt*)$_2$-dH2A/dH2B)$_2$ complex including cartoons of the proteins and CID sub-complexes. Calculated and experimental masses and stoichiometries are given in table represented by the symbols.

We next analysed the yNap1core-xH2AΔ14/xH2BΔ28 complex. Oligomers containing up to six copies of the (yNap1core)$_2$-xH2AΔ14/xH2BΔ28 unit were observed (Figure 16A). Notably, the same stoichiometry is found in the asymmetric unit of the crystal structure described in section 3.1.3. All the intermediate complexes containing one, two, three, and four copies of the repeating unit were also detected. CID analysis triggered the dissociation of the

$((yNap1core)_2$-xH2AΔ14/xH2BΔ28$)_6$ complex and revealed an assembly containing five copies of the repeating unit (Figure 16B). Together, these data indicate that yNap1core assembles into dimers and tetramers and that addition of H2A/H2B might trigger further assembly into complexes containing up to six copies of the repeating unit: $((yNap1core)_2$-xH2AΔ14/xH2BΔ28$)_6$.

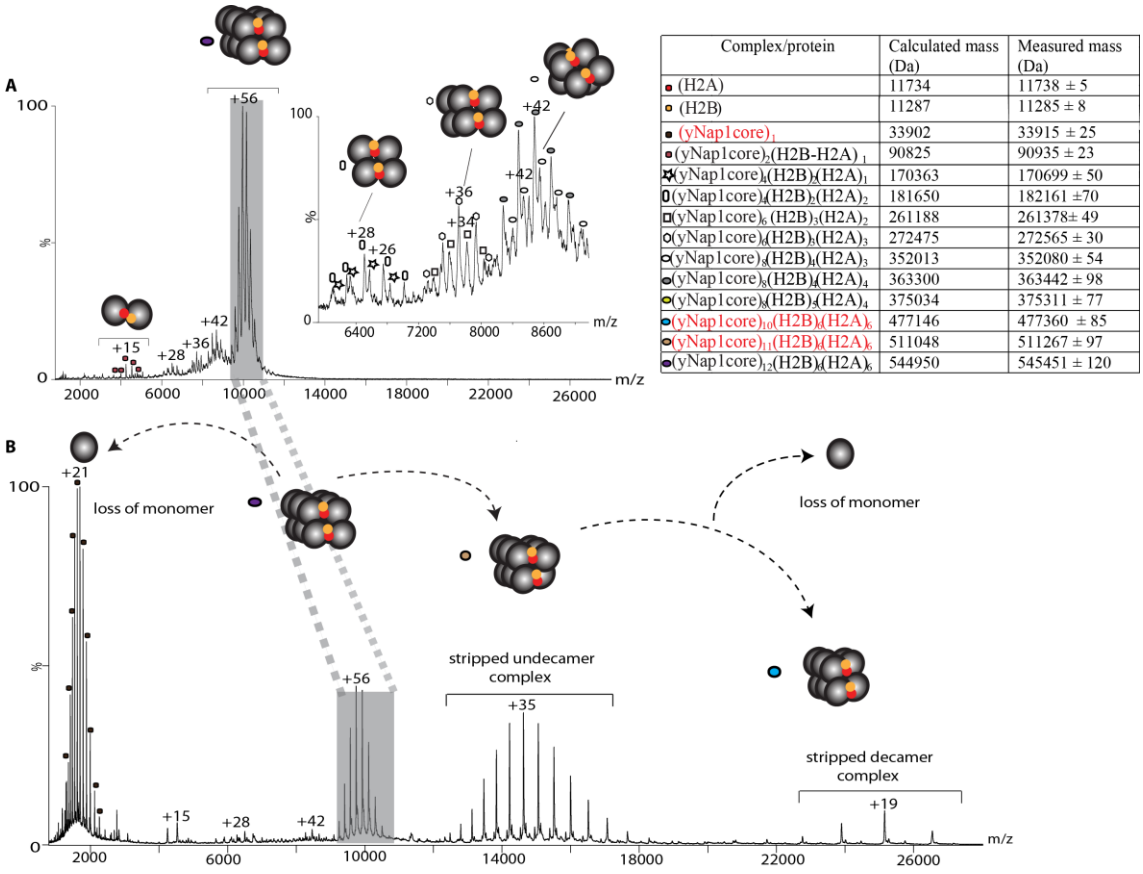

Complex/protein	Calculated mass (Da)	Measured mass (Da)
(H2A)	11734	11738 ± 5
(H2B)	11287	11285 ± 8
$(yNap1core)_1$	33902	33915 ± 25
$(yNap1core)_2(H2B\text{-}H2A)_1$	90825	90935 ± 23
$(yNap1core)_4(H2B)_2(H2A)_1$	170363	170699 ± 50
$(yNap1core)_4(H2B)_2(H2A)_2$	181650	182161 ±70
$(yNap1core)_6(H2B)_3(H2A)_2$	261188	261378± 49
$(yNap1core)_6(H2B)_3(H2A)_3$	272475	272565 ± 30
$(yNap1core)_8(H2B)_4(H2A)_3$	352013	352080 ± 54
$(yNap1core)_8(H2B)_4(H2A)_4$	363300	363442 ± 98
$(yNap1core)_8(H2B)_5(H2A)_4$	375034	375311 ± 77
$(yNap1core)_{10}(H2B)_5(H2A)_5$	477146	477360 ± 85
$(yNap1core)_{11}(H2B)_6(H2A)_5$	511048	511267 ± 97
$(yNap1core)_{12}(H2B)_6(H2A)_6$	544950	545451 ± 120

Figure 16 Oligomeric states of yNap1core-xH2AΔ14/xH2BΔ28 complex. (A) Non-denaturing MS spectrum of the complex including cartoons of the proteins and zoom in between 6000 and 9000 m/z. (B) CID of the $((yNap1core)_2$-xH2AΔ14/xH2BΔ28$)_6$ complex including cartoons of the proteins. Calculated and experimental masses are given in the table with CID products shown in red.

The crystal structure of the yNap1core dimer has revealed a β-hairpin structure (comprising residues 284-308) that forms a crystal contact and it was shown to be involved in yNap1 oligomerization in solution (Park et al. 2008). We next investigated if removal of the β-hairpin abolishes oligomerization of the complex. yNap1coreΔ284-308 alone assembles into dimers and tetramers similar to the other yNap1 constructs, as shown in Figure 14D. In the

presence of H2A/H2B, mostly tetramers and only a small fraction of dimers were observed, but no higher-order oligomerization (Figure 17). In agreement with previous studies, these results suggest that the β-hairpin structure might support higher-order oligomerization.

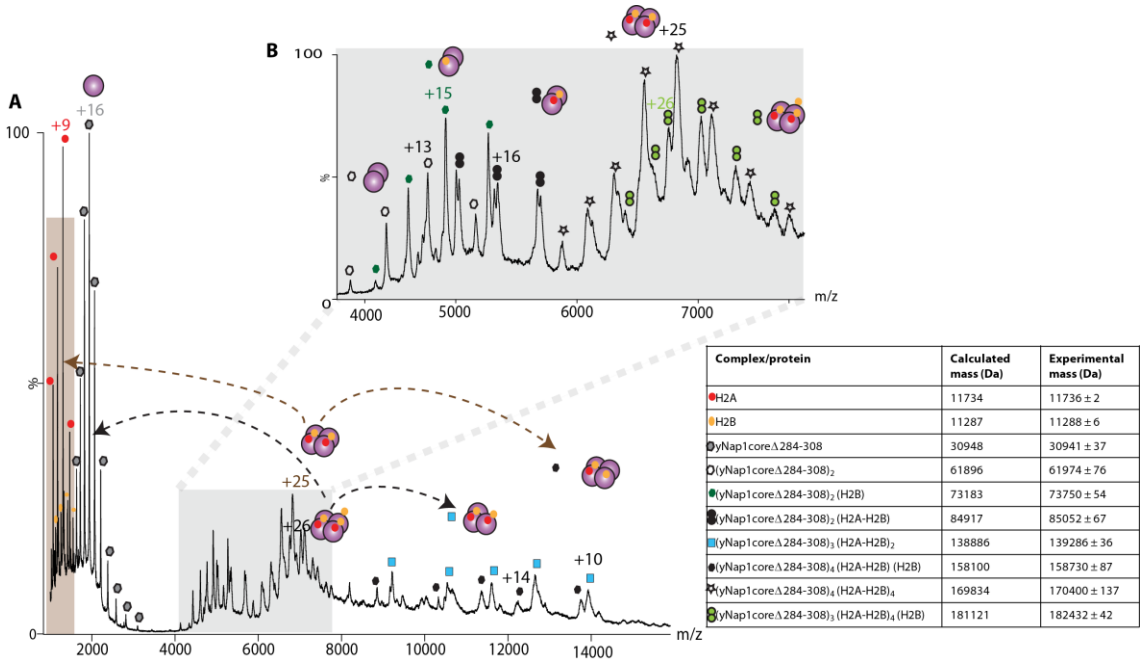

Complex/protein	Calculated mass (Da)	Experimental mass (Da)
H2A	11734	11736 ± 2
H2B	11287	11288 ± 6
yNap1coreΔ284-308	30948	30941 ± 37
$(yNap1coreΔ284-308)_2$	61896	61974 ± 76
$(yNap1coreΔ284-308)_2$ (H2B)	73183	73750 ± 54
$(yNap1coreΔ284-308)_2$ (H2A-H2B)	84917	85052 ± 67
$(yNap1coreΔ284-308)_3$ $(H2A-H2B)_2$	138886	139286 ± 36
$(yNap1coreΔ284-308)_4$ (H2A-H2B) (H2B)	158100	158730 ± 87
$(yNap1coreΔ284-308)_4$ $(H2A-H2B)_4$	169834	170400 ± 137
$(yNap1coreΔ284-308)_3$ $(H2A-H2B)_4$ (H2B)	181121	182432 ± 42

Figure 17 Oligomeric state of yNap1coreΔ284-308-xH2AΔ14/xH2BΔ28 complex. (A) MS spectrum of the complex including cartoons of the proteins. (B) Detailed MS spectrum between 4000 and 8000 m/z of the complex including cartoons. Calculated and experimental masses are given in table.

Finally, the importance of the N- and C-termini of yNap1 for the oligomerization of the complex was tested. Upon deletion of the N-terminus, oligomers containing up to two copies of the $(yNap1Δ1\text{-}73)_2$-xH2AΔ14/xH2BΔ28 complex were observed (Figure 18A), similarly to the yNap1*wt*$_2$-dH2A/dH2B complex. Deletion of the C-terminus resulted in an oligomer containing up to five copies of the $(yNap1Δ366\text{-}417)_2$- xH2AΔ14/xH2BΔ28 complex (Figure 18B). These results suggest a role for the flexible and acidic C-terminal region of yNap1 in the regulation of the oligomerization of the complex, probably due to a structural rearrangement of binding.

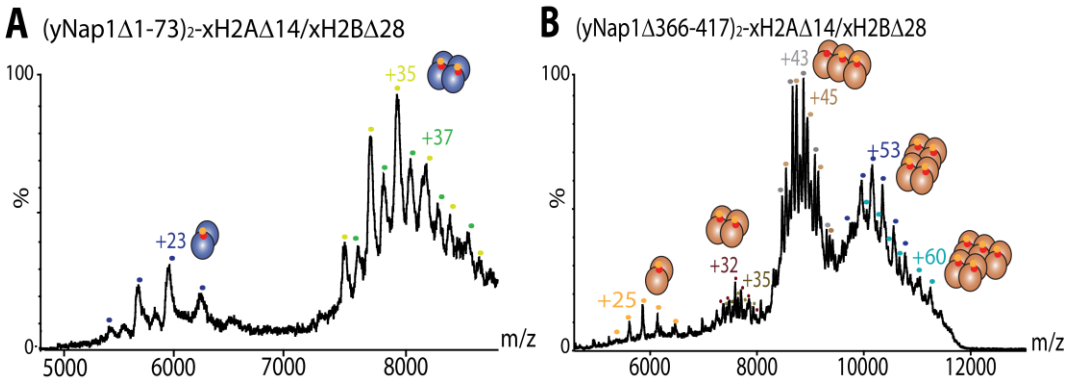

Figure 18 Oligomeric states of yNap1Δ1-74-xH2AΔ14/xH2BΔ28 complex (A) and yNap1Δ366-417-xH2AΔ14/xH2BΔ28 (B) complexes. MS spectrum of the complexes including cartoons of the proteins.

In summary, all yNap1 constructs analysed showed some propensity of dimers to further oligomerize into tetramers indicating the presence of a yNap1 tetramerization interface. We demonstrate that in the presence of H2A/H2B, yNap1 dimers bind a single H2A/H2B heterodimer, resulting in a stoichiometry of 1:1 (dimer/dimer). This $yNap1_2$-H2A/H2B complex further oligomerizes into assemblies containing up to six copies of the repeating unit depending on the experimental conditions used (ionic strength and protein concentration). Such higher-order assemblies have only been observed in the presence of H2A/H2B indicating that the heterodimer contributes to yNap1 assembly either by providing novel oligomerization interfaces or by allosterically regulating yNap1 assembly. For example, by modulating the structure of the β-hairpin structure which appears to be involved in higher-order oligomerization. Finally, the acidic C-terminal region of yNap1 might play a role in the regulation of oligomerization, possibly by inhibiting it.

3.1.2.1. Role of yeast Nap1 phosphorylation in oligomerization

Previously it has been reported that that yNap1 is extensively phosphorylated by CKII *in vivo* (Calvert et al. 2008). Nap1 phosphorylation may be necessary for the histone chaperone to efficiently function as histone donor and acceptor in chromatin assembly during S phase (Calvert et al. 2008). However, the role of CKII phosphorylation in regulating yNap1 function remains unclear.

To investigate if phosphorylation regulates yNap1 assembly, we phosphorylated the (yNap1*wt*)$_2$-dH2A/dH2B complex *in vitro*. CKII phosphorylation was verified by mass spectrometry and revealed eight phosphorylated residues on yNap1*wt* at positions T53, S82, S140, S159, T163, T177, S343, S397. Analysis of CKII-phosphorylated (yNap1wt)$_2$-dH2A/dH2B complexes by non-denaturing MS showed no higher-order oligomerization (Figure 19). This result indicates that CKII phosphorylation inhibits the formation of higher-order oligomers, possibly by interfering with yNap1 tetramerization.

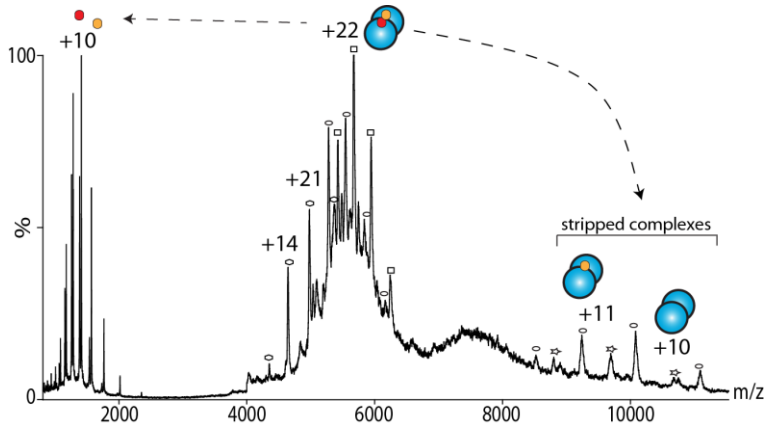

Figure 19 Analysis of yNap1*wt*-dH2A/H2B complex after phosphorylation by CKII. MS spectrum of the complex including cartoons of the proteins.

3.1.3. Low resolution X-ray crystal structure of yNap1-H2A/H2B complex

In order to investigate how Nap1 interacts with histone H2A/H2B dimers, X-ray crystallographic studies were performed on the yNap1$_2$-H2A/H2B complex. A number of crystallization trials on different constructs of yNap1 (Figure 12) in complex with full-length and truncation mutants of the histones H2A and H2B were performed. All of them yielded crystallisable samples that diffracted poorly. Extensive screening of crystals (>400 samples analysed) allowed us to obtain crystals containing the yNap1core-xH2AΔ14/xH2BΔ28 complex that diffracted to 6.7 Å resolution and allowed data collection.

Attempts to improve diffraction were carried out by using (a) *in situ* proteolysis, (b) additive screening, (c) dehydration, and (d) crystal annealing. The best-diffracting yNap1core-xH2AΔ14/xH2BΔ28 complex crystals were obtained in hanging drops in 10% w/v PEG 3350,

100 mM sodium fluoride after manual dehydration (Figure 20A-B). The content of the crystals was verified by SDS-PAGE gel and silver stain (Figure 20C).

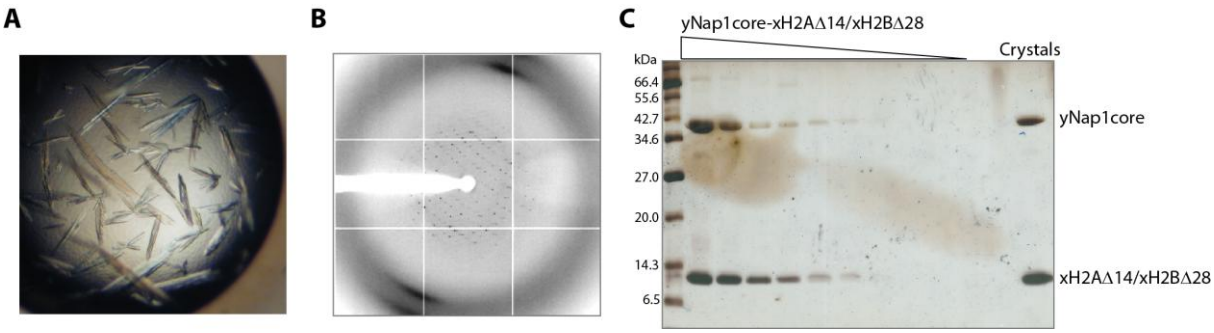

Figure 20 yNap1core-xH2AΔ14/xH2BΔ28 crystals and diffraction pattern. (A) yNap1core-xH2AΔ14/H2BΔ28 crystals obtained by hanging drop in 10% w/v PEG 3350, 100 mM sodium fluoride. (B) Example of diffraction pattern obtained from the yNap1core-xH2AΔ14/H2BΔ28 crystals. Images were collected on ID14-4 (ESRF, Grenoble). (C) SDS-PAGE gel showing a serial dilution of the yNap1core-xH2AΔ14/H2BΔ28 complex and the content of 20 crystals. *Note that H2A and H2B migrate at equivalent positions on this gel.* Visualization of the gel by silver staining. Molecular weight marker (kDa) is given.

Data on the yNap1core-xH2AΔ14/xH2BΔ28 complex crystals were collected on ID14-4 (ESRF, Grenoble). These crystals belong to the primitive monoclinic space group $P2_1$ (Table 5). Calculation of the Matthews coefficient suggested that the asymmetric unit contains 6-7 copies of the $(yNap1core)_2$-xH2AΔ14/xH2BΔ28 complex and a solvent content of 46-54% (

Table 6).

Table 5 Data collection, phasing and refinement statistics. **Values in parentheses are for highest-resolution shell.**

	Native
Data collection	
Space group	$P2_1$
Cell dimensions□□	
a, *b*, *c* (Å)	111.47, 211.13, 126.57
□□(°)	99.7
Wavelength (Å)	0.974
Resolution (Å)	50-6.7
R_{sym} or R_{merge}	11.5 (78)
$I / \sigma I$	9.2 (1.5)
Completeness (%)	96.2 (92.9)
Redundancy	1.9 (1.9)
Refinement	
Resolution (Å)	50-6.7
No. of reflections	10150
R_{work} / R_{free}	0.30 / 0.31
No. of atoms	32826
B-factors	
Protein	388.5
R.m.s deviations values	
Bond lengths (Å)	0.0028
Bond angles (°)	0.732

Table 6 Matthews coefficient calculations. Estimated molecular weight 90855.0 Da, corresponding to $(yNap1core)_2$-xH2AΔ14/xH2BΔ28.

Nmol/asym	Matthews Coefficient	% Solvent	P (6.75)	P (tot)
1	16.19	92.41	0.00	0.00
2	8.09	84.81	0.00	0.00
3	5.40	77.22	0.00	0.00
4	4.05	69.62	0.03	0.02
5	3.24	62.03	0.12	0.09
6	**2.70**	**54.43**	**0.30**	**0.26**
7	2.31	46.84	0.38	0.40
8	2.02	39.24	0.15	0.21
9	1.80	31.65	0.01	0.02
10	1.62	24.05	0.00	0.00
11	1.47	16.46	0.00	0.00
12	1.35	8.81	0.00	0.00
13	1.25	1.27	0.00	0.00

Considering that the asymmetric crystallographic unit contains 6-7 copies of a $(yNap1core)_2$-xH2AΔ14/xH2BΔ28 complex, the presence of non-crystallographic symmetry (NCS) in the asymmetric unit was verified by calculation of a self-rotation function (MolRep in CCP4

package). This analysis revealed the presence of a 2-fold and two perpendicular 3-fold non-crystallographic symmetry axis (Figure 21). Together, the NCS symmetry and the number of predicted (yNap1core)$_2$-xH2AΔ14/xH2BΔ28 complexes in the asymmetric unit predicted a high-order assembly, possibly a hexamer.

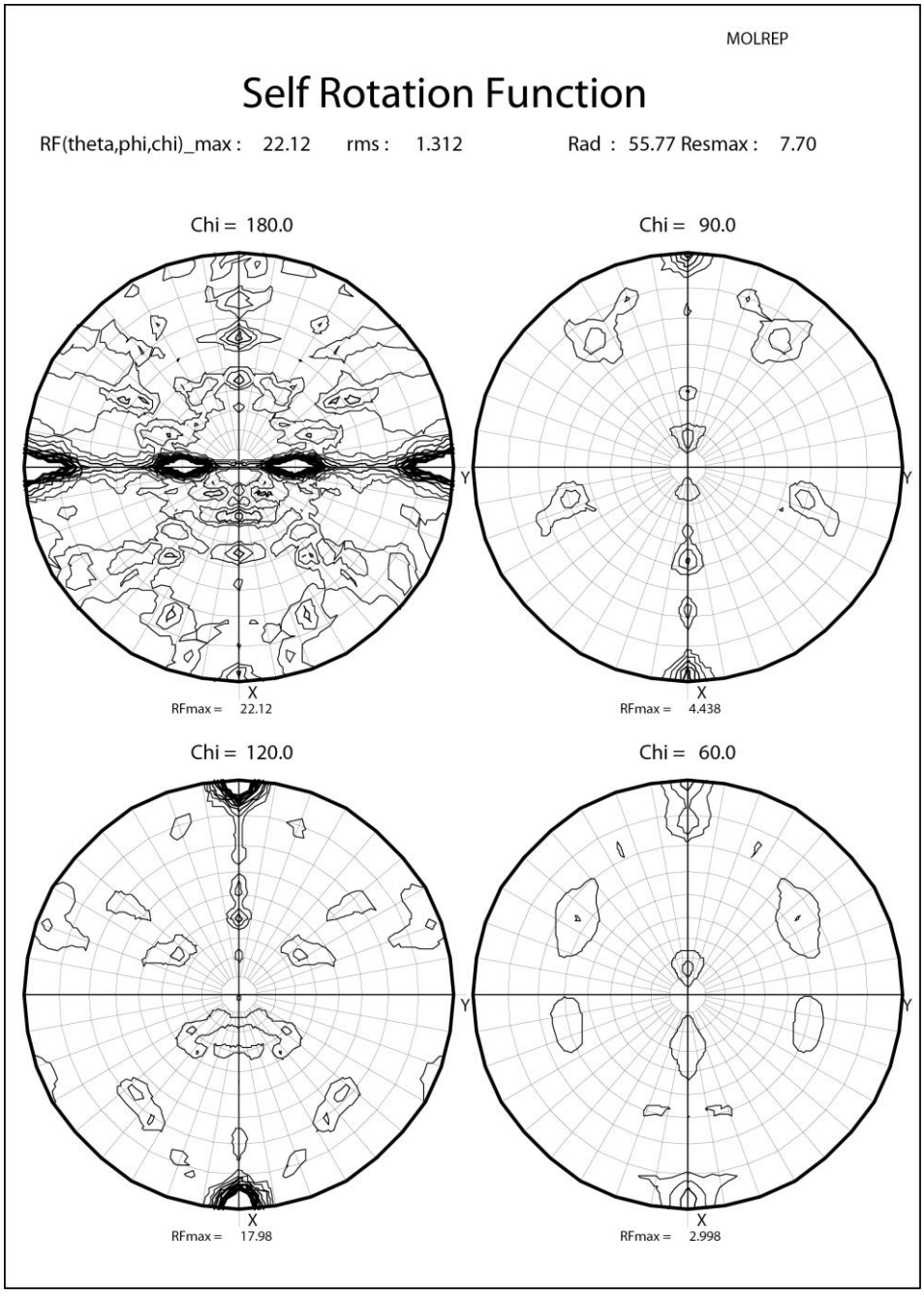

Figure 21 Self-rotation function calculated for the space group P2$_1$ yNap1core-xH2AΔ14/xH2BΔ28 crystals. Peaks in the Chi=120 section indicate a 3-fold NCS, while peaks in the Chi=180 section indicate a 2-fold NCS perpendicular to the 3-fold. Six copies of the macromolecular complex are present per asymmetric unit.

In order to determine the structure we attempted molecular replacement (MR) with PHASER (McCoy et al. 2007) using the yNap1 structure (PDB Code 2AYU) and a histone H2A/H2B heterodimer from the nucleosome structure (PDB Code 1AOI). However, the low resolution together with the fact that a single yNap1 chain only represents around 6% of the scattering mass made this approach very challenging. As the first MR attempts did not result in a clear solution, yNap1core and xH2BΔ28 were selenomethionine-labelled in order to experimentally determine phase angles by using anomalous scattering. Although good SeMet incorporation (approximately 90%) was obtained, the resulting crystals did not diffract to better than 15 Å resolution precluding experimental phasing.

Further attempts of MR were then made. Considering the Matthews coefficient, we searched for 12 copies of yNap1core and 6 copies of H2A/H2B containing truncated flexible N- terminal tails (LLG score 675, RFZ: 3.5, TFZ: 4.7). Visual inspection showed one partial solution containing one yNap1core homodimer with one H2A/H2B heterodimer bound in the dome-shaped cavity of yNap1. This $(yNap1core)_2$-xH2AΔ14/xH2BΔ28 complex was then fixed and used to search for 5 more copies. This approach resulted in a high-scoring MR solution (LLG score 629, RFZ: 4.1, TFZ: 13.6) containing 6 copies of the $(yNap1core)_2$-xH2AΔ14/xH2BΔ28 complex in the asymmetric unit. Visual inspection of a 2F0-Fc electron density map indicated the presence of all six copies of the $(yNap1core)_2$-xH2AΔ14/xH2BΔ28 complex. After initial rigid body refinement with Phenix Refine (Afonine et al. 2012), we obtained a R factor of 0.31 and a R_{free} of 0.35.

Molecular replacement and subsequent refinement is challenging at low resolution. However, the quality and number of methods for refining low-resolution structures are improving (DiMaio et al. 2011; Schröder et al. 2007; Murshudov et al. 2011). To improve the accuracy of the rigid body refined structure, we employed DEN Refinement. This method utilizes known high-resolution structures of homologous proteins or domains as reference-model (Brunger & Adams 2012). Two adjustable parameters are important in this approach: γ (deformation factor) and W_{DEN} (weight of the DEN distance restraints). The deformation factor (γ) balances the influences of the diffraction data and the reference-model (Schröder et al. 2010), while W_{DEN} depends on the overall similarity between the refined structure and its reference-model (Brunger et al. 2012; O'Donovan et al. 2012). For the success of DEN Refinement, it is essential to perform a global search for an optimum parameter pair. For

each parameter pair tested, multiple refinements are carried out with different randomly selected DEN distances restraints. Here, we performed refinement cycles for 509 pairs of γ, W_{DEN}. Considering that we have 6 copies of the (yNap1core)$_2$-xH2AΔ14/xH2BΔ28 complex in the asymmetric unit, we also applied 6 fold NCS averaging with tight restraints (weights = 500). For B-factor refinement we maintained the original B-factor distribution from the high-resolution models at 6.7 Å and applied an overall anisotropic B-factor refinement, which resulted in an unusual high value of 388.5 (Table 5). The best DEN parameter pair was γ = 0.5 and W_{DEN} = 100, resulting in the lowest R_{free} of 0.31 (Table 5) (Schröder et al. 2010). A schematic representation, including the secondary structure annotation, of the individual components of the complex in the crystal is reported in Figure 22A.

The structure revealed that a single yNap1 dimer binds to one histone H2A/H2B dimer, which means in a stoichiometry of 1:1. That is in agreement with the non-denaturing MS results described in section 3.1.2. The asymmetric unit of the crystal contains six copies of the minimal yNap1core$_2$-xH2AΔ14/xH2BΔ28 complex organized in two layers: three copies at the front and three at the back (Figure 22B-C). yNap1 contains an extended helical dimerization domain and a globular domain that contains a 4-stranded β-sheet (β1-4) on one face and helices α4-8 on the opposite face (Park & Luger 2006b). The yNap1 dimer is arranged in an antiparallel fashion, in a way that the globular domains are positioned on opposite ends and the dimer results in a dome-shaped architecture (Park & Luger 2006b). The concave face of the yNap1 homodimer is the binding site for the H2A/H2B heterodimer (Figure 22D). The yNap1 dimerization domain of each complex is oriented to the center of the structure, while the xH2AΔ14/xH2BΔ28 dimers are orientated to the outer face (Figure 22B). The antiparallel β-hairpin (β5-6) that contains a nuclear localization sequence is disordered in our structure (Figure 22E).

Even though the present structure at low resolution does not allow us to see the amino acids side-chains, the availability of the high-resolution yNap1core and H2A/H2B structures effectively provides atomic details to the structure of the complex and protein interaction interfaces (Figure 22E). The histone heterodimer is position in the Nap1 electronegative cavity in an asymmetric way, being the protein interface mediated by both yNap1 monomers and almost exclusively by H2A (Figure 22D-E). As H2A contains an extra αN

compared to H2B, which interacts with Nap1, the histone heterodimer can only bind Nap1 in such a way and histone H2A/H2B dimer cannot be flipped (Figure 22D-E). Additionally, the N-terminal tails of histones H2A and H2B are pointing towards the acidic cavity of the Nap1 homodimer, suggesting that additional contacts might occur between the histone tails and the Nap1 cavitiy. Analysis of the $2F_0$-F_c electron density map indicates that there would be enough space for the N-terminal tails of H2A and H2B to be accommodated in the Nap1 cavity (Figure 22E). However, further experiments are required to validate this hypothesis.

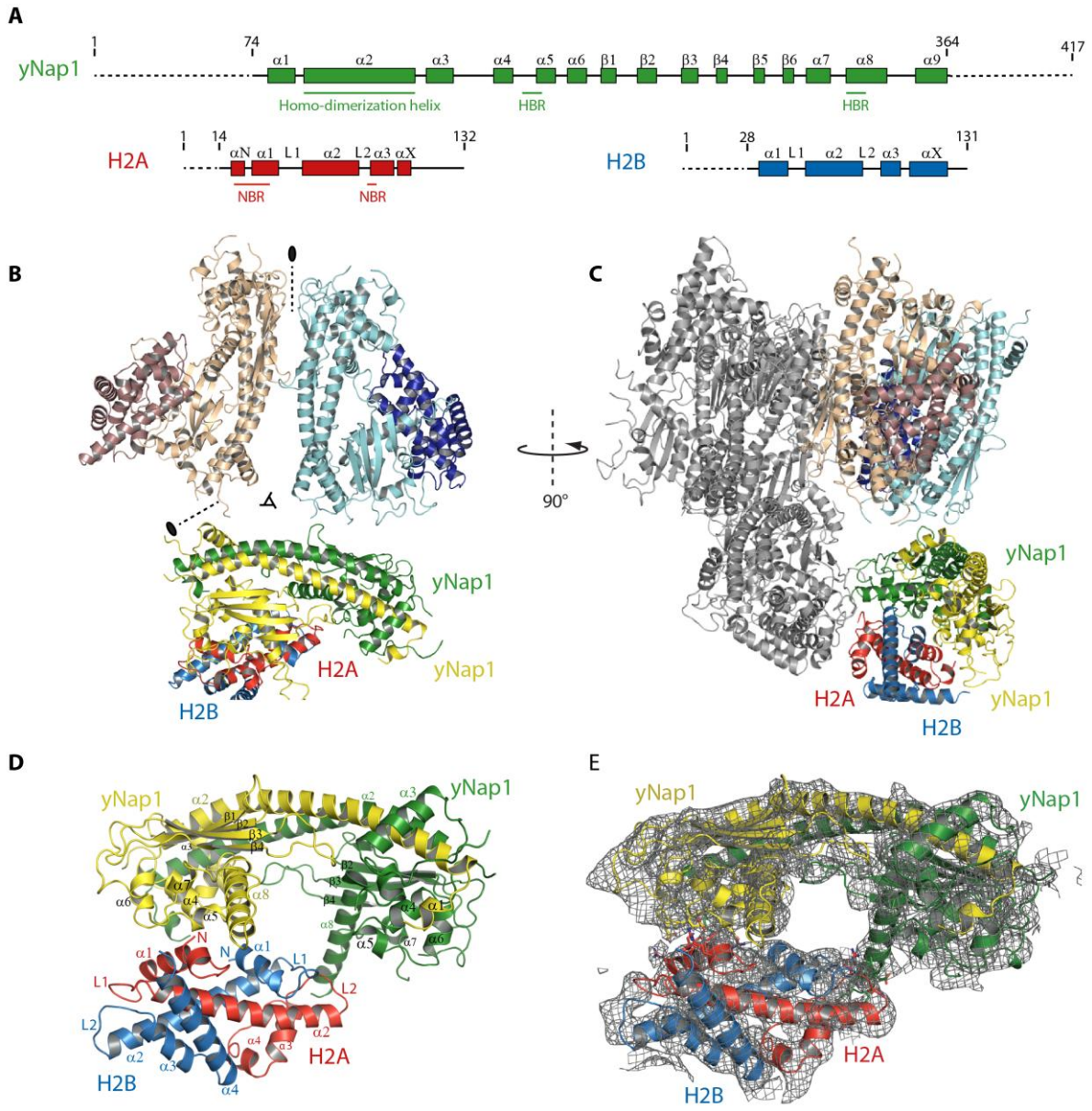

Figure 22 Structure of (yNap1core)$_2$-xH2AΔ14/xH2BΔ28 complex. (A) Schematics of domain architecture of yNap1, xH2A and xH2B. HBR: histone binding region. NBR: Nap1 binding region (B), (C) Alternative views of the crystal structure of (yNap1core)$_2$-xH2AΔ14/xH2BΔ28 complex in the asymmetric unit. Three copies at the back in (B) are omitted for clarity. (D) Detailed view of one repeating unit of the complex. Red: H2A; blue: H2B; green and yellow: yNap1 monomers.

In order to evaluate the potential for model bias of our structure, we calculated a composite omit electron density map for the region comprising xH2AΔ14/xH2BΔ28. Such calculation gave as a result the appearance of the electron density map of the histone heterodimer as in the low-resolution structure discussed here (Figure 23A-B). This indicates that our structural solution is correct.

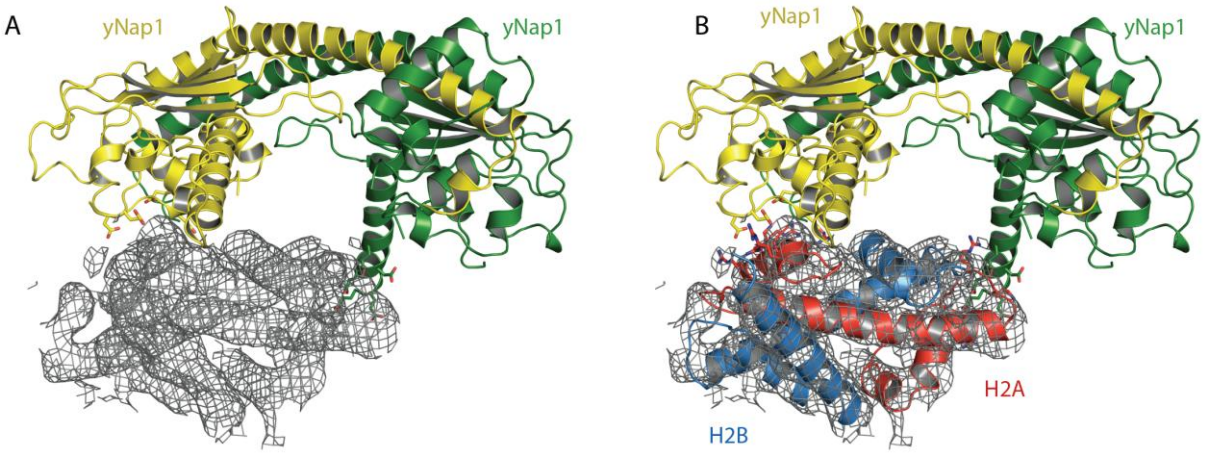

Figure 23 Omit electron density map. (A)(B) $2F_0$-F_c omit electron density map for the region comprising xH2AΔ14/xH2BΔ28 contoured at 1σ. Red: H2A; blue: H2B; green and yellow: yNap1 monomers. *Note: amino acid side-chains are illustrative.*

The H2A/H2B heterodimer, when in complex with yNap1, retains the configuration as seen in the nucleosome structure (Luger, Mäder, et al. 1997a). In the nucleosome core particle, the H2A/H2B heterodimers bind 2.5 turns of DNA double helix, which arcs around them along their long axes to generate a 140° bend (Figure 24B). In this context, the H2A/H2B dimer makes contacts with the nucleosomal DNA through three interaction interfaces which comprise: (a) H2A L1 and H2B L2, (b) H2A α1, and (c) H2A L2 and H2B L1 (Figure 24B). The yNap1 dimer mimics the structure and electrostatics of DNA and provides a concave surface for H2A/H2B binding. This results in yNap1 blocking two of the three DNA interaction interfaces with H2A/H2B (Figure 24).

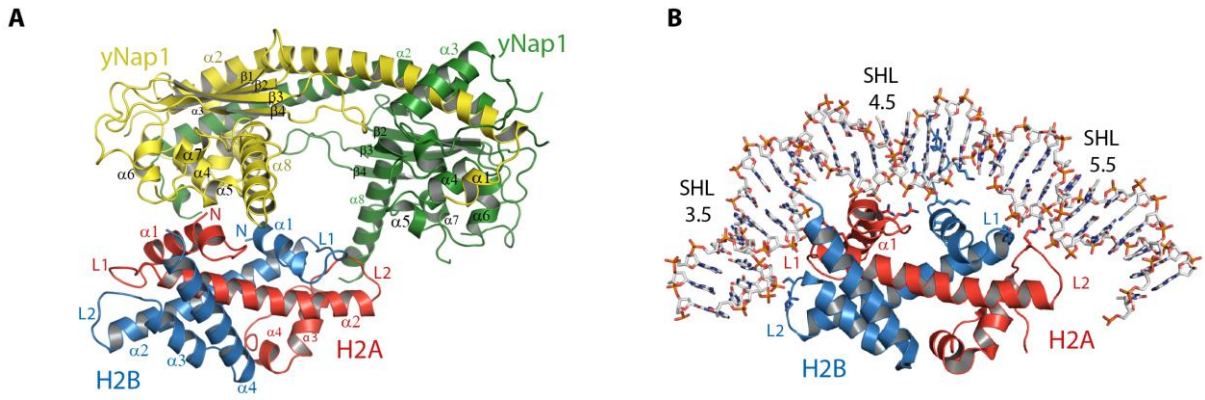

Figure 24 H2A/H2B in complex with Nap1 and in the nucleosomal DNA context. (A) Detailed view of one repeating unit of the complex. (B) H2A/H2B interaction with the nucleosomal DNA. Red: H2A; blue: H2B; green and yellow: yNap1 monomers. *Note: amino acid side-chains are illustrative.*

The H2A/H2B heterodimer is positioned asymmetrically in the electronegative binding cavity of yNap1. As a result, yNap1 engages two of the three DNA binding surfaces of the H2A/H2B with the majority of the contacts towards H2A (Figure 25A). In the centre of the heterodimer, contacts occur between H2A α1 and a segment of yNap1 spanning the C-terminal end of α4 to the N-terminal of α5 (residues 194-205) (Figure 25C). The unique N-terminal helix αN of H2A (residues 16-21) complements this binding interface by packing against E310 of yNap1, which is located in the C-terminal extension of the disordered β-hairpin (β5-β6) (Figure 25C).

On the right side of the H2A/H2B heterodimer, the DNA biding loops L1 of H2B and L2 of H2A pack against the N-terminus of helix α6 of the second yNap1 monomer (residues 328-336) (Figure 25B). The majority of contacts occur between H2A L2 (residues 75-81) and helix α6 of yNap1 (residues 328-336). The positive dipole moments of helix α2 of H2B and α3 of H2A, which are used to bind to the DNA phosphodiester backbone in context of the nucleosome, is capped by this negatively charged patch on helix α6 of yNap1.

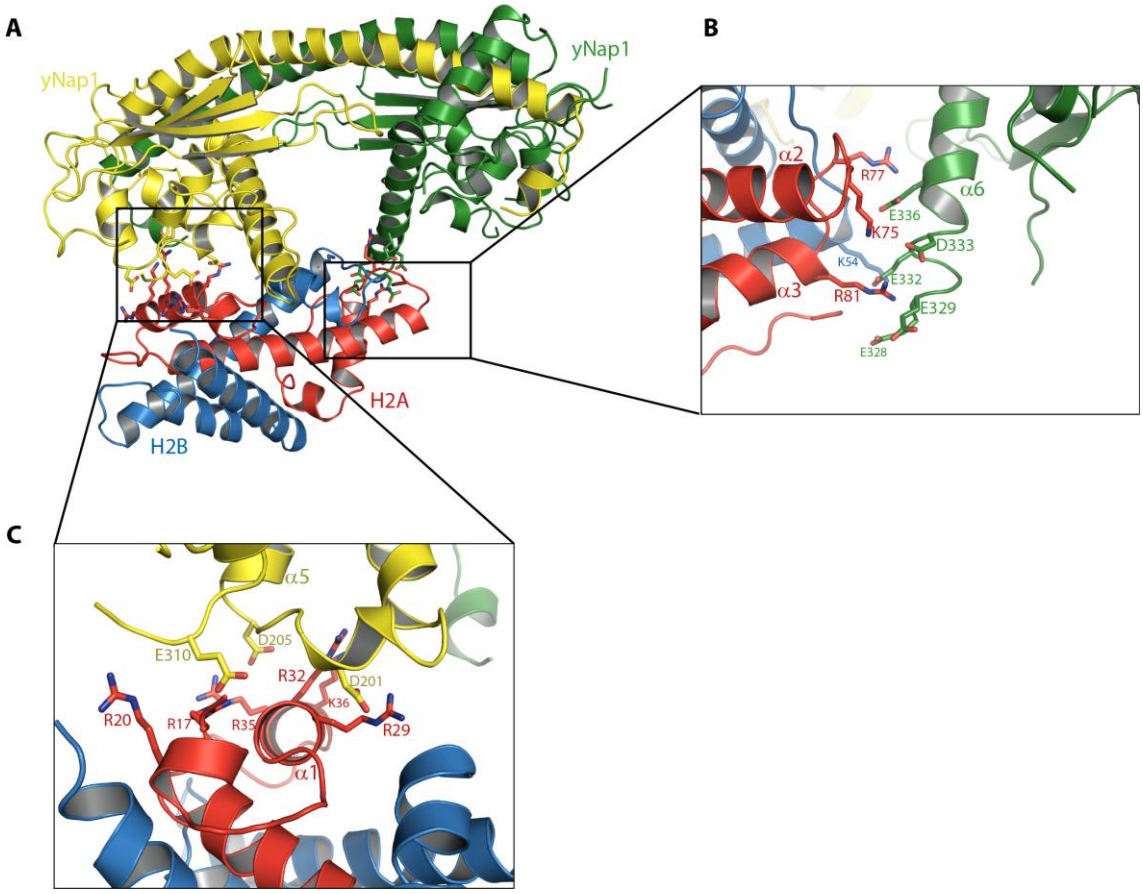

Figure 25 Nap1-H2A/H2B interactions. (A) Ribbon view of the crystal structure of the Nap1-H2A/H2B ternary complex, with the two interaction interfaces highlight boxed in black. (B), (C) Close-up views of interactions made by Nap1 and H2A/H2B heterodimer in the complex. Red, H2A; blue, H2B; green and yellow, Nap1. *Note: amino acid side-chains are illustrative.*

With this structural knowledge in hand, we set out to assess the importance of each of the residues in Nap1 responsible for the interaction with H2A/H2B heterodimers. In order to revert the polarity of the yNap1 interacting surface, residues D201, D205, E310, E332, D333, and E336 were mutated to arginine (R) in the full-length protein. GST-yNap1FL_mutants were used to pull-down untagged dH2A/dH2B heterodimers. All the mutants maintained their capacity to bind histones (Figure 26), indicating that none of these residues is essential for the interaction. However, yNap1 containing single mutations at residues D201, D205 and E310 showed a slightly lower affinity than the *wt*. That suggests that this binding region might contribute more strongly to the interaction.

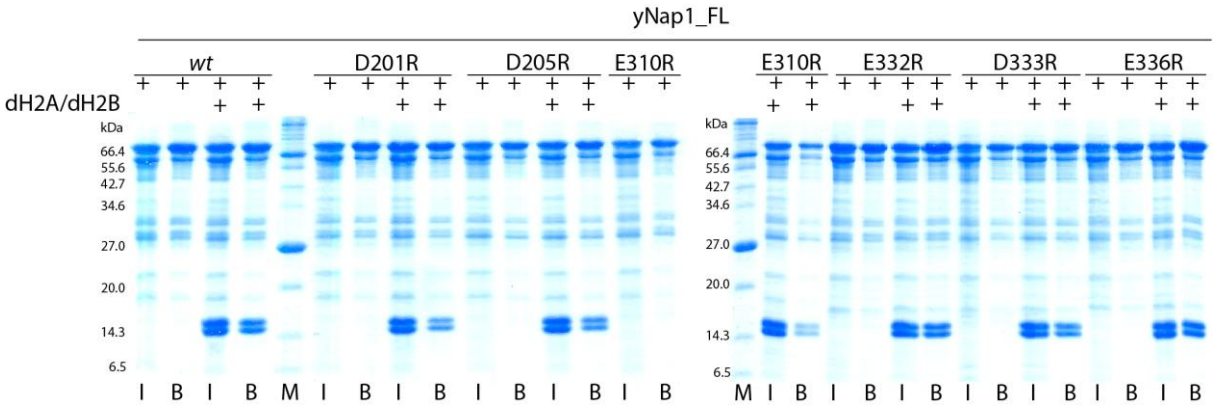

Figure 26 GST pull-down with yNap1_FL and dH2A/dH2B heterodimers. Protein names and mutations are indicated above the gels. The molecular weight (kDa) of the marker is given. M, marker; I, input; B, bound. Proteins are visualized by Coomassie blue staining.

This structure also provides insights in the oligomerization process. It shows the presence of six copies of the repeating unit (yNap1$_2$-H2A/H2B) in the asymmetric unit, which might correspond to the biggest oligomer observed by non-denaturing MS. yNap1$_2$-H2A/H2B oligomerization might be driven by two small polar interfaces present in the asymmetric unit between (a) two Nap1 monomers (Figure 27A-B) and (b) two H2A proteins (Figure 27C-D) from different sub-complexes. These interfaces are either positively or negatively charged, consistent with the salt-dependence of oligomerization suggesting that it is driven largely by electrostatic interactions.

The yNap1 interface is made up of residues from the flexible loop connecting β1 and β2 and the beginning of β3 (Figure 27A-B). This interface is rich in serine and threonine residues, which suggests that upon phosphorylation, oligomerization might be abolished. In order to test that hypothesis, two residues on that loop (S237 and T244) were substituted by aspartic acid (D) in yNap1*wt*; mutations to D are used to mimic the volume and charge of a phosphorylated residue. In addition, the residue D246, also located in that loop, was substituted by arginine (R).

The H2A interface involves the C-terminal docking domain containing residues of α3 and αC (Figure 27C-D). This C-terminal docking domain interacts with H3/H4 tetramer in the context of the nucleosome. We predicted that four residues in this interface are important for oligomerization: N94, G98, R99, and T101. These residues were mutated to glutamic acid (E)

and aspartic acid (D), respectively the first residue and the following three. Analysis of these mutations in these interfaces is currently on-going.

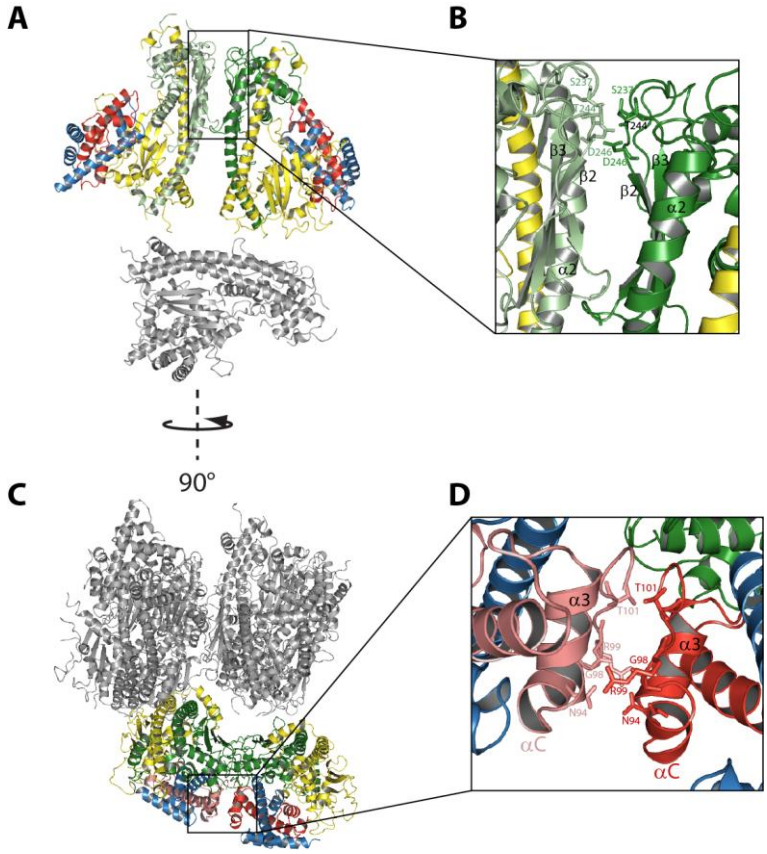

Figure 27 Putative oligomerization interfaces. (A), (C) A ribbon view of the crystal structure of the yNap1-H2A/H2B ternary complex, with the two putative oligomerization interfaces highlight boxed in black. In (A) three copies from the back are removed for clarity. (B), (C) Close-up views of interactions made in the putative oligomerization interfaces. H2A is coloured in red, H2B in blue and yNap1 in green and yellow. *Note: amino acid side-chains are illustrative.*

3.1.4. Electron microscopy of yNap1 – histone complexes

In order to further investigate how the crystal structure relates to yNap1$_2$-H2A/H2B assembly in solution, the (yNap1core)$_2$-xH2AΔ14/xH2BΔ28 complex, which is the same construct present in the crystal structure, was visualized by negative stain electron microscopy (EM). Electron micrographs revealed particles of similar size, about 15 nm in diameter, but with varying structural features. This observation indicated that there are different orientations of the particles on the carbon support film (Figure 28A). Size and shape of representative negatively-stained particles marched well with projections from a 20 Å resolution filtered crystal structure of the ((yNap1core)$_2$-xH2AΔ14/xH2BΔ28)$_6$ complex

(Figure 28B-C). Similar particles were seen with the complex containing full-length versions of the proteins (data not shown). Together, both the non-denaturing MS and EM measurements confirm that the assembly seen in the asymmetric crystallographic unit is relevant for yNap1$_2$-H2A/H2B oligomerization in solution.

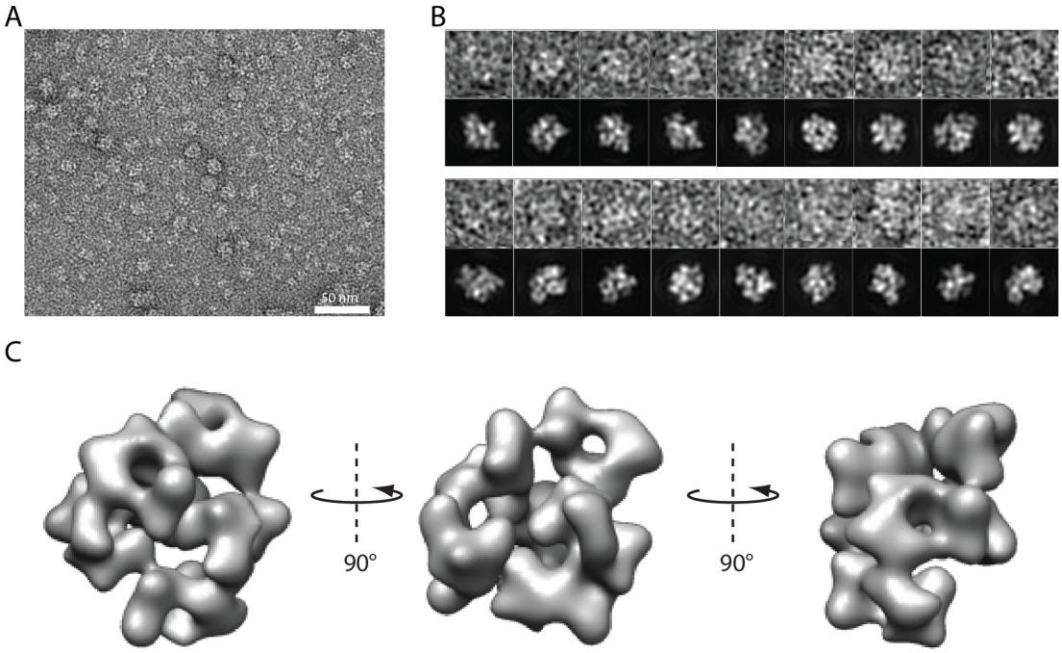

Figure 28 Negative stain EM images of yNap1core-xH2AΔ14/xH2BΔ28 complex. (A) Negative stain EM image. (B) Comparison between single particles (upper row) and yNap1core-xH2AΔ14/xH2BΔ28 structure projections (lower row). (C) Low resolution map of the yNap1core-xH2AΔ14/xH2BΔ28 structure.

3.2. STRUCTURAL STUDIES ON MOUSE NAP1 – HISTONE COMPLEXES

3.2.1. Binding studies of mouse Nap1 and linker Histone H1 complexes

In higher eukaryotes, binding of Nap1 with the linker histone H1 induces a more open and extended chromatin conformation with an increased internucleosomal distance (Kepert et al. 2005). To understand this interaction in more detail, we decided to study the interaction between mNap1 and the linker histone H1. Knowing that the interaction between the yeast chaperone and the core histones H2A/H2B is occurring through the globular domain of the histones, we hypothesized that it would be the same for the linker histone H1. In order to test this hypothesis, pull-down assays were performed using His-tagged mNap1*wt* and untagged histone H1Δ100 or GH1 (Figure 29A). Control reactions showed that only His-tagged mNap1*wt* interacted with the Ni^{2+} beads (Figure 29B). The mNap1*wt*-H1Δ100 interaction was confirmed by this assay (Figure 29C). However, GH1 was not sufficient to form a complex with mNap1*wt* (Figure 29C). These results suggest that the N-terminal tail and/or residues 112-127 of H1 are important for mNap1 interaction. From here on, only H1Δ100 was used for further characterization of the mNap1-H1 complex.

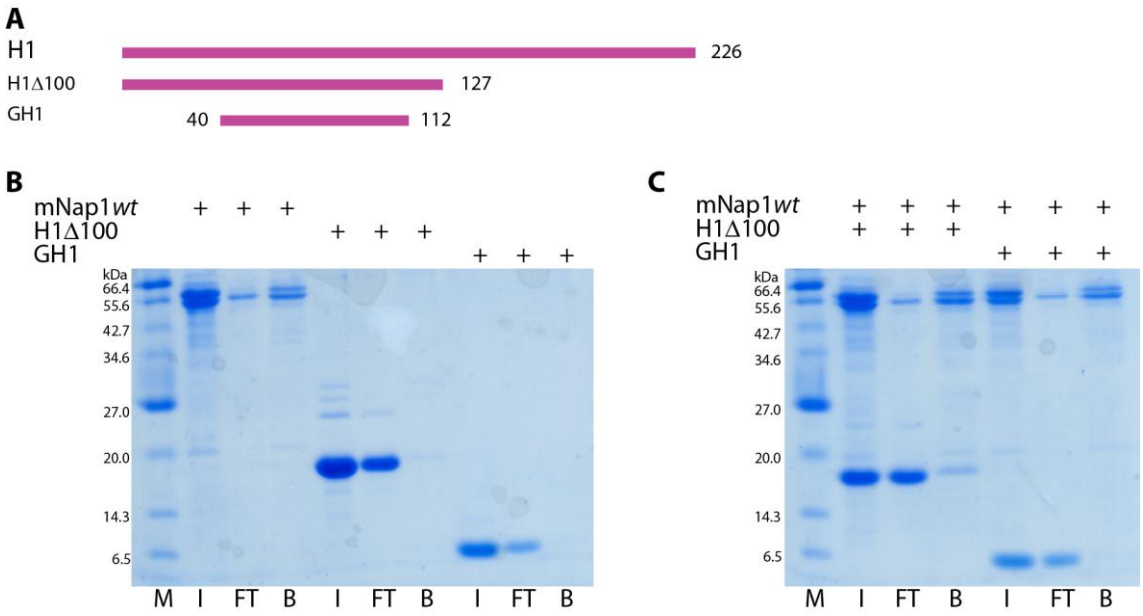

Figure 29 His pull-down with mNap1*wt* and linker histone H1. (A) Schematic representation of the H1 constructs used in this study. SDS-PAGE gels showing His pull-downs: controls (B) and reactions (C). Protein names are indicated above the gels. The molecular weight (kDa) of the marker is given. M, marker; I, input; FT, flow through; B, bound. Proteins are visualized by Coomassie blue staining.

In order to identify the regions of mNap1 that interact with the linker histone H1, limited proteolysis on the mNap1*wt*-H1Δ100 complex was performed using an initial set of twelve proteases. Samples exhibiting interesting banding patterns are shown in Figure 30A. Identification of the fragments of interest by N-terminal sequencing and MS showed that the N-terminal region of mNap1 is very sensitive to proteolysis. These results indicate that the interaction between the two components of the complex occurs through the central and the C-terminal region of mNap1 or both.

Accordingly to the results obtained from the limited proteolysis, MS, and N-terminal sequencing, new constructs lacking the N-terminus of mNap1 were designed: mNap1Δ36, mNap1Δ50 and mNap1Δ63. In addition, a fourth construct was designed base on the sequence alignment with yNap1: mNap1core (residues 63 to 347). A schematic representation of these mutants is shown in Figure 30B.

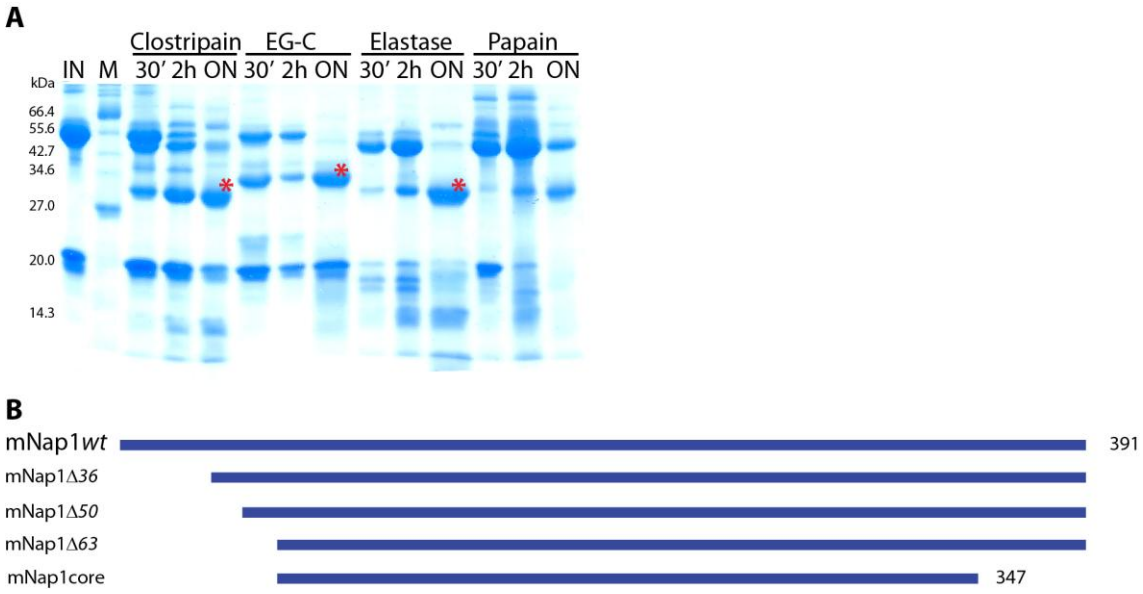

Figure 30 Identification of the mNap1*wt* interacting regions with H1Δ100. (A) SDS-PAGE analysis of the limited proteolysis of the mNap1*wt*–H1Δ100 complex. Incubation time in minutes (‘), hours (h) and overnight (ON) is indicated above the gels. Proteases as well as molecular weight (kDa) of the marker are given; EG-C, Endoproteinase Glu-C. Protein fragments were visualized by Coomassie blue straining. Bands analysed by N-terminal sequencing are indicated by *. (B) Schematic representation of the mNap1 constructs used in this study.

Finally, the mNap1–H1 interacting regions were confirmed by *in vitro* complex reconstitution and size-exclusion chromatography. Complex formation between mNap1 and H1Δ100 was always achieved when the linker histone was mixed with mNap1*wt* or deletion mutants at the N-terminus (Figure 31A-B). However, when H1Δ100 was mixed with mNap1core, no complex formation was observed (Figure 31C). From these results, we conclude that the C-terminal region of mNap1 is important for complex formation.

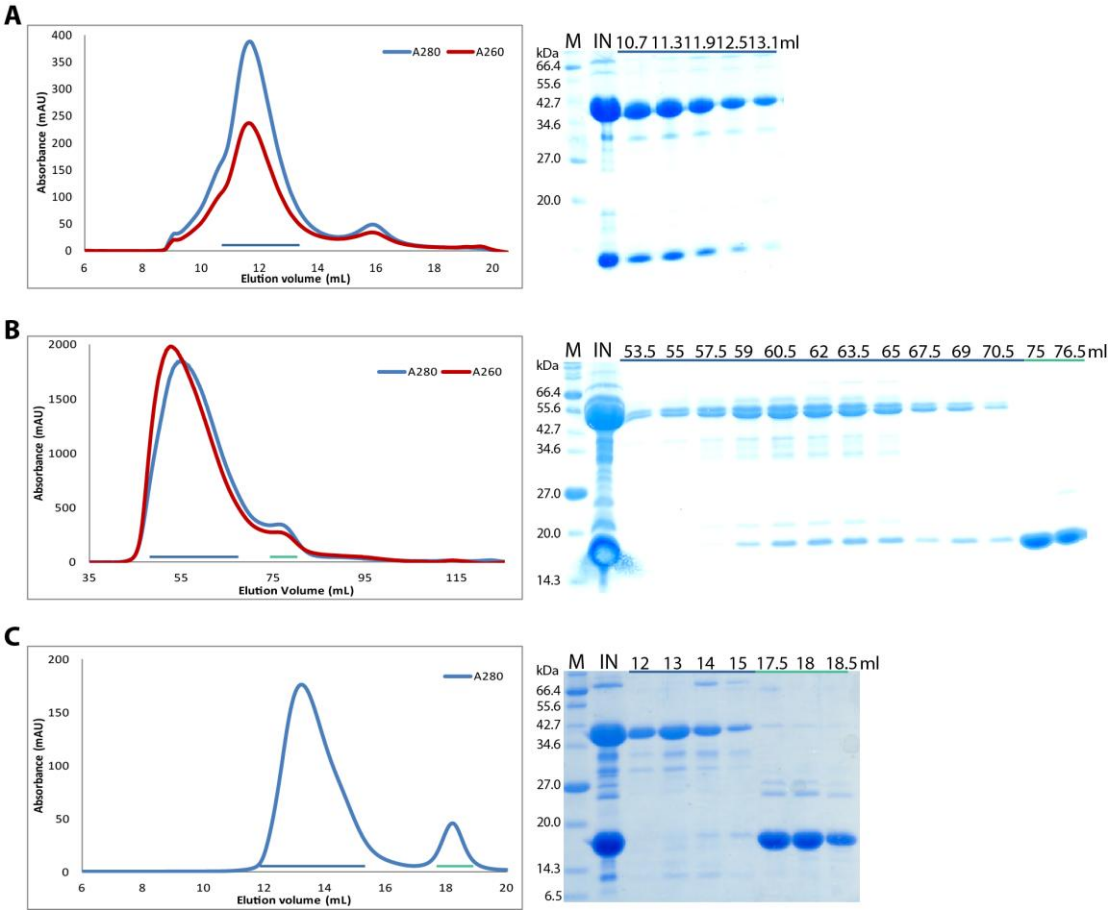

Figure 31 mNap1-H1 complex reconstitution. Chromatograms showing the elution profiles of mNap1*wt* – H1Δ100 complex (A), mNap1Δ63 – H1Δ100 complex (B) and mNap1core-H1Δ100 complex (C) using a Superdex S200 or a Superose 6 size-exclusion column. Absorbance at 280 nm (blue) and 260 nm (red) were measured to detect protein and nucleic acid elution, respectively. Each panel contains the corresponding SDS-PAGE gel showing the protein content of the peak fractions. The name of the proteins as well as the molecular weight (kDa) of the protein marker is given. mNap1Δ36 and mNap1Δ50 in complex with H1Δ100 are not shown to avoid repetition.

Our observations are in accordance with the literature. It has been reported that the C-terminal acidic segment of *Xenopus* Nap1 is required for complex formation with the linker histone B4, a histone H1 variant in *Xenopus* eggs (Shintomi et al. 2005).

3.2.2. Crystallization of mouse Nap1 – Linker Histone H1 complexes

Crystallization trials of the complex formed by mNap1*wt*-H1Δ100, mNap1Δ36-H1Δ100, mNap1Δ50-H1Δ100, and mNap1Δ63-H1Δ100 were carried out at 20ºC and 4ºC with several protein concentrations. Yet they have not yielded crystals. Further optimization of the protein constructs might be needed in the future.

3.2.3. Characterization of the oligomeric state of mNap1 – H1Δ100 complex

The mNap1*wt*-H1Δ100 complex has been characterized by native PAGE gels, which showed the co-existence of several oligomers. A titration of mNap1 with increasing concentration of H1Δ100 revealed the formation of four species (Figure 32). Additional analysis by non-denaturing MS confirmed the heterogeneity of the sample and allowed us to assign the bands observed in the native PAGE gels to mNap1wt_2, mNap1wt_2-H1Δ100, (mNap1wt_2)$_2$ and (mNap1wt_2-H1Δ100)$_2$ (Figure 33A).

The stoichiometry of Nap1 – Histone complexes has been of interest. By non-denaturing MS analysis, we identified the stoichiometry of the (mNap1*wt*)$_2$-H1Δ100 complex as a ratio of 1:1 (dimer/monomer) (Figure 33A).

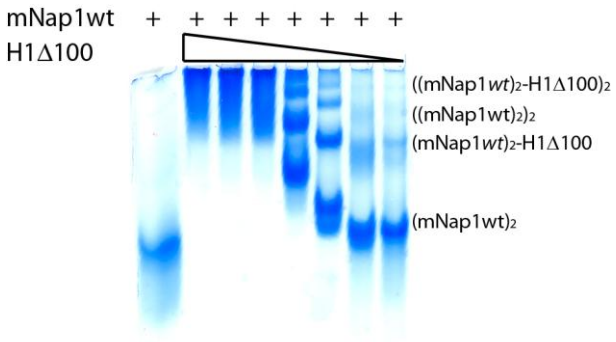

Figure 32 First evidences of mNap1-H1 oligomerization. Titration of mNap1*wt* with increasing concentration of H1Δ100 analysed by Native-PAGE gels and visualized by Coomassie blue staining.

Post-translational modifications are known to modify the activity of enzymes or the localization of proteins in the cell. *Drosophila* Nap1 is phosphorylated by CKII, which induces its translocation between cytoplasm and nucleus (M. Li et al. 1999). We hypothesised that phosphorylation may not only influence the cellular localization of the protein but also its oligomeric state. In order to test this hypothesis, the mNap1wt_2-H1Δ100 complex was phosphorylated by CKII and its phosphorylation state was confirmed by MS (six phosphorylated residues were detected per mNap1 monomer). Analysis of the phosphorylated sample by non-denaturing MS detected only (mNap1*wt*)$_2$-H1Δ100 complexes and not higher ordered oligomers (Figure 33B). This result revealed that phosphorylation of the mNap1-H1 complex might abolish oligomerization.

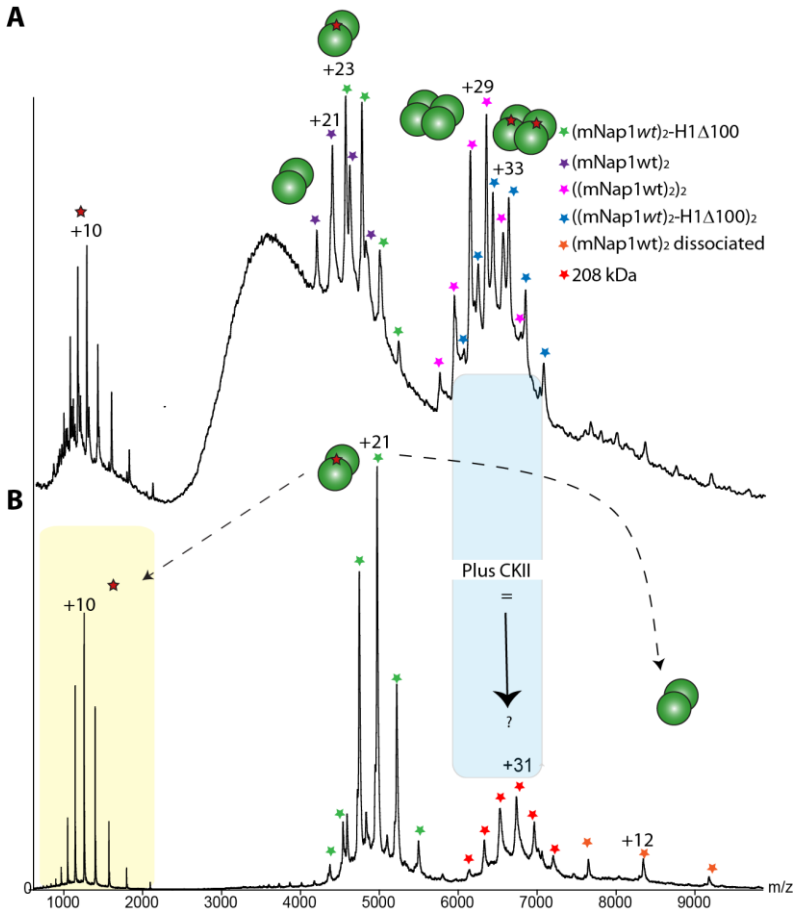

Figure 33 mNap1-H1 complex oligomerization. Non-denaturing mass spectrometry of non-phosphorylated (A) and phosphorylated (B) mNap1*wt* – H1Δ100 complex.

3.3. DISCUSSION

A pure yNap1 – H2A/H2B complex was obtained. A number of variants for the yNap1 protein and the histones H2A and H2B have been used in this study. All of them have been successfully cloned and recombinantly expressed in *E. coli* BL21 (DE3). After purification of the individual components and refolding of the histone H2A/H2B dimer, the yNap1–H2A/H2B complex was *in vitro* reconstituted and isolated by size-exclusion chromatography to high yields and purity.

yNap1$_2$ interacts with H2A/H2B dimers in a stoichiometry of 1:1. The binding stoichiometry of the yNap1–H2A/H2B complex is surrounded by controversy. It has been proposed that Nap1 interacts with H2A/H2B dimers using two distinct stoichiometries: (a) in a 1:1 ratio where one Nap1 dimer binds one histone dimer (McBryant et al. 2003; Newman et al. 2012), and (b) in a 1:2 ratio where one Nap1 dimer binds two histone dimers (Andrews et al. 2008). It has also been claimed that human Nap1 binds to H2A/H2B dimers in both stoichiometries depending on the preparation of the sample (Noda et al. 2011). Here, we demonstrate using MS and X-ray crystallography that yNap1$_2$ binds to one H2A/H2B heterodimer. Indeed, visual inspection of the yNap1$_2$-H2A/H2B complex indicates that a second copy of the H2A/H2B heterodimer cannot be accommodated in the yNap1 cavity.

The structure presented here also provides insights in the interaction of the histone chaperone with the H2A/H2B heterodimer. This interaction is mediated by both yNap1 monomers and almost exclusively by H2A. The H2A/H2B heterodimer showed the same configuration as in the nucleosome, while Nap1 dimer mimics the structure and the electrostatics of the DNA, providing a concave surface for the histone binding. This structural "mimicry" by yNap1 of DNA interactions with H2A/H2B heterodimers provides a mechanism for the yNap1 chaperone activity and its role in nucleosome assembly/disassembly. yNap1 does not block association of H2A/H2B with the tetrasome, suggesting that nucleosome assembly occurs through a transient yNap1-H2A/H2B-tetrasome complex that is resolved by DNA binding to the free H2A L1 and H2B L2 loops. DNA "strand invasion" into the yNap1-H2A/H2B complex is then predicted to result in yNap1 displacement and full nucleosome assembly. This model needs further investigation.

Histone H2A/H2B dimer triggers $(yNap1)_2$ – H2A/H2B oligomerization to a final $((yNap1)_2$-H2A/H2B$)_6$. yNap1 is an obligate dimer (Park & Luger 2006b) that has been described to further self-associate in an equilibrium of dimer-octamer-hexadecamer in solution under physiological conditions (Tóth et al. 2005). In our studies, we could only detect self-association of yNap1 to dimer-tetramer equilibrium at low ionic strength. However, when H2A/H2B dimers were in complex with yNap1, distinct oligomerization states were observed at low ionic strength by non-denaturing MS. Analysis of (yNap1*wt*)$_2$-dH2A/dH2B, (yNap1coreΔ284-308)$_2$-xH2AΔ14/H2BΔ28 and (yNap1Δ1-73)$_2$-xH2AΔ14/H2BΔ28 samples showed the formation of complexes that contain up to two copies of the repeating unit: ((yNap1)$_2$-H2A/H2B)$_2$. And analysis of the (yNap1Δ366-417)$_2$-xH2AΔ14/H2BΔ28 sample showed complexes containing five copies, while (yNap1core)$_2$-xH2AΔ14/H2BΔ28 sample showed complexes containing six copies (corresponding to a molecular weight of 545 kDa). That allowed us to identify the regions of yNap1 that play important roles in oligomerization. The acidic C-terminal region might inhibit oligomerization. Previously it was shown that a β-hairpin structure (residues 284 to 308) that is involved in a crystal contact in the yNap1 dimer structure is also involved in yNap1 oligomerization in solution (Park et al. 2008). Removal of the β-hairpin abolishes formation of the ((yNap1)$_2$-H2A/H2B)$_6$ but still allows formation of a complex containing two copies of the repeating unit: ((yNap1)$_2$-H2A/H2B)$_2$.

As mention above, (yNap1core)$_2$-xH2AΔ14/H2BΔ28 forms a complex containing six copies of this repeating unit. Interestingly, the asymmetric unit of the crystal of that complex contains six copies of the (yNap1core)$_2$-xH2AΔ14/H2BΔ28 repeating unit. That suggests that the crystallized oligomeric state is exactly the complex detected by non-denaturing MS and negative stain EM, which could be the biological relevant oligomer of the (yNap1)$_2$-H2A/H2B complexes. Two novel putative oligomerization interfaces were identified in the crystal structure between two Nap1 monomers and two histones H2A. Mutagenesis of key residues in these interfaces and analysis of the chaperone-histones complexes by non-denaturing MS is now on-going. Phosphorylation of the Nap1-H2A/H2B complex abolished oligomerization, suggesting that this post-translational modification might regulate the oligomeric state of the complex *in vivo*. Phosphopeptide mapping studies indicate that residues T53, S82, S140, S159, T163, T177, S343, S397 of yNap1 are phosphorylated by CKII, as already described (Calvert et al. 2008). However, positioning of these residues on the (yNap1$_2$-H2A/H2B)$_6$

structure indicated that they are not in the putative Nap1-Nap1 oligomerization interface. This observation suggests that CKII phosphorylation might regulate Nap1 oligomerization not by disrupting the Nap1-Nap1 surface but by another mechanism. Further investigation is needed to understand how phosphorylation regulates oligomerization.

The H1 globular domain is not sufficient for binding with mNap1. In higher eukaryotes, Nap1 has been described to not only bind H2A/H2B dimers but also the linker histone H1. Pull-down assays were used to identify the essential regions of the linker histone H1 that interact with mNap1. Our results showed that GH1 does not bind mNap1*wt*. However, H1Δ100 formed a stable complex with mNap1*wt* and its N-terminal deletion mutants, which survived size-exclusion chromatography. These results suggest that either the N-terminus and residues 113 to 127 in the linker histone H1 or both are essential for mNap1 binding. On the other hand, limited proteolysis, N-terminal sequencing and MS of the mNap1*wt*-H1Δ100 complex, as well as the sequence alignment of Nap1 homologs, allowed us to design a new mNap1 construct: mNap1core (residues 63 to 347). *In vitro* reconstitution and size-exclusion chromatography of the mNap1core-H1Δ100 complex showed no binding between the two proteins. This suggests that **the acidic C-terminal region of mNap1 is essential for binding of the linker histone H1**.

mNap1$_2$ interacts with the linker histone H1 in a stoichiometry of 1:1. In *Xenopus* eggs, xNap1 monomer has been shown to bind the linker histone B4 (an histone H1 variant) in a stoichiometry of 2:1 (Shintomi et al. 2005). Non-denaturing MS revealed that mNap1 also binds to linker histones in a stoichiometry of one Nap1 dimer to one H1 monomer. We also detected oligomerization of the mNap1-H1 complex up to two copies of the repeating unit: ((mNap1)$_2$-H1Δ100)$_2$. Phosphorylation of the complex inhibits oligomerization.

4. SYNERGISTICAL ACTION OF Nap1 AND p300 IN TRANSCRIPTION

RESUME EN FRANÇAIS

L'histone chaperonne Nap1 et l'histone acétyle-transférase p300 travaillent en synergie dans la phase de transcription afin d'expulser le nucléosome dans les régions promotrices de l'ADN. Dans cette étude, nous avons analysé l'interaction entre ces deux facteurs en présence et en l'absence d'histone H2A/H2B hétérodimère, par des expérience de *pull-down*. Celles-ci ont montré que l'interaction entre Nap1 et p300 n'est pas médiée par l'histone H2A/H2B dimère et que l'interaction directe entre les deux facteurs est faible ou non existante.

Il a été suggéré que cette interaction est médiée par le KIX et le CH3 domaines de p300. Ici, nous nous focaliserons sur le domaine CH3 en raison de sa proximité avec la région catalytique centrale de p300. L'hypothèse du rôle de régulation du domaine CH3 sur l'activité de p300 a été proposée ((Reynoird et al. 2010)). Il suggère que le domaine CH3 se replie sur la région catalytique de p300 (domaine HAT) ce qui a pour effet d'inhiber l'activité acétyle-transférase de p300. Lors de la liaison d'un des partenaire de p300 tel que Nap1, le domaine HAT serait libéré ce qui permet son (trans-) auto-acétylation et par conséquent l'activation de p300. Cependant les expériences de pull-down réalisées n'ont montrées aucune interaction significative entre le domaine CH3 de p300 avec d'autres domaines de p300 tels que le Bromodomain, le RING, le PHD ou le HAT de la région centrale de p300. Ceci vient donc nuancer le modèle établi sans toutefois l'infirmer.

4.1. CHARACTERIZATION OF HISTONE CHAPERONES AND ACETYL-TRANSFERASES INTERACTION

It has been suggested that the histone acetyltransferase p300 and the histone chaperone Nap1 work synergistically to remove the nucleosomes at the promoter regions and allow transcription to start. Here, we attempt to demonstrate that p300 and Nap1 physically interact, as it has been suggested in the literature (Shikama et al. 2000; Asahara et al. 2002).

We used three hNap1 homologs: hNap1-L1, hNap1-L2, and hNap1-L4. GST-tagged hNap1-L# constructs were used to pull-down FLAG-tagged p300_short (residues 324 to 2094) encompassing the KIX and the CH3 domains. Control samples of the proteins alone against the GST beads showed high binding of the GST-tagged proteins and no binding of the untagged dH2A/H2B dimers (Figure 34A). However, a small fraction of p300_short exhibited unspecific binding with the beads (Figure 34A). As shown in Figure 34B, none of the pull-down reactions showed direct interaction between Nap1 and p300. These results reveal that Nap1 and p300 do not interact strongly in this assay.

Furthermore, these results suggest that the interaction might occur through a mutual binding partner. We proposed that the intermediate could be the histone H2A/H2B dimer. However, GST-tagged hNap1-L# could not pull-down p300_short in the presence of histone H2A/H2B dimers (Figure 34B), indicating that the histone dimer is not the intermediate that we were looking for.

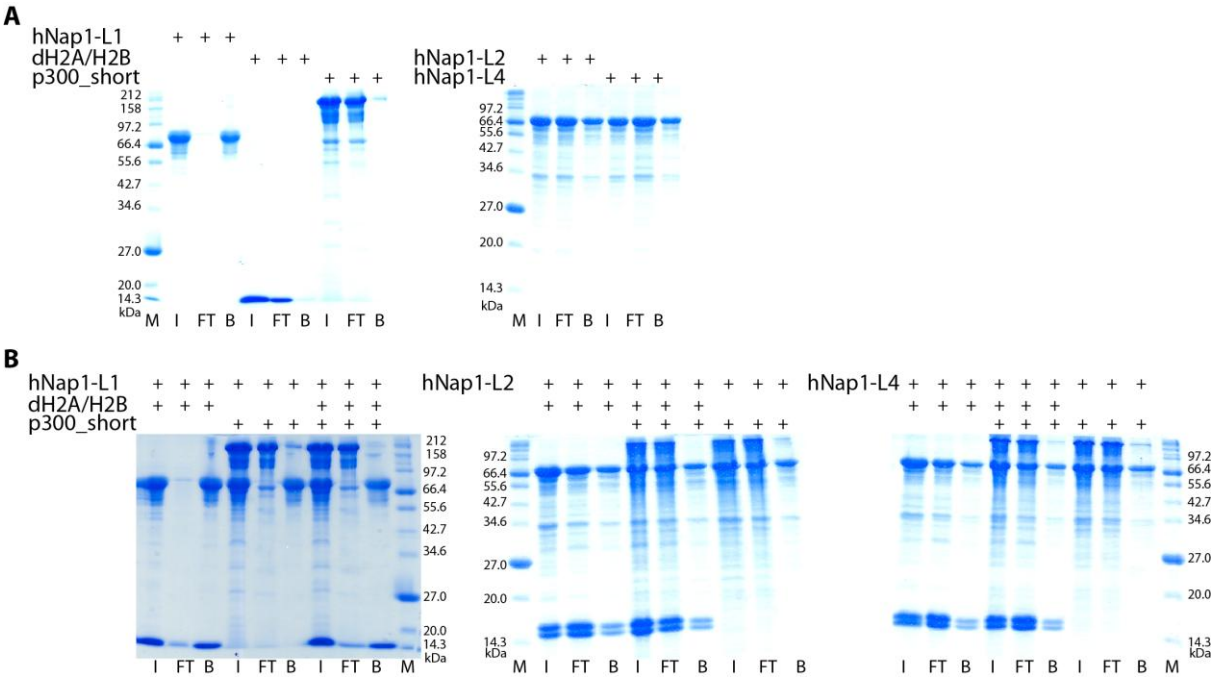

Figure 34 Nap1-p300 interaction in presence and absence of H2A/H2B. SDS-PAGE gels showing GST pull-down assays: controls (A) and GST_hNap1-L1, GST_hNap1-L2 and GST_hNap1-L4 with FLAG_p300_short, in presence or absence of H2A/H2B dimers (untagged) (B). Protein names are indicated above the gels. The molecular weight (kDa) of the marker is given. M, marker; I, input; FT, flow through; B, bound. Proteins are visualized by Coomassie blue staining.

4.2. REGULATORY ROLE OF P300_CH3 DOMAIN IN HAT ACTIVITY

It has been suggested that Nap1 interacts with the CH3 domain of p300 (Shikama et al. 2000). A number of other ligands are also known to interact with the CH3 region and to modulate p300 HAT activity. For example, NUT (nuclear protein in testis) has been suggested to regulate the HAT activity of p300 upon binding to the CH3 domain by making the enzyme more active (Reynoird et al. 2010). However, how ligand binding to the CH3 domain regulates p300 HAT activity is poorly understood. We hypothesized that the CH3 domain folds back to the central region of p300 auto-inhibiting the HAT domain.

To test this hypothesis, two constructs were designed: one containing the p300'core' plus the ZZ motive (p300'core'_ΔloopY1467F_ZZ) and another comprising the entire CH3 domain (p300'core'_ΔloopY1467F_ZZ_TAZ2) (Figure 35A). The proteins were recombinantly expressed in insect cells and purification yielded good amounts of the protein samples at good purity. MS analysis revealed that the samples were not homogeneous, containing up

to six acetylations for p300'core'_ΔloopY1467F_ZZ and four acetylations for p300'core'_ΔloopY1467F_ZZ_TAZ2 (Figure 35B-C).

In order to get a more homogeneous sample, both constructs were deacetylated by SIRT2. Analysis of the proteins by MS after deacetylation revealed that p300'core'_ΔloopY1467F_ZZ was deacetylated (Figure 35B), whearas the p300'core'_ΔloopY1467F_ZZ_TAZ2 construct showed the identical MS profile as seen before SIRT2 treatment (Figure 35C).

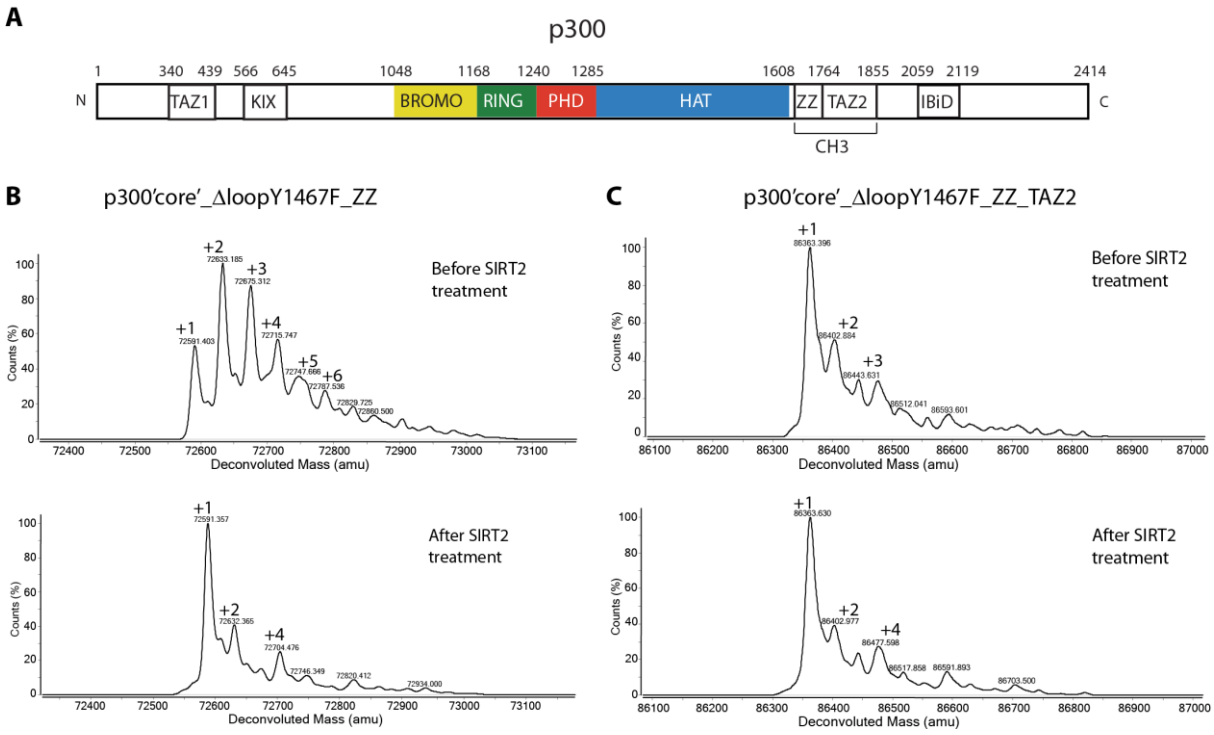

Figure 35 Schematic representation of the domain organization of p300 (A). Regular mass spectrometry analysis of p300'core'_ZZ (B), and p300'core'_ZZ_TAZ2 (C) before and after deacetylation by SIRT2. *Note: each acetylation increases the molecular weight of the protein by 42 Da.*

These results support the hypothesis that the CH3 domain plays a role in the auto-regulation of the HAT activity of p300. They also suggest that the TAZ2 domain alone is necessary to inhibit (auto-) acetylation of p300, and therefore most likely its activation. The fact that the construct containing the entire CH3 presents only one acetylation might be an indication that the CH3 domain folds back on the central region of p300 and prevents acetylation of

other residues, making them less accessible for an active p300 or another acetyl-transferases.

Determination of the crystal structure of any of those constructs would bring insights in the arrangement of the CH3 domain in respect to the p300'core'. And interpretation of that arrangement would allow us to understand the mechanism by which the CH3 domain auto-regulates p300. Crystallization trials of p300'core'_ΔloopY1467F_ZZ and p300'core'_ΔloopY1467F_ZZ_TAZ2 at 20ºC and 4ºC were performed. Unfortunately, it has not been possible to obtain crystals of any of these constructs.

Because of the lack of structural information on the p300'core'_ΔloopY1467F_ZZ and p300'core'_ΔloopY1467F_ZZ_TAZ2 constructs, we studied the interaction by pull-down assays. The GST-p300_CH3 construct was used to pull-down individual domains or modules of p300. Controls of the GST-p300_CH3 and the untagged p300_BRP, p300_BPΔR, and p300_HATΔloopY1467F against GST beads were performed. The results showed that only the tagged protein was able to bind to the GST resin, and discarded any non-specific interaction of the untagged proteins with the resin (Figure 36A-B).

However, GST-p300_CH3 was not able to pull-down p300_BRP, p300_BPΔR, and p300_HATΔloopY1467F (Figure 36A-B). These results suggest that the CH3 domain do not strongly bind to the effector module or the catalytic domain of the enzyme. But we cannot discard a scenario where both, the BRP module and the HAT domain, are needed to detect the interaction.

We tested this hypothesis by pull-down of the untagged p300'core'_Y1467F against GST-p300_CH3, and we could not detect any interaction (Figure 36C). These results indicate that the interaction of the CH3 domain with the central region of p300 is weak or not existing.

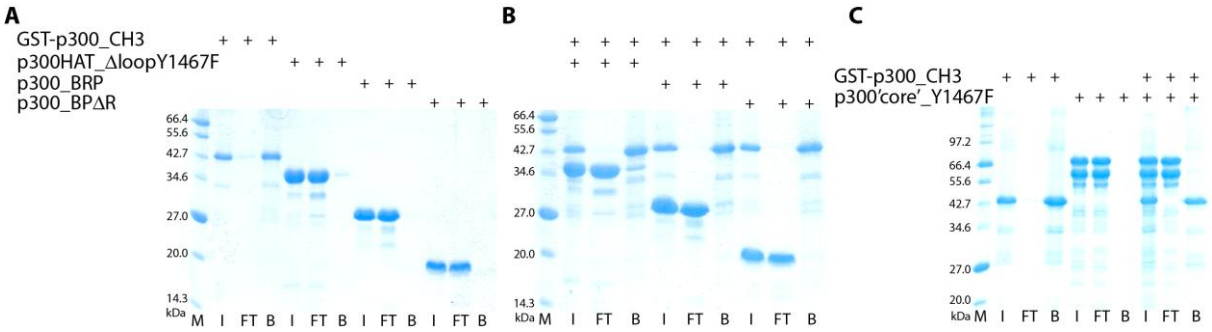

Figure 36 p300 central region interaction with the CH3 domain. SDS-PAGE gels showing GST pull-down assays: individual domain controls (A), GST-p300_CH3 with p300HAT_DloopY1467F, p300_BRP, and p300_BPΔR (B), and GST-p300_CH3 with p300'core'_Y1467F controls and reaction (C). Protein names are indicated above the gels. The molecular weight (kDa) of the marker is given. M, marker; I, input; FT, flow through; B, bound. Proteins are visualized by Coomassie blue staining.

4.3. DISCUSSION

hNap1 does not directly interact with p300. Our results contrast with those of (Asahara et al. 2002), who reported binding between mNap1 and the mouse p300 homolog CBP. Asahara et al. used whole cell extracts for pull-down assays while we used purified recombinant proteins. This suggests two possibilities, one where Nap1 and p300 do not bind each other directly but indirectly through a mutual binding partner. We have shown here that the intermediate is not the H2A/H2B dimer. Another possibility is that the interaction between Nap1 and p300 is not strong enough to be detected by our assay, meaning that the two proteins don't form a stable complex.

The TAZ2 motive inhibits (auto-) acetylation of p300. The p300 central region contains four domains: a Bromodomain, a RING domain, a PHD finger (effector module), and a HAT domain (catalytic domain). C-terminal to the core is a CH3 domain, which can be divided in two zing-binding motives: ZZ and TAZ2. Analysis of the acetylation state of constructs containing the central region of p300 plus the ZZ or plus both motives suggests that the TAZ2 domain plays a regulatory role on the HAT activity of the enzyme. Moreover, we could conclude that the TAZ2 domain has an auto-inhibitory effect on p300 HAT activity.

The CH3 domain does not strongly bind to the central region of p300. Attempts to crystallize the p300'core'_ZZ and the p300'core'_ZZ_TAZ2 constructs were performed. A

structure of the core including the CH3 domain would have yielded to important insights in the regulatory mode of this domain. Unfortunately, these constructs did not crystallize. GST pull-down experiments revealed no interaction between these domains. These experiments revealed that there is no interaction between these domains. However, weak binding cannot be discarded and it is still possible that the CH3 domains folds back on the central region preventing (auto-) acetylation of p300 and, therefore its activation. Further experiments are needed to confirm this hypothesis.

5. FINAL DISCUSSION

RÉSUMÉ EN FRANÇAIS

La stoechiométrie des complexes Nap1-H2A/H2B et Nap1-H1 est très controversée. Dans cette étude, nous avons pu montrer qu'un dimère de Nap1 peut lier un dimère de H2A/H2B ou un monomère de H1. Ces résultats concordent avec la plupart des études publiées à ce jour.

La structure cristalline du complexe $Nap1_2$-H2A/H2B montre que les deux monomères de Nap1 interagissent principalement avec l'histone H2A, via deux interfaces. Ces interfaces situées au niveau de la face concave de l'homodimère de Nap1 sont très conserves au sein des membres de la famille Nap1 excepte au sein des chaperones Vps75 et hSET aussi connues pour interagir avec H3/H4. Ceci suggère que ces deux interfaces sont importantes pour spécificité d'interaction des chaperones avec les histones.

D'autre part nous avons pu observer que le complexe Nap1-H2A/H2B est capable de former de larges oligomères en solution. Cet oligomère, qui peut atteindre jusqu'à six copie du complexe, est aussi présent au sien de l'unité asymétrique du cristal. Ainsi de nouvelles interfaces d'oligomerisation ont pu être mis a jour et leur fonction biologique est en cours de caractérisation. It a été suggéré que ces oligomères pourraient faciliter le stockage des histones de façon similaire à la Nucleoplasmin dans les œufs de *Xenopus*.

Ces nouvelles données nous ont permit de peindre un portrait moléculaire des étapes d'assemblage du nucléosome via Nap1. Le complexe Nap1-H2A/H2B pourrait se lier au tetrasome contentant H3/H4 et former un complexe intermédiaire avant le déplacement de Nap1 par l'ADN pour former le nucléosome.

Une autre partie de ce projet consiste a mieux caractériser la fonction de p300 et Nap1 dans l'assemblage et le désassemblage des nucléosomes. En effet il a été montre que ces facteurs peuvent interagir et réguler ce processus. Des investigations sont actuellement en cours.

5.1. Nap1 – HISTONE COMPLEXES

The exact binding stoichiometry of yNap1-H2A/H2B complexes has been a controversy of this field. In this study, we provide substantial evidence that a Nap1 homodimer binds to one H2A/H2B heterodimer or one linker histone H1, and that this represents the elemental repeat unit for further oligomerization of each complex. This observation is in agreement with the majority of prior publications (English et al. 2006; McBryant et al. 2003; Tóth et al. 2005; Zlatanova et al. 2007; Kepert et al. 2005; Newman et al. 2012; Shintomi et al. 2005). Our structural studies exclusively support a 1:1 stoichiometry and provide a clear understanding of how this histone chaperone interacts with the histone H2A/H2B heterodimer.

Our yNap1$_2$-H2A/H2B structure yields detailed molecular insights in the interaction between the Nap1 chaperone and the canonical H2A/H2B heterodimer. This interaction is mediated by both Nap1 monomers and predominantly by histone H2A (Figure 37, Figure 38). Despite the low resolution achieved, we were able to determine that the H2A/H2B heterodimer present in this complex has the same overall structure as observed within the context of the nucleosome, whereas the Nap1 homodimer appears to mimic the architecture and the charges of DNA, providing a concave surface for the histone binding as was suggested by the structure of the Nap1 dimer in isolation (Park & Luger 2006b).

This concave surface accommodates two histone interacting regions one per Nap1 monomer. Both regions are highly conserved among the Nap1 family members (Figure 37), suggesting that other Nap1 family members may recognize the histone H2A/H2B heterodimer through the same interface. However, the Vps75 and SET subsets of the Nap family differ at these regions (Figure 37A). Both subsets of proteins harbour distinct histone binding specificity; while Nap1 proteins bind preferentially H2A/H2B *in vivo* (Ito et al. 1996; Mosammaparast et al. 2001) and also H3/H4 *in vitro* (McQuibban et al. 1998), Vps75 and SET have been described as H3/H4-specific chaperones (Tang et al. 2008; Muto et al. 2007). As the two regions identified in the structure are a key source of variation between the subfamilies, we propose that the divergent features of these regions represent critical determinants of histone binding specificity.

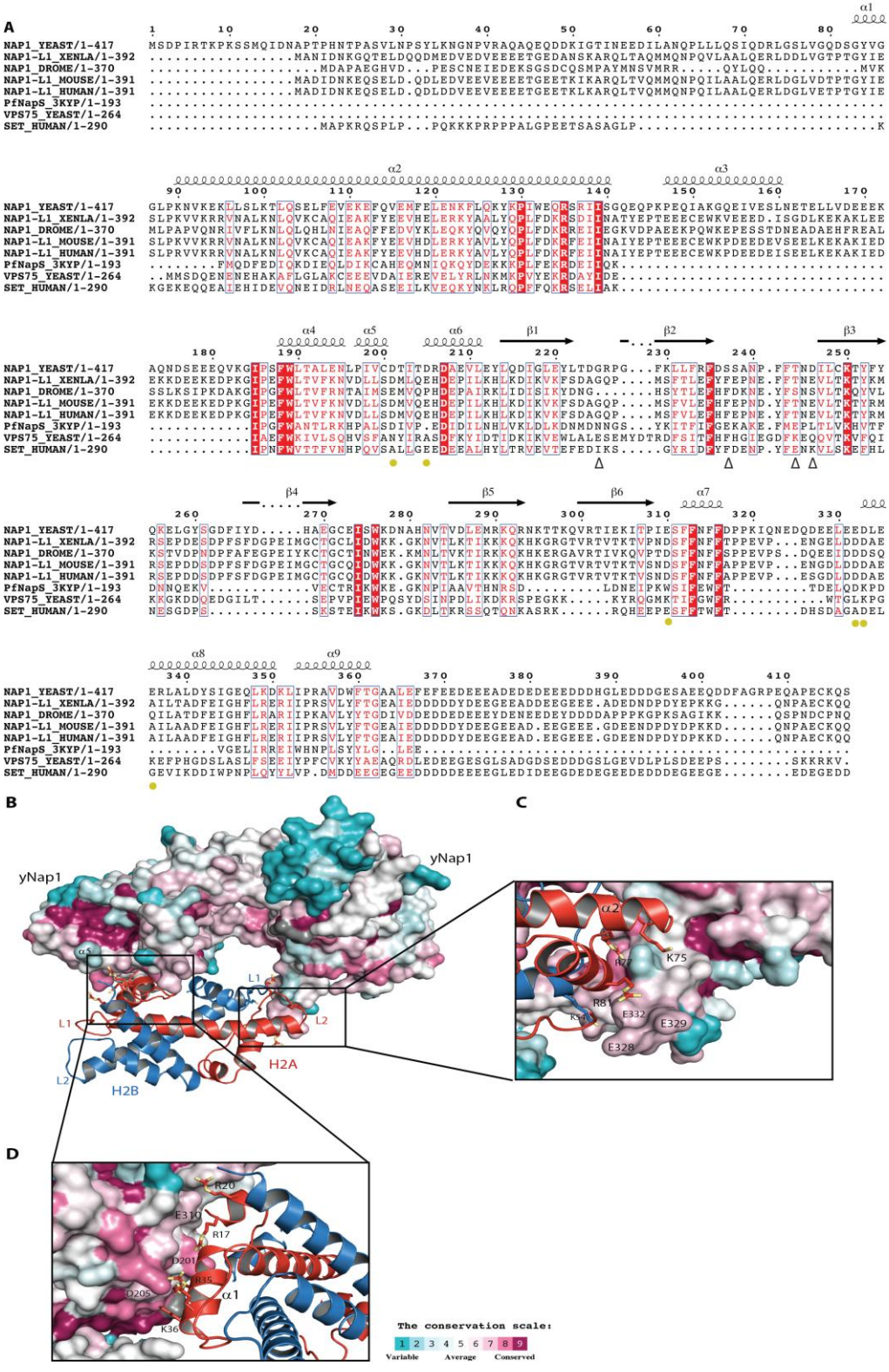

Figure 37 Sequence alignment and surface representation of conservation between Nap1 othologs and yeast Vps75 and human SET. (A) Sequence alignment Secondary structure of Nap1 is shown above the sequence alignment of the Nap1 othologs. A sequence alignment of yeast Vps75 and human SET is shown below the alignment of the Nap1 homologs. Residues implicated in binding histone H2A/H2B heterodimers and Nap1-Nap1 oligomerization are indicated with dots and triangles respectively, below the alignment. (B) Conservation surface representation of Nap1 homologues on the yNap1core2-xH2AD14/xH2BD28 complex. Conservation scale is given. (C) (D) Close-up views of contacts made by Nap1 and H2A/H2B heterodimer in the complex. H2A is coloured in red, H2B in blue. *Note: amino acids side-chains are illustrative.*

Both Nap1 monomers mainly interact with histone H2A (Figure 37B-D). These two interfaces mimic the DNA interactions with H2A/H2B heterodimers, an observation previously postulated by (Mazurkiewicz et al. 2006), and compete for binding to the same residues on H2A (Figure 38A). This structural "mimicry" also presents a mechanism for how Nap1 may prevent the non-productive association of DNA and histones and offers an explanation for the thermodynamic model proposed by Andrews et al. 2010, in which Nap1 promotes nucleosome assembly by disfavoring non-nucleosomal interactions between H2A/H2B and DNA.

In addition, H2A and H2A.Z share the same residues at the interacting regions (Figure 38A), indicating that Nap1 may make similar contacts with both canonical and variant histones. This suggests that Nap1 might not be able to discriminate between canonical H2A/H2B heterodimers and H2A.Z/H2B heterodimers, which reinforces the current model for Nap1-mediated nucleosome assembly proposed by Mazurkiewicz et al. 2006.

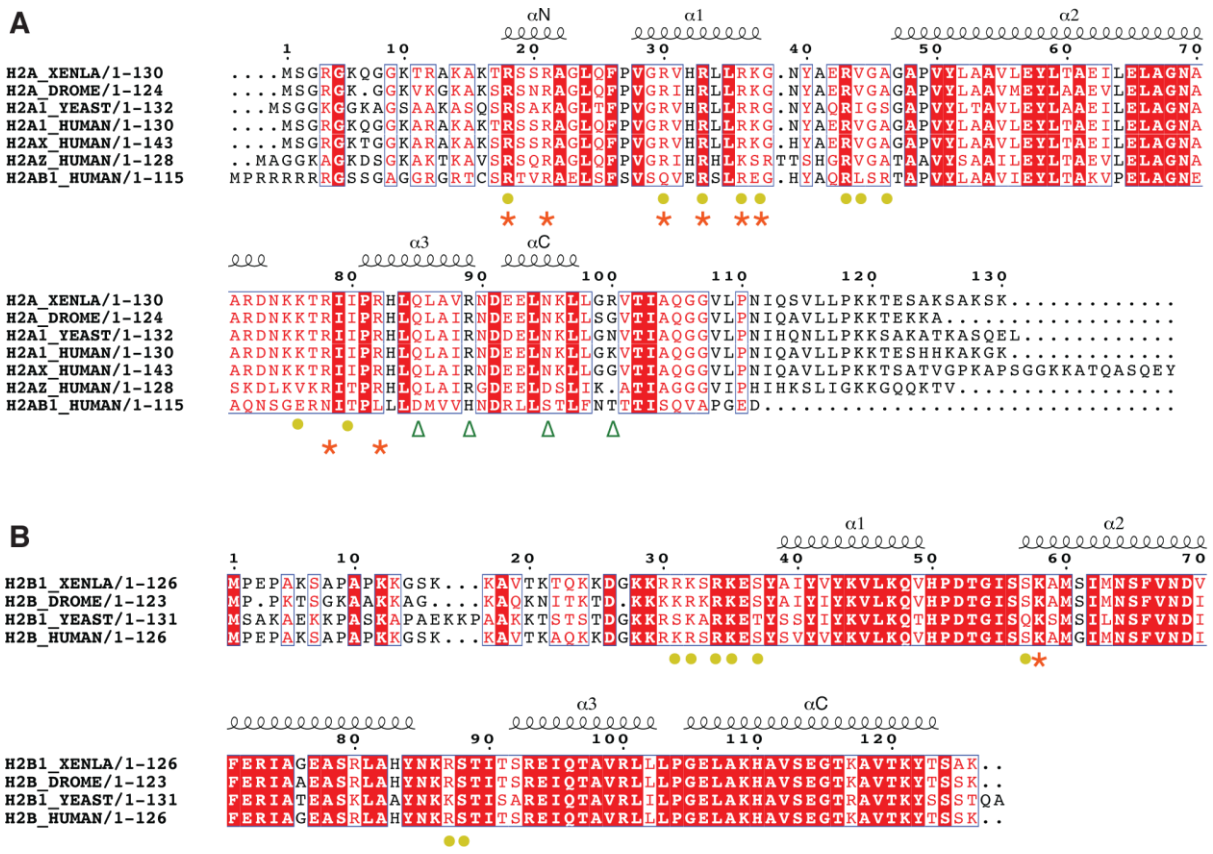

Figure 38 Sequence alignment and domain structure of H2A (A) and H2B (B). Secondary structure of H2A and H2B is shown above the sequence alignment of H2A and H2B homologs and variants. Residues implicated in histone-Nap1 binding, the H2A-H2A oligomerization interface and histone-DNA binding are indicated with asterisk, triangles and dots respectively.

At physiological conditions, Nap1 forms an obligate dimer (Park & Luger 2006b) that further self-associates in an equilibrium of dimer-octamer-hexadecamer (Tóth et al. 2005; Noda et al. 2011). In our studies, we detected self-association of yNap1 as a dimer-tetramer equilibrium. In contrast, upon addition of H2A/H2B dimers, distinct oligomerization states arise (from one to six repeating units) and were characterized by non-denaturing MS using various yNap1 constructs to determine which particular features of the protein facilitate higher-order complexes (Table 7). For example, it was previously suggested in the literature that removal of the β-hairpin structure (residues 284 to 308) may be detrimental to such oligomerization (Park et al. 2008). Additionally we found that removal of the C-terminal acidic tail of Nap1 may regulate the oligomeric state of these complexes. Furthermore, this acidic region has been shown to be important for nucleosome disassembly *in vitro* (Park et al. 2005).

Table 7 Summary of the oligomerization states of Nap1 before and after H2A/H2B binding.

Construct	Oligomer (x # of monomers)	Oligomer upon H2A/H2B binding (x # of repeating units)
yNap1*wt*	x2, x4	x1, x2
yNap1core	x2, x4	x1, x2, x3, x4, x5, x6
yNap1coreΔ284-308	x2, x4	x1, x2,
yNap1Δ1-73	x2, x4	x1, x2
yNap1Δ366-417	x2, x4	x1, x2, x3, x4, x5

Oligomerization has also been observed in other histone chaperones, Np forms a pentamer that binds five histone H2A/H2B heterdimers, which appears to serve as a histone storage complex (Dutta et al. 2001; Ramos et al. 2010). The role of the higher-order Nap1-H2A/H2B complexes remains unclear. One possibility is that oligomerization is used for histone storage or in order to buffer the cellular pool of soluble histones to allow controlled assembly and exchange of histones in chromatin (Cook et al. 2011). It is probable that the relevant oligomer for this function is the $(yNap1_2\text{-}H2A/H2B)_6$ complex seen in the asymmetric crystallographic unit and, as we were able to reproduce this finding independently in solution, by non-denaturing MS and negative stain EM measurements.

We additionally investigated whether phosphorylation of Nap1 might control the oligomerization state of the macromolecule. CKII phosphorylation of Nap1 abolished oligomerization, however it is not immediately clear why, as the phosphorylated residues,

which have been identified by (Calvert et al. 2008) and this thesis, are neither located in nor proximate to the putative oligomerization interfaces available in the $(Nap1_2\text{-}H2A/H2B)_6$ structure. The molecular basis for $Nap1_2$-H2A/H2B oligomer disruption by CKII-mediated phosphorylation remains unclear and needs further investigation.

Based on the crystal structure of the yNap1core (residues 75 to 365), it was postulated that the β-hairpin structure (residues 284 to 308) might play an important role in oligomerization (Park et al. 2008). This β-hairpin is not visible in our $yNap1_2$-H2A/H2B, thus we were unable to corroborate this putative role in $yNap1_2$-H2A/H2B complex oligomerization. However, the crystal structure reported in this study suggests two alternative oligomerization interfaces: (a) a Nap1-Nap1 interface and (b) a H2A-H2A interface. Both interfaces reside between two $yNap1_2$-H2A/H2B complex monomers and they are related by a two-fold symmetry axis in the asymmetric unit of the crystal.

Interestingly, sequence alignment of the Nap superfamily suggests that only the Nap1 and Nap1-like members of the family might have the capacity to oligomerize via the identified Nap1-Nap1 interface (Figure 37A), due to the conservation of critical residues in positions S237, T244, and G246. In contrast, Vps75 and SET do not exhibit sequence conservation at this interface (Figure 37A), which may offer an explanation for functional divergence of these Nap subsets observed in the cell.

At the H2A-H2A interface there is also conservation between canonical H2A and its variants (Figure 38A), which suggests Nap1-histone variant (H2A.X and H2A.Z) complexes may also be competent for oligomerization. However both interfaces, Nap1-Nap1 and H2A-H2A, require further biochemical characterization to determine their precise contribution, if any, to oligomerization.

5.2. THE PROPOSED MODEL

The structural “mimicry” by Nap1 of the DNA moiety of DNA-H2A/H2B complexes observed in our structure provides mechanistic insights regarding Nap1 functions. Furthermore, we believe our structure enables us to present a coherent mechanism by which stepwise assembly, and conversely the disassembly, of the nucleosome may be achieved. As

discussed previously, tetrasome deposition, by an H3/H4 histone chaperone such as Asf1, initiates nucleosome formation (Figure 39A) (Tyler 2002). As the configuration of Nap1 in our structure does not occlude the protein-protein interactions between the tetrasome and the H2A/H2B heterodimer, it is likely that the next step of nucleosome assembly occurs through a transient Nap1-H2A/H2B-tetrasome complex (Figure 39B). Subsequently, DNA associated with the tetrasome binds to the free H2A L1 and H2B L2 loops, and by "strand invasion" of the Nap1-H2A/H2B complex the histone chaperone is displaced (Figure 39C) and the hexasome intermediate is formed (Figure 39D). Finally, consequent deposition of a second H2A/H2B heterodimer by Nap1 at the alternative face of the hexasome, following a similar mechanism, would complete the formation of the nucleosome. A similar model was proposed over a decade prior to this thesis (Smith & Stillman 1991; Tyler 2002), in the absence of comprehensive molecular evidence. The structure presented in the current study provides structural and molecular evidence for this hypothesis, and moreover is in agreement with the previously determined thermodynamics of the nucleosome assembly process (Mazurkiewicz et al. 2006; Andrews et al. 2010).

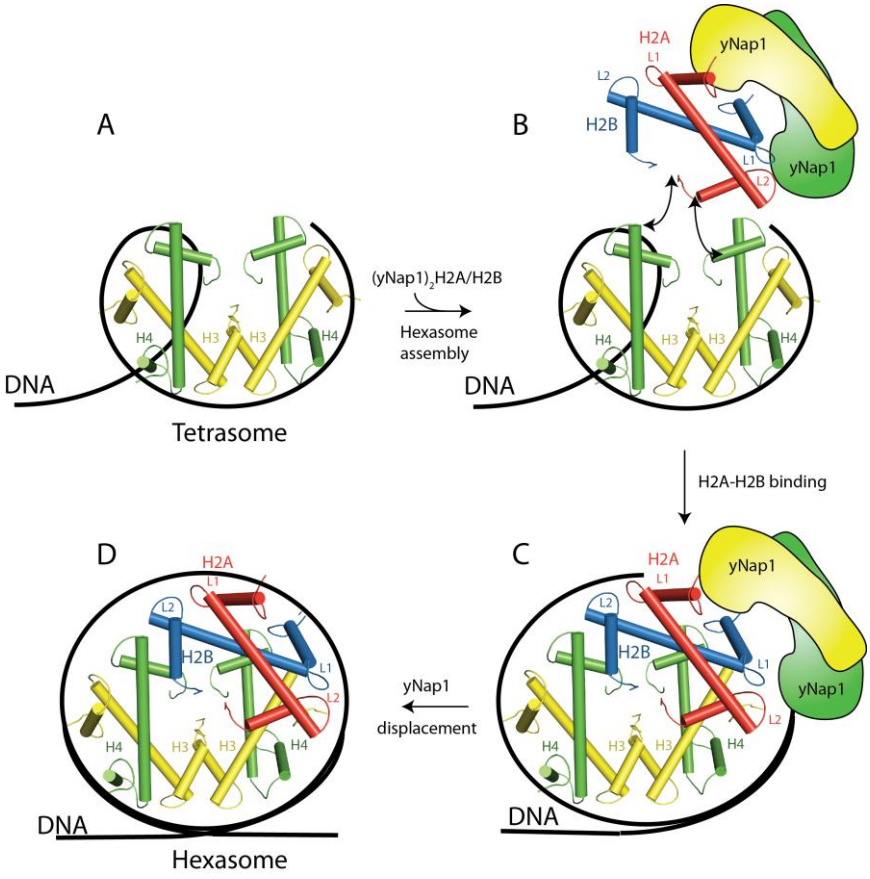

Figure 39 Proposed model for Nap1 mediated H2A/H2B deposition.

In conclusion, this study represents an extensive investigation of the structural, biophysical and biochemical characteristics of the interaction between the histone chaperone Nap1 and its preferred binding partner, the H2A/H2B heterodimer. The structural analysis of the yNap1-H2A/H2B complex provides the molecular basis for Nap1 chaperone function and Nap1-mediated nucleosome assembly; however further, detailed experimentation is required to determine the precise mechanism at work and whether this is consistent with the hypothesis we propose.

5.3. THE ROLE OF Nap1 IN TRANSCRIPTION

Currently, the cooperation p300 and Nap1 is thought to be essential in acetylation-dependent nucleosome eviction at promoter regions during transcription (Luebben et al. 2010). Indirect evidence for interaction of these proteins was reported in the literature (Asahara et al. 2002; Shikama et al. 2000), thus we sought to confirm this. However no direct interaction between the two factors could be determined, in this thesis, by pull-down assays using purified proteins. Our results suggest that, whilst both proteins might interact indirectly though a mutual binding partner, we have shown herein that this intermediate is not the histone H2A/H2B heterodimer dimer.

Nap1 purportedly interacts with the CH3 domain of p300 (Shikama et al. 2000), which is divided in two motifs: ZZ and TAZ2 (Yuan & Giordano 2002). Characterization of the p300'core', corresponding to the catalytic region of the enzyme, containing either the ZZ or both motives suggested that the TAZ2 domain inhibits (auto-) acetylation of p300. This observation, together with other studies (Reynoird et al. 2010), indicates that the CH3 domain might fold back on the catalytic region of p300 preventing its acetylation. Therefore recruitment of a CH3-interacting partner, such as Nap1 or NUT, may displace the CH3 domain, rendering the catalytic region of p300 more accessible for acetylation and therefore activation.

Pull-down experiments between the CH3 domain and the catalytic core of p300 were performed in order to test this hypothesis. However, it was not possible to detect any strong binding between them.

6. CONCLUDING REMARKS AND FUTURE PERSPECTIVES

RÉSUMÉ EN FRANÇAIS

Il est évident que la résolution de la structure de $Nap1_2$-H2A/H2B est importante pour comprendre le rôle des histones chaperons dans la cellule. Les mécanismes par lesquels les nucléosomes sont assemblé sont de mieux en mieux définies grâces aux études menées pendant cette thèse. Cependant, des études complémentaires devraient être faites afin de déterminer dans le détail les différentes étapes nécessaires à l'oligomerization du complexe Nap12-H2A/H2B *in vivo* et *in vitro*, aussi que la vérification du model d'assemblage du nucléosome.

Les mécanismes d'oligomerization et d'assemblage du nucléosome, un fois mieux définie, représenteront une information clé pour la compression de ces procès dans les cellules. A l'avenir, des efforts seront faits afin de mieux caractériser l'oligomerization du complexe. En outre, des études seront effectuées afin de rechercher le rôle de ces oligomères *in vivo*. Aussi, des études sur model d'assemblage du nucléosome pour Nap1 seront faits, qui aidera a une mieux compression moléculaire de ce procès.

6.1. CONCLUDING REMARKS

The basic repeating unit of chromatin is the nucleosome, which is composed of 147 bp of double stranded DNA wrapped around an octamer of histone proteins (Luger, Rechsteiner, et al. 1997b; Luger, Mäder, et al. 1997a). Nucleosome assembly requires initial deposition of H3/H4 tetramers followed by addition of two copies of H2A/H2B dimers (Smith & Stillman 1991). An additional linker histone H1 is located on the linker DNA between nucleosomes (Happel & Doenecke 2009). Histone deposition is mediated by histone chaperones, which are a diverse group of acidic proteins that facilitate the specific association and dissociation of histones with DNA, thus regulating nucleosome formation (Avvakumov et al. 2011; Eitoku et al. 2008).

High-resolution structures of the Asf1 histone chaperone in complex with the histone H3/H4 heterodimer have yielded detailed insights into the process of tetrasome assembly (English et al. 2006), the so-called first step in nucleosome assembly. However, it remains unclear how histone chaperones mediate H2A/H2B deposition to complete nucleosome assembly. In this study, to address this question, we have investigated the role of the H2A/H2B histone chaperon Nap1 in nucleosome assembly.

We determined the hitherto controversial stoichiometry of the Nap1-H2A/H2B complex to be 1:1 (dimer/dimer), via non-denaturing MS experiments, as further confirmed with the low-resolution crystal structure of this complex. The $Nap1_2$-H2A/H2B complex structure shows that both Nap1 monomers interact predominantly with H2A through two interaction surfaces to facilitate histone heterodimer recruitment. In addition, a large oligomer containing 6 copies of the $Nap1_2$-H2A/H2B complex is seen in the asymmetric crystallographic unit, which is concurrent with the predominating species we observed in solution. Inspection of the asymmetric crystallographic unit suggested two putative oligomerization interfaces, which are the subject of on-going characterization in our laboratory, in order to understand how higher order species are achieved.

Interpretation of the $Nap1_2$-H2A/H2B complex structure allows us to advance a model for the deposition of H2A/H2B heterodimers on the tetrasome and subsequently the hexasome to form the final NCP. We hypothesize that after binding of the H2A/H2B dimer in complex with $Nap1_2$ to the H3/H4 tetramer in the tetrasome, the H2A L1 and H2B L2 loops play a role

as sensor loops for the presence of the DNA. Upon its recognition by H2A/H2B, DNA strand invasion of the $Nap1_2$-H2A/H2B complex displaces $Nap1_2$ enablisng incorporation of H2A/H2B into the hexasome. A second copy of H2A/H2B heterodimer would then be deposited on the hexasome via a similar mechanism, thus facilitating completion of the nucleosome. Naturally, however, this model requires experimental validation.

Collectively these data provide to a better understanding of the $Nap1_2$-H2A/H2B complex stoichiometry and oligomerization process, as well as establishing a molecular basis for Nap1-mediated nucleosome assembly. This research represents significant progress in our understanding of chromatin structure and its assembly process.

6.2. FUTURE PERSPECTIVES

To better understand $Nap1_2$-H2A/H2B oligomerization, the first step will be to characterize the two putative oligomerization surfaces identified in the low-resolution structure of the $Nap1_2$-H2A/H2B complex. To this end, point mutations of the Nap1-Nap1 and H2A-H2A interfaces were designed and are under investigation. These mutants will allow us to define the molecular determinants of complex oligomerization. Identification of the residues involved in this process will also help in the understanding of its regulation, which might occur by phosphorylation. Upon clarification of the oligomerization sites *in vitro*, experiments will need to be conducted *in vivo* in order to analyse how perturbation of these interfaces influences oligomerization in the cell. Furthermore, understanding where this oligomerization takes place, and if oligomers might function as storage molecules, would yield key insights into the functional relevance of such higher order species.

To examine in molecular detail the interaction surface between the chaperone and the histone heterodimer, further attempts to obtain a high-resolution structure of the $Nap1_2$-H2A/H2B complex will be made. After the residues important for oligomerization are identified, point mutants on these surfaces will be used for crystallization. This might allow us to obtain a new crystal form that might diffract to higher resolution. In parallel, it will be interesting to test point mutations in the binding interface by pull-down assays in order to confirm the present structure. *In vivo* validation of this interaction is also required. Immuno-

precipitaion (IP) of point mutants in the full-length Nap1, expressed in *Saccharomyces cerevisiae*, would be a good approach to confirm the interaction surfaces *in vivo*.

A third important aspect that will be covered in the future is the validation of the Nap1-mediated nucleosome assembly model. The establishment of a nucleosome assembly assay utilizing Nap1 to deposit H2A/H2B dimers will be optimized in the near future. Then, point mutants on the H2A L1 and H2B L2 loops, suggested to function as a sensor loop for the DNA, will be used to stop the assembly process. In such scenario, Nap1 will remain bound to the H2A/H2B-tetrasome intermediate and the hexasome would not be assembled.

LIST OF FIGURES

LIST OF TABLES

REFERENCES

Afonine, P.V. et al., 2012. Towards automated crystallographic structure refinement with phenix.refine. *Acta Cryst (2012). D68, 352-367 [doi:10.1107/S0907444912001308]*, pp.1–16.

Akey, C.W. & Luger, K., 2003. Histone chaperones and nucleosome assembly. *Current Opinion in Structural Biology*, 13(1), pp.6–14.

Andrews, A.J. et al., 2008. A thermodynamic model for Nap1-histone interactions. *The Journal of biological chemistry*, 283(47), pp.32412–32418.

Andrews, A.J. et al., 2010. The histone chaperone Nap1 promotes nucleosome assembly by eliminating nonnucleosomal histone DNA interactions. *Molecular cell*, 37(6), pp.834–842.

Asahara, H. et al., 2002. Dual roles of p300 in chromatin assembly and transcriptional activation in cooperation with nucleosome assembly protein 1 in vitro. *Molecular and cellular biology*, 22(9), pp.2974–2983.

Attia, M. et al., 2007. Nap1l2 promotes histone acetylation activity during neuronal differentiation. *Molecular and cellular biology*, 27(17), pp.6093–6102.

Avvakumov, N., Nourani, A. & Côté, J., 2011. Histone chaperones: modulators of chromatin marks. *Molecular cell*, 41(5), pp.502–514.

Berndsen, C.E. et al., 2008. Molecular functions of the histone acetyltransferase chaperone complex Rtt109-Vps75. *Nature structural & molecular biology*, 15(9), pp.948–956.

Brunger, A.T. & Adams, P.D., 2012. *Chapter 108 - 1.7 Refinement of X-ray Crystal Structures*, Elsevier Ltd.

Brunger, A.T. et al., 2012. Improving the Accuracy of Macromolecular Structure Refinement at 7 Å Resolution. *Structure (London, England : 1993)*, 20(6), pp.957–966.

Calvert, M.E.K. et al., 2008. Phosphorylation by casein kinase 2 regulates Nap1 localization and function. *Molecular and cellular biology*, 28(4), pp.1313–1325.

Campos, E.I. & Reinberg, D., 2010. New chaps in the histone chaperone arena. *Genes & development*, 24(13), pp.1334–1338.

Cook, A.J.L. et al., 2011. A specific function for the histone chaperone NASP to fine-tune a reservoir of soluble H3-H4 in the histone supply chain. *Molecular cell*, 44(6), pp.918–927.

Daganzo, S.M. et al., 2003. Structure and function of the conserved core of histone deposition protein Asf1. *Current biology : CB*, 13(24), pp.2148–2158.

Davey, C.A. et al., 2002. Solvent mediated interactions in the structure of the nucleosome

core particle at 1.9 a resolution. *Journal of molecular biology*, 319(5), pp.1097–1113.

De Guzman, R.N. et al., 2000. Solution structure of the TAZ2 (CH3) domain of the transcriptional adaptor protein CBP. *Journal of molecular biology*, 303(2), pp.243–253.

Delvecchio, M., 2011. Mechanism of regulation of the p300/CBP acetyltransferase. pp.1–195.

DiMaio, F. et al., 2011. Modeling symmetric macromolecular structures in Rosetta3. *PloS one*, 6(6), p.e20450.

Drane, P. et al., 2010. The death-associated protein DAXX is a novel histone chaperone involved in the replication-independent deposition of H3.3. *Genes & development*, 24(12), pp.1253–1265.

Dutta, S. et al., 2001. The crystal structure of nucleoplasmin-core: implications for histone binding and nucleosome assembly. *Molecular cell*, 8(4), pp.841–853.

Earnshaw, W.C. et al., 1980. Assembly of nucleosomes: the reaction involving X. laevis nucleoplasmin. *Cell*, 21(2), pp.373–383.

Eitoku, M. et al., 2008. Histone chaperones: 30 years from isolation to elucidation of the mechanisms of nucleosome assembly and disassembly. *Cellular and molecular life sciences : CMLS*, 65(3), pp.414–444.

Elsässer, S.J. & D'Arcy, S., 2012. Towards a mechanism for histone chaperones. *Biochimica et biophysica acta*, 1819(3-4), pp.211–221.

Elsässer, S.J. et al., 2012. DAXX envelops an H3.3-H4 dimer for H3.3-specific recognition. *Nature*.

English, C.M. et al., 2005. ASF1 binds to a heterodimer of histones H3 and H4: a two-step mechanism for the assembly of the H3-H4 heterotetramer on DNA. *Biochemistry*, 44(42), pp.13673–13682.

English, C.M. et al., 2006. Structural basis for the histone chaperone activity of Asf1. *Cell*, 127(3), pp.495–508.

Finch, J.T. et al., 1977. Structure of nucleosome core particles of chromatin. *Nature*, 269(5623), pp.29–36.

Franzetti, B. et al., 2002. Tetrahedral aminopeptidase: a novel large protease complex from archaea. *The EMBO Journal*, 21(9), pp.2132–2138.

Fujii-Nakata, T. et al., 1992. Functional analysis of nucleosome assembly protein, NAP-1. The negatively charged COOH-terminal region is not necessary for the intrinsic assembly activity. *The Journal of biological chemistry*, 267(29), pp.20980–20986.

Fussner, E. et al., 2012. Open and closed domains in the mouse genome are configured as 10-nm chromatin fibres. *EMBO reports*, 13(11), pp.992–996.

Gamble, M.J. et al., 2005. The Histone Chaperone TAF-I/SET/INHAT Is Required for Transcription In Vitro of Chromatin Templates. *Molecular and cellular biology*, 25(2), pp.797–807.

Gill, J. et al., 2009. Crystal structure of malaria parasite nucleosome assembly protein: distinct modes of protein localization and histone recognition. *The Journal of biological chemistry*, 284(15), pp.10076–10087.

Gill, J. et al., 2010. Structure, localization and histone binding properties of nuclear-associated nucleosome assembly protein from Plasmodium falciparum. *Malaria journal*, 9, p.90.

Goldberg, A.D. et al., 2010. Distinct Factors Control Histone Variant H3.3 Localization at Specific Genomic Regions. *Cell*, 140(5), pp.678–691.

Grigoryev, S.A. et al., 2009. Evidence for heteromorphic chromatin fibers from analysis of nucleosome interactions. *Proceedings of the National Academy of Sciences of the United States of America*, 106(32), pp.13317–13322.

Hansen, J.C., 2002. Conformational dynamics of the chromatin fiber in solution: determinants, mechanisms, and functions. *Annual review of biophysics and biomolecular structure*, 31, pp.361–392.

Hansen, J.C. et al., 2010. Histone chaperones, histone acetylation, and the fluidity of the chromogenome. *Journal of cellular physiology*, 224(2), pp.289–299.

Happel, N. & Doenecke, D., 2009. Histone H1 and its isoforms: contribution to chromatin structure and function. *Gene*, 431(1-2), pp.1–12.

Haushalter, K.A. & Kadonaga, J.T., 2003. Chromatin assembly by DNA-translocating motors. *Nature reviews. Molecular cell biology*, 4(8), pp.613–620.

Henikoff, S. & Ahmad, K., 2005. Assembly of variant histones into chromatin. *Annual review of cell and developmental biology*, 21, pp.133–153.

Henikoff, S., Furuyama, T. & Ahmad, K., 2004. Histone variants, nucleosome assembly and epigenetic inheritance. *Trends in genetics : TIG*, 20(7), pp.320–326.

Hieb, A.R. et al., 2012. Fluorescence strategies for high-throughput quantification of protein interactions. *Nucleic acids research*, 40(5), p.e33.

Horn, P.J., 2002. MOLECULAR BIOLOGY: Chromatin Higher Order Folding--Wrapping up Transcription. *Science (New York, N.Y.)*, 297(5588), pp.1824–1827.

Ishimi, Y. & Kikuchi, A., 1991. Identification and molecular cloning of yeast homolog of nucleosome assembly protein I which facilitates nucleosome assembly in vitro. *The Journal of biological chemistry*, 266(11), pp.7025–7029.

Ishimi, Y. et al., 1987. Binding mode of nucleosome-assembly protein (AP-I) and histones. *European journal of biochemistry / FEBS*, 162(1), pp.19–24.

Ito, T. et al., 1996. Drosophila NAP-1 is a core histone chaperone that functions in ATP-facilitated assembly of regularly spaced nucleosomal arrays. *Molecular and cellular biology*, 16(6), pp.3112–3124.

Ito, T. et al., 2000. p300-mediated acetylation facilitates the transfer of histone H2A-H2B dimers from nucleosomes to a histone chaperone. *Genes & development*, 14(15), pp.1899–1907.

Kabsch, W., 2010. XDS. *Acta crystallographica. Section D, Biological crystallography*, 66(Pt 2), pp.125–132.

Kepert, J.F. et al., 2005. NAP1 modulates binding of linker histone H1 to chromatin and induces an extended chromatin fiber conformation. *The Journal of biological chemistry*, 280(40), pp.34063–34072.

Kolonko, E.M. et al., 2010. Catalytic activation of histone acetyltransferase Rtt109 by a histone chaperone. *Proceedings of the National Academy of Sciences of the United States of America*, 107(47), pp.20275–20280.

Kornberg, R.D. & Thomas, J.O., 1974. Chromatin structure; oligomers of the histones. *Science (New York, N.Y.)*, 184(4139), pp.865–868.

Laskey, R.A. et al., 1978. Nucleosomes are assembled by an acidic protein which binds histones and transfers them to DNA. *Nature*, 275(5679), pp.416–420.

Legge, G.B. et al., 2004. ZZ domain of CBP: an unusual zinc finger fold in a protein interaction module. *Journal of molecular biology*, 343(4), pp.1081–1093.

Levchenko, V. & Jackson, V., 2004. Histone release during transcription: NAP1 forms a complex with H2A and H2B and facilitates a topologically dependent release of H3 and H4 from the nucleosome. *Biochemistry*, 43(9), pp.2359–2372.

Lewis, P.W. et al., 2010. Daxx is an H3.3-specific histone chaperone and cooperates with ATRX in replication-independent chromatin assembly at telomeres. *Proceedings of the National Academy of Sciences of the United States of America*, 107(32), pp.14075–14080.

Li, B., Carey, M. & Workman, J.L., 2007. The role of chromatin during transcription. *Cell*, 128(4), pp.707–719.

Li, M. et al., 1999. Casein kinase 2 binds and phosphorylates the nucleosome assembly protein-1 (NAP1) in Drosophila melanogaster. *Journal of molecular biology*, 293(5), pp.1067–1084.

Liu, C.-P. et al., 2012. Structure of the variant histone H3.3-H4 heterodimer in complex with its chaperone DAXX. *Nature structural & molecular biology*, 19(12), pp.1287–1292.

Liu, X. et al., 2008. The structural basis of protein acetylation by the p300/CBP transcriptional coactivator. *Nature*, 451(7180), pp.846–850.

Luebben, W.R., Sharma, N. & Nyborg, J.K., 2010. Nucleosome eviction and activated transcription require p300 acetylation of histone H3 lysine 14. *Proceedings of the National Academy of Sciences of the United States of America*, 107(45), pp.19254–19259.

Luger, K. & Richmond, T.J., 1998. The histone tails of the nucleosome. *Current opinion in genetics & development*, 8(2), pp.140–146.

Luger, K., Dechassa, M.L. & Tremethick, D.J., 2012. New insights into nucleosome and chromatin structure: an ordered state or a disordered affair? *Nature reviews. Molecular cell biology*, 13(7), pp.436–447.

Luger, K., Mäder, A.W., et al., 1997a. Crystal structure of the nucleosome core particle at 2.8 A resolution. *Nature*, 389(6648), pp.251–260.

Luger, K., Rechsteiner, T.J., et al., 1997b. Characterization of nucleosome core particles containing histone proteins made in bacteria. *Journal of molecular biology*, 272(3), pp.301–311.

Luk, E. et al., 2007. Chz1, a nuclear chaperone for histone H2AZ. *Molecular cell*, 25(3), pp.357–368.

Mazurkiewicz, J., Kepert, J.F. & Rippe, K., 2006. On the mechanism of nucleosome assembly by histone chaperone NAP1. *The Journal of biological chemistry*, 281(24), pp.16462–16472.

McBryant, S.J. & Peersen, O.B., 2004. Self-association of the yeast nucleosome assembly protein 1. *Biochemistry*, 43(32), pp.10592–10599.

McBryant, S.J. et al., 2003. Preferential binding of the histone (H3-H4)2 tetramer by NAP1 is mediated by the amino-terminal histone tails. *The Journal of biological chemistry*, 278(45), pp.44574–44583.

McCoy, A.J. et al., 2007. Phaser crystallographic software. *Journal of Applied Crystallography*, 40(4), pp.658–674.

McQuibban, G.A., Commisso-Cappelli, C.N. & Lewis, P.N., 1998. Assembly, remodeling, and histone binding capabilities of yeast nucleosome assembly protein 1. *The Journal of biological chemistry*, 273(11), pp.6582–6590.

Mello, J.A. & Almouzni, G., 2001. The ins and outs of nucleosome assembly. *Current opinion in genetics & development*, 11(2), pp.136–141.

Mills, A.D. et al., 1980. An acidic protein which assembles nucleosomes in vitro is the most abundant protein in Xenopus oocyte nuclei. *Journal of molecular biology*, 139(3), pp.561–568.

Miyaji-Yamaguchi, M. et al., 2003. Involvement of nucleocytoplasmic shuttling of yeast Nap1 in mitotic progression. *Molecular and cellular biology*, 23(18), pp.6672–6684.

Mizuguchi, G. et al., 2004. ATP-driven exchange of histone H2AZ variant catalyzed by SWR1 chromatin remodeling complex. *Science (New York, N.Y.)*, 303(5656), pp.343–348.

Mosammaparast, N. & Pemberton, L.F., 2004. Karyopherins: from nuclear-transport mediators to nuclear-function regulators. *Trends in cell biology*, 14(10), pp.547–556.

Mosammaparast, N. et al., 2001. Nuclear import of histone H2A and H2B is mediated by a network of karyopherins. *The Journal of cell biology*, 153(2), pp.251–262.

Mosammaparast, N., Del Rosario, B.C. & Pemberton, L.F., 2005. Modulation of histone deposition by the karyopherin kap114. *Molecular and cellular biology*, 25(5), pp.1764–1778.

Mosammaparast, N., Ewart, C.S. & Pemberton, L.F., 2002. A role for nucleosome assembly protein 1 in the nuclear transport of histones H2A and H2B. *The EMBO Journal*, 21(23), pp.6527–6538.

Mousson, F. et al., 2005. Structural basis for the interaction of Asf1 with histone H3 and its functional implications. *Proceedings of the National Academy of Sciences of the United States of America*, 102(17), pp.5975–5980.

Murshudov, G.N. et al., 2011. REFMAC5 for the refinement of macromolecular crystal structures. *Acta crystallographica. Section D, Biological crystallography*, 67(Pt 4), pp.355–367.

Muto, S. et al., 2007. Relationship between the structure of SET/TAF-Ibeta/INHAT and its histone chaperone activity. *Proceedings of the National Academy of Sciences of the United States of America*, 104(11), pp.4285–4290.

Nakagawa, T. et al., 2001. Multistep chromatin assembly on supercoiled plasmid DNA by nucleosome assembly protein-1 and ATP-utilizing chromatin assembly and remodeling factor. *The Journal of biological chemistry*, 276(29), pp.27384–27391.

Natsume, R. et al., 2007. Structure and function of the histone chaperone CIA/ASF1 complexed with histones H3 and H4. *Nature*, 446(7133), pp.338–341.

Newman, E.R. et al., 2012. Large multimeric assemblies of nucleosome assembly protein and histones revealed by small-angle X-ray scattering and electron microscopy. *The Journal of biological chemistry*, 287(32), pp.26657–26665.

Noda, M. et al., 2011. Assembly states of the nucleosome assembly protein 1 (NAP-1) revealed by sedimentation velocity and non-denaturing MS. *The Biochemical journal*, 436(1), pp.101–112.

O'Donovan, D.J. et al., 2012. A grid-enabled web service for low-resolution crystal structure refinement. *Acta crystallographica. Section D, Biological crystallography*, 68(Pt 3), pp.261–267.

Ohkuni, K., Shirahige, K. & Kikuchi, A., 2003. Genome-wide expression analysis of NAP1 in Saccharomyces cerevisiae. *Biochemical and biophysical research communications*,

306(1), pp.5–9.

Olins, A.L. & Olins, D.E., 1974. Spheroid chromatin units (v bodies). *Science (New York, N.Y.)*, 183(4122), pp.330–332.

Oudet, P., Gross-Bellard, M. & Chambon, P., 1975. Electron microscopic and biochemical evidence that chromatin structure is a repeating unit. *Cell*, 4(4), pp.281–300.

Park, Y.-J. & Luger, K., 2006a. Structure and function of nucleosome assembly proteins. *Biochemistry and cell biology = Biochimie et biologie cellulaire*, 84(4), pp.549–558.

Park, Y.-J. & Luger, K., 2006b. The structure of nucleosome assembly protein 1. *Proceedings of the National Academy of Sciences of the United States of America*, 103(5), pp.1248–1253.

Park, Y.-J. et al., 2005. Nucleosome assembly protein 1 exchanges histone H2A-H2B dimers and assists nucleosome sliding. *The Journal of biological chemistry*, 280(3), pp.1817–1825.

Park, Y.-J., McBryant, S.J. & Luger, K., 2008. A beta-hairpin comprising the nuclear localization sequence sustains the self-associated states of nucleosome assembly protein 1. *Journal of molecular biology*, 375(4), pp.1076–1085.

Ramos, I. et al., 2010. Nucleoplasmin binds histone H2A-H2B dimers through its distal face. *The Journal of biological chemistry*, 285(44), pp.33771–33778.

Ransom, M., Dennehey, B.K. & Tyler, J.K., 2010. Chaperoning histones during DNA replication and repair. *Cell*, 140(2), pp.183–195.

Reynoird, N. et al., 2010. Oncogenesis by sequestration of CBP/p300 in transcriptionally inactive hyperacetylated chromatin domains. *The EMBO Journal*, 29(17), pp.2943–2952.

Rocha, W. & Verreault, A., 2008. Clothing up DNA for all seasons: Histone chaperones and nucleosome assembly pathways. *FEBS letters*, 582(14), pp.1938–1949.

Rodriguez, P. et al., 2000. NAP-2: histone chaperone function and phosphorylation state through the cell cycle. *Journal of molecular biology*, 298(2), pp.225–238.

Schröder, G.F., Brunger, A.T. & Levitt, M., 2007. Combining efficient conformational sampling with a deformable elastic network model facilitates structure refinement at low resolution. *Structure (London, England : 1993)*, 15(12), pp.1630–1641.

Schröder, G.F., Levitt, M. & Brunger, A.T., 2010. Super-resolution biomolecular crystallography with low-resolution data. *Nature*, 464(7292), pp.1218–1222.

Selth, L. & Svejstrup, J.Q., 2007. Vps75, a new yeast member of the NAP histone chaperone family. *The Journal of biological chemistry*, 282(17), pp.12358–12362.

Seo, S.B. et al., 2001. Regulation of histone acetylation and transcription by INHAT, a human cellular complex containing the set oncoprotein. *Cell*, 104(1), pp.119–130.

Sharma, N. & Nyborg, J.K., 2008. The coactivators CBP/p300 and the histone chaperone NAP1 promote transcription-independent nucleosome eviction at the HTLV-1 promoter. *Proceedings of the National Academy of Sciences of the United States of America*, 105(23), pp.7959–7963.

Shen, H.-H. et al., 2001. Identification and Characterization of a SET/NAP Protein Encoded by a Brain-Specific Gene, MB20. *Genomics*, 71(1), pp.21–33.

Shikama, N. et al., 2000. Functional interaction between nucleosome assembly proteins and p300/CREB-binding protein family coactivators. *Molecular and cellular biology*, 20(23), pp.8933–8943.

Shintomi, K. et al., 2005. Nucleosome assembly protein-1 is a linker histone chaperone in Xenopus eggs. *Proceedings of the National Academy of Sciences of the United States of America*, 102(23), pp.8210–8215.

Simpson, R.T., 1978. Structure of the chromatosome, a chromatin particle containing 160 base pairs of DNA and all the histones. *Biochemistry*, 17(25), pp.5524–5531.

Smith, S. & Stillman, B., 1991. Stepwise assembly of chromatin during DNA replication in vitro. *The EMBO Journal*, 10(4), pp.971–980.

Steer, W.M. et al., 2003. Xenopus nucleosome assembly protein becomes tissue-restricted during development and can alter the expression of specific genes. *Mechanisms of development*, 120(9), pp.1045–1057.

Straube, K., Blackwell, J.S. & Pemberton, L.F., 2010. Nap1 and Chz1 have separate Htz1 nuclear import and assembly functions. *Traffic (Copenhagen, Denmark)*, 11(2), pp.185–197.

Studier, F.W., 2005. Protein production by auto-induction in high density shaking cultures. *Protein expression and purification*, 41(1), pp.207–234.

Taneva, S.G. et al., 2009. A mechanism for histone chaperoning activity of nucleoplasmin: thermodynamic and structural models. *Journal of molecular biology*, 393(2), pp.448–463.

Tang, Y. et al., 2008. Structure of Vps75 and implications for histone chaperone function. *Proceedings of the National Academy of Sciences of the United States of America*, 105(34), pp.12206–12211.

Tóth, K.F., Mazurkiewicz, J. & Rippe, K., 2005. Association states of nucleosome assembly protein 1 and its complexes with histones. *The Journal of biological chemistry*, 280(16), pp.15690–15699.

Tyler, J.K., 2002. Chromatin assembly. Cooperation between histone chaperones and ATP-dependent nucleosome remodeling machines. *European journal of biochemistry / FEBS*, 269(9), pp.2268–2274.

Wong, H., Victor, J.-M. & Mozziconacci, J., 2007. An all-atom model of the chromatin fiber

containing linker histones reveals a versatile structure tuned by the nucleosomal repeat length. *PloS one*, 2(9), p.e877.

Wong, L.H. et al., 2010. ATRX interacts with H3.3 in maintaining telomere structural integrity in pluripotent embryonic stem cells. *Genome Research*, 20(3), pp.351–360.

Woodcock, C.L. & Ghosh, R.P., 2010. Chromatin Higher-order Structure and Dynamics. *Cold Spring Harbor Perspectives in Biology*, 2(5), pp.a000596–a000596.

Woodland, H.R. & Adamson, E.D., 1977. The synthesis and storage of histones during the oogenesis of Xenopus laevis. *Developmental biology*, 57(1), pp.118–135.

Wu, W.-H. et al., 2005. Swc2 is a widely conserved H2AZ-binding module essential for ATP-dependent histone exchange. *Nature structural & molecular biology*, 12(12), pp.1064–1071.

Yuan, L.W. & Giordano, A., 2002. Acetyltransferase machinery conserved in p300/CBP-family proteins. *Oncogene*, (21), pp.2253–2260.

Zhou, Z. et al., 2008. NMR structure of chaperone Chz1 complexed with histones H2A.Z-H2B. *Nature structural & molecular biology*, 15(8), pp.868–869.

Zhu, Y. et al., 2006. Arabidopsis NRP1 and NRP2 encode histone chaperones and are required for maintaining postembryonic root growth. *The Plant cell*, 18(11), pp.2879–2892.

Zlatanova, J., Seebart, C. & Tomschik, M., 2007. Nap1: taking a closer look at a juggler protein of extraordinary skills. *FASEB journal : official publication of the Federation of American Societies for Experimental Biology*, 21(7), pp.1294–1310.

ACKNOWLEDGEMENTS

I would like to give a special thanks to my supervisor, Dr. Daniel Panne, for giving me the opportunity to work in his lab and in that fascinating project.

I would like to thank the PhD jury members Dr. John McGeehan, Dr. Stefan Dimitrov and Dr. Christophe Müller for taking the time to revise this thesis. I would also like to acknowledge the members of my TAC Committee: Dr. Winfried Weissenhorn, Dr. Christian Häring, and Dr. Darren Hart, for their support and for helpful discussion during our annual meetings. I would also like to extend these acknowledgements to Helke Hillebrand and Milanka Strojkovic for their support over the years. They help me in my adaptation to EMBL and made everything easier.

I would like to express my gratitude to the EMBL and PSB facilities as well as the EMBL community and the non-scientific staff, who are always ready to help. This work would have been a bit more complicated without you.

Over the last years, I discovered that science could be discouraging and sometimes frustrating. But the encouragement of the members of the Panne lab, past and present, helped greatly along the way. I would like to send a special thanks to Juliette Devos, Amédé Larabi, Esther Ortega, and Kyle Muir, who kept my optimism in good shape and gave me the strength not to give up. I would also like to thank all the other members of the group: Manuela Delvecchio, for welcoming me to Grenoble; Joanna Andrecka, for her happiness and helpful discussions; Emily Newman, for insights in the project; Jonathan Gaucher, for his enthusiasm in science; Daria Bou Dargham and Siyi Zhang for their fresh air. I would like to thank once more all of them for proofreading parts of my thesis and specially Amédé and Jonathan who corrected the summaries in French.

During my time in Grenoble I have met some people to whom I will always be grateful for their personal value and for all we have shared: Juan Reguera, Amada Peñalosa, Andrés Palencia, Simon Trowitzsch, Matze Haffke, Elisa Cora… I might forget some names, do not take it personally!

I am also very grateful to all EMBL Predocs 2009, specially Kasia Tarnawska, Sander Timmer, Tze Heng Tan, Mathieu Botte and Michael Lipp. Thanks you all for the time during the predoc course but also for all the trips and magic friendship we have been able to construct.

Please let me now write some words in my mother tongue to my friends and family back home in Barcelona.

Per començar m'agradaria donar les gràcies a la Mercè i la Natalia. Gràcies per ser sempre allí, per no decaure mai i mantenir viva l'amistat des de la distància.

També voldria donar les gràcies a la meva família, a tots: Micu, Mare, Jordi, Mar, etc. Per confiar tant en mi i donar-me el suport necessari per no deixar de mirar endavant quan més ho necessitava.

Oriol, sí ara et toca a tu. Com agrair-te tots aquests anys, els alts i baixos de la tesi i en definitiva de la vida. No tinc massa paraules, només puc donar-te les gràcies. Aquesta tesi també és una mica teva.